Department of Chemistry | Lancaster University

MRes Chemistry Research Project

Thesis

Name: Ethan Evans

Supervisors: Dr Verena Görtz & Dr John Griffin

Project Title:

Photochromic Polymers as Solar Thermal Fuels

2020-2021

Abstract

Solar thermal fuels could provide a move away from open cycle storage, being a renewable resource that utilises photochromic molecules such as azobenzene, to achieve solar energy harvesting, storage and release in a single material. The synthesis of an azobenzene based monomer and mildly syndiotactic polymer, alongside the characterisation of energy storage, energy release, thermal properties and structural properties is presented. The tailoring of azobenzene based polymers to achieve certain levels of crystallinity and how that could increase the energy density of a solar thermal fuel is discussed.

It was found that free-radical polymerisation could achieve a polymer of mild syndiotacticity however, this tacticity did not appear to produce any form of crystallinity in the polymer when characterised by differential scanning calorimetry, with no additional recrystallisation exotherm present. This result was contradicted by wide angle X-ray scanning measurements, which showed a small level of crystallinity in the unirradiated form of the polymer, indicated by an additional peak at the q value of 0.33 $Å^{-1}$, corresponding to a d-spacing of 19.04 Å, attributed to the ordered spacing between polymer layers.

The synthesised polymer was irradiated with 365 nm light, to explore its energy release properties, with a comparatively high energy density of 134 J g^{-1} being recorded. The effect of solvents on these energy release properties was also explored however, P1 samples dried from DCM and THF were recorded as 83.64 J g^{-1} (cis percentage: 61.8 %) and -90.96 J g^{-1} (cis percentage: 63.1 %) respectively, indicating that there was little to no difference between the use of the two solvents. This result was not conclusive due to not fully optimal drying conditions in samples dried from THF.

No evidence was found to show any contribution of crystallinity in the synthesised polymer, to an increased overall energy density of the polymer solar thermal fuel system. Solid-state charging of the polymer via drop casting and irradiation at 365 nm was unsuccessful with the polymer only reaching a low cis percentage of around 19.5 %. 13 C CPMAS experiments were carried out to assess the sensitivity of the experiment to differences in P1 isomers, overall, it appeared that SSNMR is not very sensitive to changes in P1 isomers, however, there were some small differences present.

Acknowledgements

I would like to thank my supervisors John Griffin and Verena Görtz for giving me the opportunity to study and work on this project. It has been a longer than planned journey, but they have given me the utmost support, guidance, and very valuable patience over the course of the whole project and through the ongoing COVID 19 pandemic. Verena and John have been extremely kind and helpful to me throughout my entire time at university and have gone above and beyond to help me improve as a chemist and a person along the way. I have a lot of respect for them both.

Jack Kaufman, Stuart Berrow and Callum Wallace also deserve a lot of praise, for their support and guidance in the lab over the course of the project. There were countless times when I asked the same question twice, but they would answer it again in the same kind and understanding manner every time as if to say, “we’ve all been there”.

Thank you to my family and friends, who have supported me throughout and have shown an unwavering amount of support and patience, while also providing a kick up the backside when times were tough (thanks Mum). I would like to thank Sarah, who has been by my side throughout the entirety of my academic journey so far and has helped me through what was perhaps the toughest stage of it yet. A special thanks to Mum, Sarah and Tom for helping me to proofread the whole piece, your contributions are greatly appreciated.

Covid 19 Impact Statement

The COVID 19 pandemic led to several factors that were detrimental to me during the project, causing several delays early-on in the project. Delays included a slow start to lab work, due to fume hood scheduling issues, because of the reduced lab capacity caused by COVID 19 restrictions. Due to social distancing, the lab was run with a rota system with scheduling, meaning that I was only able to use approximately 50% of the lab time that I would under normal circumstances, with fume hood needing to be shared between two or (rarely) three people at a time in each week. Social distancing also led to a reduced capacity for training in various techniques such as column chromatography and inert reaction synthesis methods, with training made significantly more complex and time consuming.

In the early stages of the project, social distancing meant that I was unable to benefit from direct supervision in the lab, that would have provided me with more confidence in the techniques required to get up to speed with the project and achieve a high level of efficiency with these techniques. This contributed to the synthesis of the initial monomer for the project taking much longer than expected, where is experienced issues in purification and reduced lab access. Also, during COVID 19 restrictions, an air compressor failure meant that the solid-state NMR instrument was running at half capacity, resulting in reduced access.

Additionally, isolation and limited access to the lab environment during lockdown contributed to a decline in mental health. Any activities that could have boosted my physical and mental wellbeing were difficult to access while living on campus, those activities were important in allowing me to separate work life from home life and therefore, impacted my ability to focus on the project and keep up the levels of self-determination that the project required in such a working environment. Not being home for ~6 months, combined with some uncertainty around living arrangements at home, also contributed to a lack of focus.

Author's Declaration

I declare that this thesis is my own work and has not been submitted in substantially the same form, as part of a higher degree elsewhere.

Table of Contents

List of Figures

List of Tables

List of Abbreviations

AIBN	Azobisisobutyronitrile
C	Concentration
cat	Catalytic
$CDCl_3$	Deuterated Chloroform
CNTs	Carbon Nanotubes
CP	Cross Polarisation
DCM	Dichloromethane
d	Doublets
dd	Doublet of Doublets
DSC	Differential Scanning Calorimetry
E_a	Activation Energy
eq	Equivalences
GPC	Gel Permeation Chromatography
m	Multiplet
MAS	Magic-Angle Spinning
mm	Isotactic Triad
mr	Atactic Triad
M_n	Number Average Molecular Weight
M_w	Weight Average Molecular Weight
M1	*Trans*-4-methacroloyloxyazobenzene
NMR	Nuclear Magnetic Resonance
OM	Optical Microscopy
PMMA	Poly(methyl methacrylate)
ppm	Parts per Million
PSS	Photostationary State
PVs	Photovoltaics
P1	Poly(t*rans*-4-methacroloyloxyazobenzene)
q	Quintuplet
rr	Syndiotactic Triad
s	Singlet
SSNMR	Solid State Nuclear Magnetic Resonance
STFs	Solar Thermal Fuels
SWCNTs	Single Walled Carbon Nanotubes
T	Temperature
t	Triplet

t	Time
TEA	Triethylamine
UV	Ultraviolet
Vis	Visible
WAXS	Wide Angle X-ray Scanning
ε	Molar Extinction Coefficient
ε_c	*Cis* Isomer Molar Extinction Coefficient
ε_t	*Trans* Isomer Molar Extinction Coefficient
λ_{max}	Wavelength of the Absorption Maximum
Φ_{ct}	Quantum Yield of *Cis* to *Trans* Conversion Photoreaction
Φ_{tc}	Quantum Yield of *Trans* to *Cis* Conversion Photoreaction

1. Introduction

Fossil fuel dependence has been a necessary and perhaps unavoidable practice for humans over the past couple of centuries. This practice has now led to a very unfamiliar and unpredictably changing climate. Anthropogenic sources of greenhouse gases are stated as the main cause of climate change and have been said to have caused a 1 °C increase in global temperatures since pre-industrial times.[1] Aside from their contribution to climate issues, fossil fuels are becoming increasingly rare and more expensive,[2] adding to the importance of new, renewable energy sources.[1]

1.1. The Importance of Renewable Energy in the Form of Solar Energy

A move away from open-cycle storage, requiring chemicals to be exchanged with the environment, towards renewables, is necessary to combat climate change. This will require new technologies and methodologies for capturing, converting, storing and releasing energy. Solar energy is among the suitors for this endeavour, releasing no CO_2 or greenhouse gases into the atmosphere as a result of the energy it provides.

The amount of energy that reaches the earth from the sun, per hour, is reported to be ~430 exajoules (EJ) or 430×10^{18} J.[3] This value is comparable to the approximate annual global energy usage of 583.9 EJ,[4] suggesting that there is potential for a huge amount of energy to be harnessed, if suitable conversion and storage technologies can be developed.

The use of solar energy has its advantages and disadvantages. For example, solar energy is an intermittent energy source and therefore, requires energy storage methods to capture any excess energy for use in poor weather conditions or during periodical darkness. Solar energy technologies are constantly looking to increase the ability to store large amounts of energy gained, in a given volume, i.e. increasing the energy density. Solar energy technologies can also be utilised in places that would not normally be suitable for energy production, such as the use of solar panels on buildings or solar windows, a recent innovation that uses windows as solar collectors.

Global annual solar energy production increased by 1.2 EJ between 2018 and 2019. A large part of that, contributing to renewable energy having a 5% share in current global energy usage, are solar photovoltaics (PV).[4] This share will likely increase in the coming years, due to increasing pressure on companies to become more environmentally friendly and sustainable. This data shows that PV technology has become well-established in recent years, with a global growth rate of 24.3% from 2018 to 2019.[4] It is safe to assume that PV technology will be a major energy provider for years to come.

A drawback for PV is that the technology requires separate materials for the capture of photons, the conversion of photons into electrons and finally the storage of those electrons in an external battery.[5] All of these components lead to PV technology taking up more physical space, as well as having a lower efficiency than technologies that only require one material for capture, conversion and storage of solar energy, such as solar thermal fuels (STF).

1.2. Solar Thermal Fuels

Recently, a new form of energy system has become prominent, in the form of so-called solar thermal fuels (STF). An STF stores solar energy in the bonds of metastable molecules (a stable state in the system that is not the ground state). This energy can be released as heat at a later time through the application of a small energy "trigger", in the form of a pulse of heat or light. Advantages of STFs are that they can be single component materials, with no moving or electrical parts, which can be highly cyclable, making them good suitors for daily or seasonal repeat uses.[6] STFs are different to classical solar thermal energy (STE) storage methods in that, STE harnesses the power of the sun and can be used in housing to save energy and decrease the use of carbon.[7]

STE works through the collection of heat from the sun via a heat transfer liquid, which is then transferred to a heat exchanger. Finally, the transferred heat increases the temperature of water inside a storage cylinder, to provide hot water to housing. There are other applications for STE with higher temperature outputs however, this is beyond the scope of this thesis. STE is another case where capture, conversion and storage of the sun's energy requires separate components to function, meaning that STFs can provide a good alternative in a one-material capture, conversion and storage solution. [6]

Certain types of STF have been shown to equal, if not better, the theoretical energy densities of Li-ion batteries.[8] STFs could be a useful complementary technology to PV, due to their robustness,[9] controlled thicknesses and properties that can be tailored for different applications.[10] STFs offer a closed-cycle storage system that can be unimolecular, involving the absorption of a photon (small energy trigger) to produce heat. There are no chemicals used from or released into the environment following a complete cycle of an STF material, with no external batteries required to store converted energy. [6]

Solid-state STFs could be integrated into numerous technologies, including de-icing coatings, solar blankets, functional fibres, or any generic heating equipment.[11]

1.3. Energy Conversion and Storage in Metastable Molecules

To store solar energy in metastable bonds, STF materials utilise photoisomerism in photoswitches or in some cases reversible photochemical reactions.[6] Photoisomerism is the process of *reversibly* changing a chemical species to a different form (photoisomer) through absorption of light. This structural change can be through changes in isomers (isomeric) or through changes in bonding (photochemical). There are many examples of potential STF materials such as: stilbenes,[12] (fulvalene)tetracarbonyldiruthenium,[13] norbornadiene/quadricyclane (NBD/QC)[14] and azobenzenes.[15,16] In STF systems, a stable lower energy photoisomer or reactant is converted into a higher energy photoisomer or product.

The general process can be explained using the azobenzene system, as an example. Upon irradiation, *trans*-azobenzene changes colour, making it a photo chromophore. Equally, upon reconversion to the *trans* isomer from *cis*-azobenzene, the colour changes again therefore *trans* and *cis*-azobenzene make up a photochromic pair. Figure 1, shown below, is an energy diagram of the azobenzene system.[17]

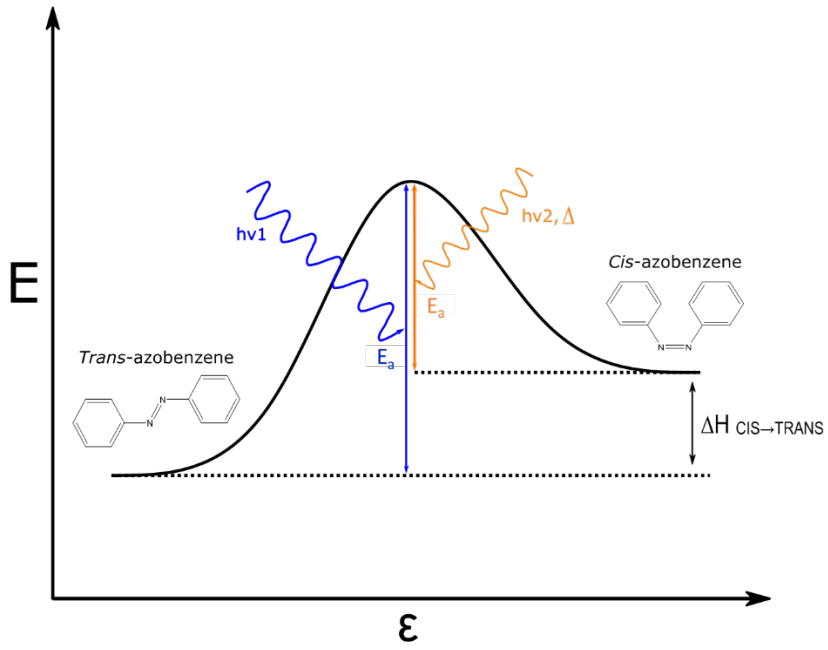

Figure 1: An energy level diagram of trans-azobenzene photoisomerising into the metastable cis-azobenzene conformation, via a transition state.[17,18] $\Delta H_{CIS \rightarrow TRANS}$ = Enthalpy of isomerisation of cis to trans, E_a = Activation energy of; the trans to cis isomerisation (blue), the cis to trans isomerisation (orange), $\mathcal{E}$ = Reaction progress.

Figure 1 shows the energy diagram of the *cis* and *trans*-azobenzene photochromic pair. Ultraviolet irradiation with the correct amount of energy to reach the activation energy ($E_{a\ trans \rightarrow cis}$) excites the more stable lower energy (*trans*-azobenzene) photoisomer into its

transition state, which then 'relaxes' into its metastable higher energy (*cis*-azobenzene) photoisomer. The energy difference between the two stable photoisomers ($\Delta H_{cis \rightarrow trans}$) is equivalent to the energy that is stored within the chemical bonds of the metastable isomer.[17,18]

1.3.1. UV-Vis Absorption Properties of Azobenzene

The UV-Vis spectrum for *trans*-azobenzene dissolved in methanol at 25 °C of a concentration of 2.5×10^{-3} M is shown below in Figure 2.

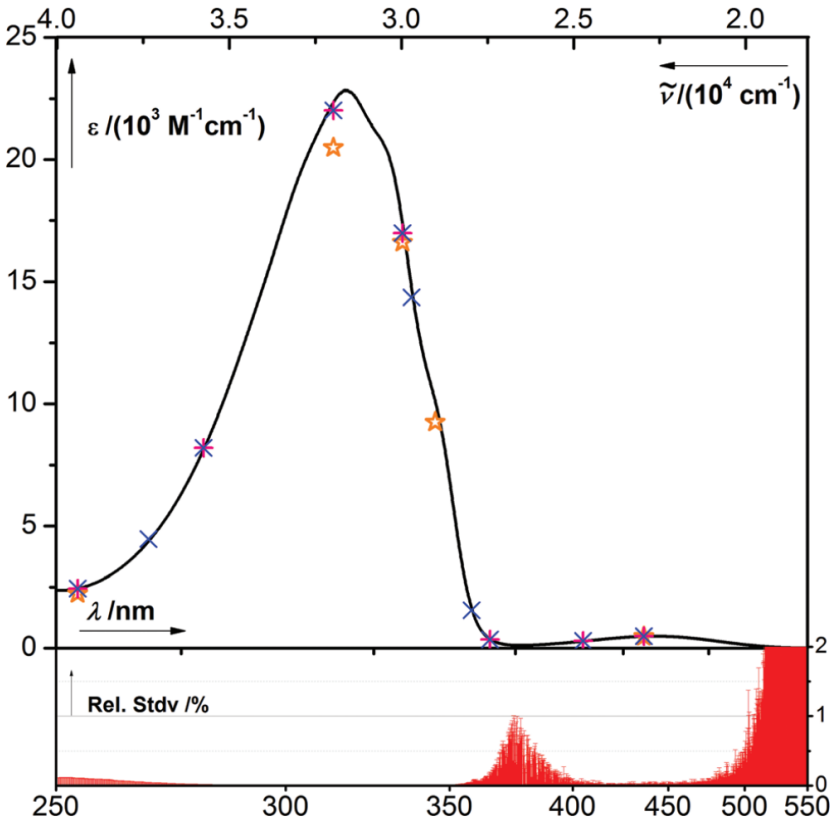

Figure 2: The molar absorption coefficients (ε_{trans}) of trans-azobenzene in methanol at 25 °C and their comparison with published data: orange stars,[19] pink plus sign,[20] and blue x.[21] Bottom: Relative standard deviations among independent samples in %. Reproduced from Photochem. Photobiol. Sci., 2017,16, 1749-1756.[22]

Figure 2 shows two main absorptions at 320 nm and 442 nm, attributed to the π→ π* and forbidden n→ π* electronic transitions respectively, with 320 nm being the wavelength with the highest level of absorption, known as the absorption maxima (λ_{max}).

The UV-Vis spectrum for *cis*-azobenzene dissolved in methanol at 35 °C is shown below in Figure 3.

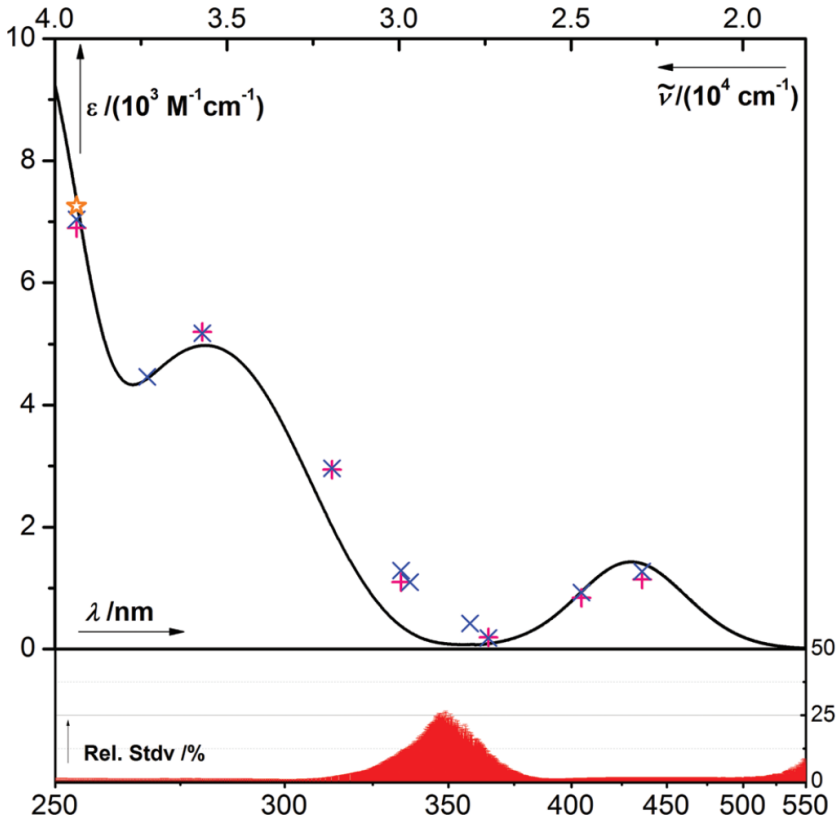

Figure 3: The molar absorption coefficients (ε_{cis}) of cis-azobenzene in methanol at 35 °C and comparison with published data: orange stars,[19] pink plus sign,[20] and blue x.[21] Bottom: Relative standard deviations among independent samples in %. Reproduced from Photochem. Photobiol. Sci., 2017,16, 1749-1756.[22]

Figure 3 shows two main absorptions at 282 nm (λ_{max}) and 430 nm, attributed to the π→ π* and forbidden n→ π* electronic transitions respectively. [22]

The Beer-Lambert Law, shown below, describes the intensity of absorption at a certain wavelength and its relationship with the concentration of material being investigated.

$$A = \varepsilon c l \quad (1)$$

Where, A = absorbance; ε = molar absorption coefficient (L mol^{-1} cm^{-1}); c = molar concentration (L mol^{-1}); l = path length (cm). The molar absorption coefficient (ε) is a measure of how strongly a material absorbs light of a certain wavelength, considering the concentration of material in solution.[23]

Both the *cis* and *trans* azobenzene isomers exhibit similar λ_{max} values. *Trans*-azobenzene exhibits absorptions at ~320 nm (ε = ~22000 L mol^{-1} cm^{-1}) and ~442 nm

(ε = ~400 L mol^{-} cm^{-1}).18 *Cis*-azobenzene exhibits absorptions at ~282 nm (ε = ~5000 L mol^{-1} cm^{-1}) and ~430 nm (ε = ~1500 L mol^{-1} cm^{-1}).[15] The isomerisation of azobenzene through irradiation at each wavelength of light is a balance between the rate of *trans* to *cis* isomerisation and vice-versa. At each wavelength, a steady state will be reached where the rate of *trans* to *cis* and *cis* to *trans* isomerisation are equal with the concentration of both isomer remaining constant. This is known as the photostationary state (PSS), at a given wavelength.[24]

The photostationary state can be described in the form of an equation shown below.

$$\mathrm{PSS} = \left(\frac{[Trans]}{[Cis]}\right)_{PSS} = \frac{\varepsilon_c(\varphi_{ct})}{\varepsilon_t(\varphi_{tc})}$$

Where, $\left(\frac{[Trans]}{[Cis]}\right)_{\mathrm{PSS}}$ is the ratio of the concentration of *cis* and *trans* isomers at the photostationary state, ε_c and ε_t are the molar absorption coefficients of *cis* and *trans* isomers respectively and (φ_{ct}) and (φ_{tc}) are the quantum yields of the *cis* to *trans* and *trans* to *cis* isomerisation, which describes the efficiency of the photoreactions at a certain wavelength.[24] The molar coefficients of these transitions are a consequence of symmetry allowed or forbidden transitions within the azobenzene isomers.

Table 1 shows the difference between molar absorption coefficients as a result of a transition being allowed or forbidden.

Table 1: Table showing the magnitude of molar absorption coefficients of trans and cis azobenzene isomers as a results of forbidden or allowed transitions. [15]

Azobenzene Isomer	**Transition symmetry** (orbitals involved, λ_{max})	**Transition state excitations**	**Allowed/ Forbidden Transition?**	**Molar absorption coefficient** (ε, L mol^{-1} cm^{-1})
Trans	**n→π***, ~450nm	$S_1(n\pi^*)$	Forbidden	~400
Cis	**n→π***, ~450nm	$S_1(n\pi^*)$	Forbidden	~1500
Trans	**π→π***, ~320nm	$S_2(\pi\pi^*)$	Allowed	~22000
Cis	**π→π***, ~270nm	$S_2(\pi\pi^*)$	Allowed	~5000
Cis	**π→π***, ~250nm	$S_2(\pi\pi^*)$	Allowed	~11000

As mentioned earlier, the *trans* and *cis* isomers of azobenzene both absorb at similar wavelengths, meaning that there will be a limit for the highest amount of *cis* azobenzene possible in solution. This limit is characterised by the ratio between *cis* to *trans* conversion

and *trans* to *cis* conversion. The higher conversion of *trans* to *cis* conversion, the higher the amount of *cis* azobenzene in solution following irradiation. This is highlighted further in Figure 4.

The ratio of molar absorption coefficients between *cis* and *trans* azobenzene isomers in methanol is shown below in Figure 4.

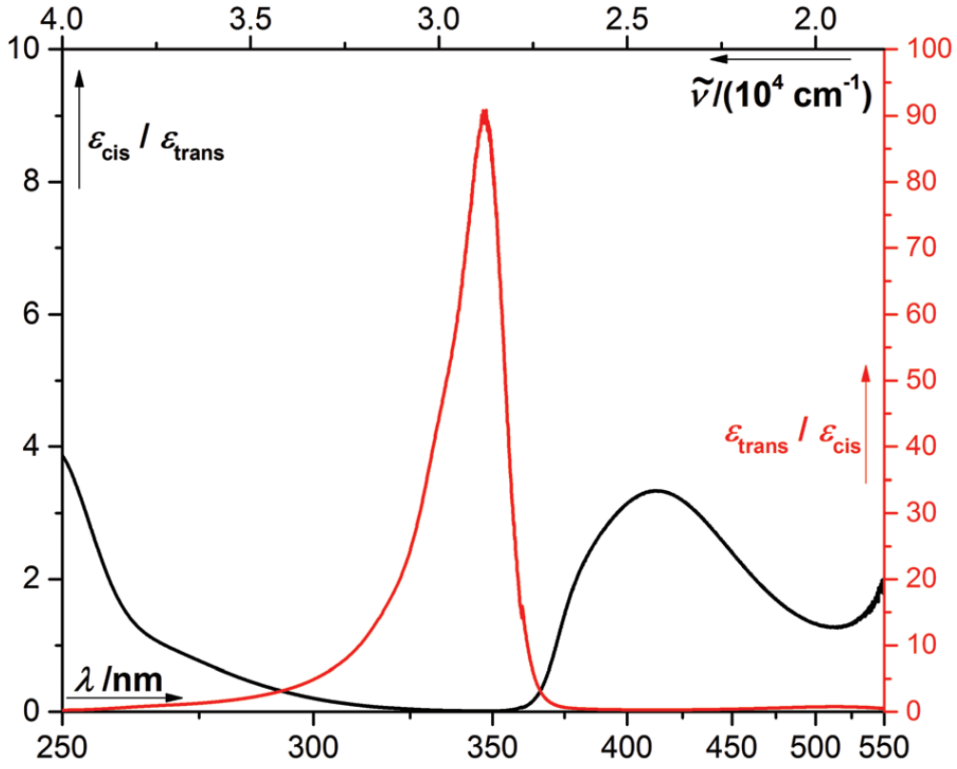

Figure 4: The ratio of molar absorption coefficients $\varepsilon_{cis}/\varepsilon_{trans}$ (black) and $\varepsilon_{trans}/\varepsilon_{cis}$ (red) of azobenzene in methanol. Reproduced from Photochem. Photobiol. Sci., 2017,16, 1749-1756. [22]

The highest ratio of $\varepsilon_{trans}/\varepsilon_{cis}$ is at a wavelength of 347 nm, showing an absorption of 91 times more than the *cis* azobenzene isomer. Despite this being an ideal wavelength to use for the highest *cis* PSS, irradiation of azobenzene at 365 nm results in a *cis* percentage PSS of ~78 %.[25] Both the *cis* and *trans* azobenzene isomers are able to absorb at a wavelength of 365 nm, however the amount of absorption in the *trans* isomer is still much higher than that of the *cis* azobenzene isomer. [22]

1.4. Desirable Solar Thermal Fuel Properties

There are a range of properties that are important for a material to function as a STF, accounting for both chemical and material considerations.[6] Equally, the properties of an STF material must be matched with the application that it is being used for, to increase the efficiency of the system.

1.4.1. High Energy and Power Densities

In the case of an azobenzene-based STF, the energy density of the material would relate directly to the density of azobenzene groups. This can be given gravimetrically as a molar-energy density and mass-energy density or volumetrically as a volumetric-energy density.[6] Referred to as the average power density delivered by a fully charged STF as it discharges, the power density or heat release rate can be given per mass.[6]

In general, STFs with high energy and power density are desirable. In some applications such as automotive/mobile technologies, it is desirable to have high gravimetric energy densities so that using the STF system comes with the minimal amount of added weight. For systems where space may be restricted, for example in phone batteries, volume-energy densities would be more suitable. In systems that are stationary, gravimetric and volumetric energy densities may not be as important as these can be less limited, but in these systems the amount of sunlight gained could be limited due to being kept at a fixed point. For the purposes of this project, energy densities will be given as mass-energy densities.

Molecular azobenzene has a gravimetric energy density of 269 J g^{-1}.[26] Kolpak *et al.* were among the first to show an appreciable energy difference between *cis* and *trans* isomers of azobenzene by adsorbing azobenzene unit onto a carbon nanotube surface. This energy density was investigated using computational calculations, with a high volumetric energy density of up to 690 W h L^{-1} using their azobenzene system, showing promise for the use of azobenzene molecules in solar thermal fuel systems. Gravimetric energy densities of that system were reported to be comparable to those achieved by Li-ion batteries, which can have upper limit energy density values of ~100-200 Wh kg^{-1} (360-720 J g^{-1}).4,27,8 This highlights that an azobenzene based STF system, is able to store a large amount of energy and could potentially, function as an solar thermal fuel with comparable energy densities to Li-ion batteries. However, azobenzene can only achieve this high energy density when in solution, with no energy storage possible in the solid state, meaning the actual energy density of the system is much lower.[28]

1.4.2. High Quantum Yield with a High Photostationary State

The efficiency of a photoreaction at a certain wavelength is known as the quantum yield. A quantum yield value of 1 would show a system where every photon absorbed results in an excitation of an STF material to its higher metastable state.[6] The quantum yield of molecular azobenzene is 0.49, which will be compared to other system later. (Section 1.5)[6]

Due to most STF systems having materials that photoisomerise and reconvert with the application of light, the two processes should not compete with each other to ensure the highest efficiency of each.[6] For example, any STF system where the ratio of $\varepsilon_{trans}/\varepsilon_{cis}$ is

high, there is little competition between absorption of the *trans* isomer and the *cis* isomer, with the *cis* isomer absorbing more than the *trans* isomer.

The photostationary state (PSS) is similar to the quantum yield and is a measure of the equilibrium between each photoisomer when excited by a light source as previously mentioned (Section 1.3.1). Complete conversion of *trans*→*cis* would be quoted as a PSS of 100 % (all *cis* isomer), whereas half conversion would be a PSS of 50 % (half *cis*, half *trans* isomer). A high PSS of between 70 - 100 % is a desirable STF property, this will be discussed frequently over the course of this thesis.

1.4.3. A Total Solar Irradiance Spectrum Match

The total solar irradiance is the measure of how much of a certain wavelength of photons reaches the earth from the sun. Each wavelength has a different intensity known as the spectral irradiance (W m^{-2} nm^{-1}). This is typically given within a range of 250-4000 nm but has been reduced to 250-2000 nm in the case of Figure 5 shown below.[29]

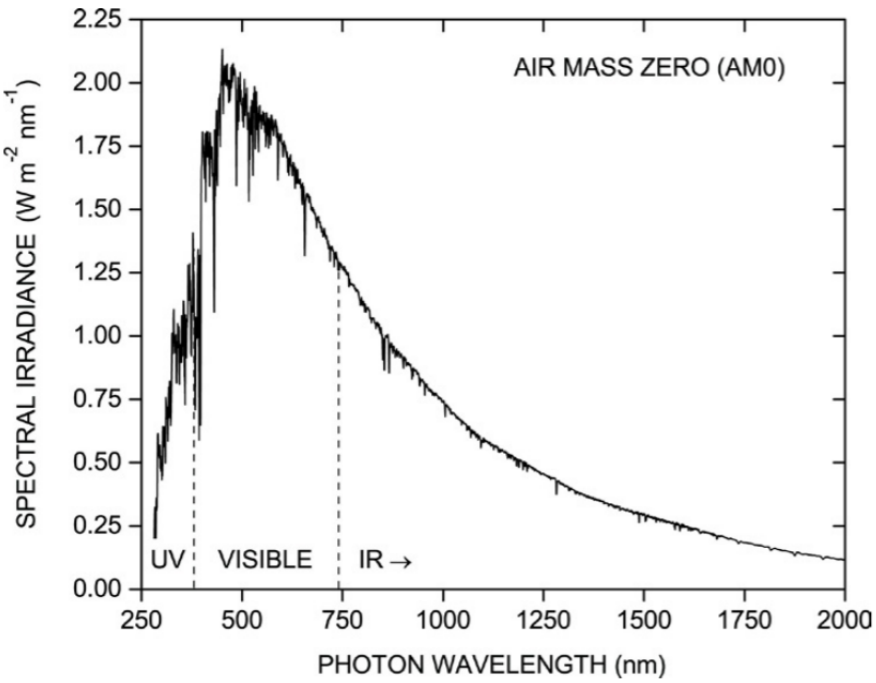

Figure 5: Air mass zero (AM0), solar spectrum showing the relative intensity of wavelengths reaching Earth from the sun in vacuum.[16]

The air mass zero (AM0) distribution of wavelength intensity from the sun is the distribution under a vacuum, without the effects of Earth's atmosphere.[29] Figure 5 shows the distribution with the sun directly above a specific position on earth (the 'Zenith' position), where the amount of sunlight will be at its highest.[29] In ideal circumstances, any solar technology would absorb in the range of ~400 - 625 nm where the intensity of sunlight is at its absolute highest, therefore, giving the solar technology the highest chance of sunlight absorption. The

consideration of Earth's atmosphere and how it affects wavelength distributions is beyond the scope of this project.

1.4.4. Long-Term Stability of the Metastable State and High Cycling Stability

The energy stored within the chemical bonds of the metastable isomer of an STF, can be released upon use of either a thermal (heat) or photochemical ($E_{a\ cis\rightarrow trans} < E_{a\ trans\rightarrow cis}$) trigger (in some cases only one of these), which excites the metastable higher energy (*cis*-azobenzene) photoisomer towards a transition state, enabling it to overcome the activation energy barrier to return to the more stable lower energy (*trans*-azobenzene) photoisomer. This then releases the energy stored in the chemical bonds of the metastable photoisomer exothermically as heat to the environment, as shown in Figure 1.[9]

A higher activation energy for the reconversion of *cis* to *trans* isomers in an STF material, means a higher stability of the *cis* isomer in its higher-energy metastable state. For many applications, STFs require a sufficiently high activation energy barrier such that, the thermal reconversion process can take place very slowly, meaning energy can be stored for long periods of days or even months, making them more promising for seasonal and intermittent use.[6] This can be measured as the half-life of an STF material, describing the stability of the metastable state upon excitation of the STF material.

Also, to make them viable for daily use, the STF system must be cyclable, with a high cycling stability, meaning the material maintains the same energy and power density over lots of charge and discharge cycles.[6] The activation energy of *cis*-azobenzene being ~521 J g^{-1} in solution, allows for a good thermal stability of *cis*-azobenzene and a half-life of 2 days in solution.[15]

1.4.5. Sustainability Considerations

The chemical system used for any STF material should be commercially viable, scalable, sustainable, easy to produce, easy to store and non-toxic. Real-world applications require well-known chemistries and easily available resources, in comparison to complex systems with an advanced or costly synthesis which are likely to increase the cost of an end product therefore, likely to make the product less competitive.[6]

1.5. Review of Previous Photoswitches

As mentioned earlier, there are numerous examples of STF materials, all with their own advantages and disadvantages. Some common STF materials are listed below.

1.5.1. Norbornadiene to Quadricyclane Solar Thermal Fuels

The norbornadiene to quadricyclane system has been shown to have a comparably-high energy density of ~1090 J g^{-1} in its most basic form by Kutal *et al.*, [30,31,32] shown in Figure 6 below.

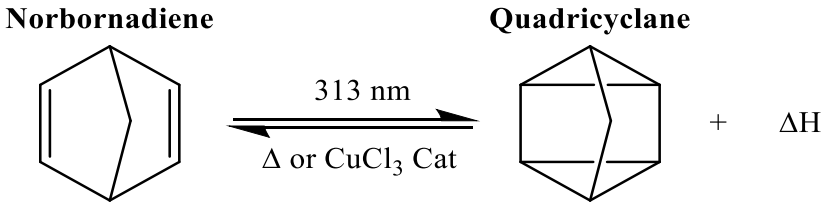

Figure 6: The photochromic reaction of norbornadiene to quadricyclane. Thermal energy (Δ), catalysis (Cat). [31]

Figure 6 shows the reversible conversion of norbornadiene to quadricyclane via thermal excitation or use of a photosensitiser/catalyst. The quantum yield of the system is said to be 0.3-0.4 in chloroform, a similar quantum yield to that of azobenzene.[32] The norbornadiene to quadricyclane system is described as having a relatively cost effective synthesis, requiring only acetylene and cyclopentadiene, therefore suggesting that it is a cost effective STF. This system is also described as having a high thermal stability.[31]

Unfortunately, the norbornadiene to quadricyclane system does not show a good total solar irradiance spectrum match, with no norbornadiene absorption beyond 295 nm, meaning that the system requires a catalyst to achieve a high enough percentage of the higher energy quadricyclane. Irradiation at 313 nm can only produce quadricyclane with the use of a $CuCl_3$ catalyst thus, the potential as a closed-cycle system is decreased with the cost of the system increased.[31] It is noted that, the norbornadiene to quadricyclane STF system can achieve a ~90 % norbornadiene to quadricyclane conversion, due to the reverse reaction of quadricyclane to norbornadiene not being catalysed by the $CuCl_3$ catalyst.

Most importantly however, the norbornadiene to quadricyclane system cannot isomerise in the solid state therefore, the system must be dissolved in a solvent therefore, decreasing the actual energy density of the system.

1.5.2. Fulvalene Dimetal Solar Thermal Fuels

The fulvalene diruthenium system has been shown to have a low energy density of ~187 J g^{-1} compared to the norbornadiene to quadricyclane system.[33]

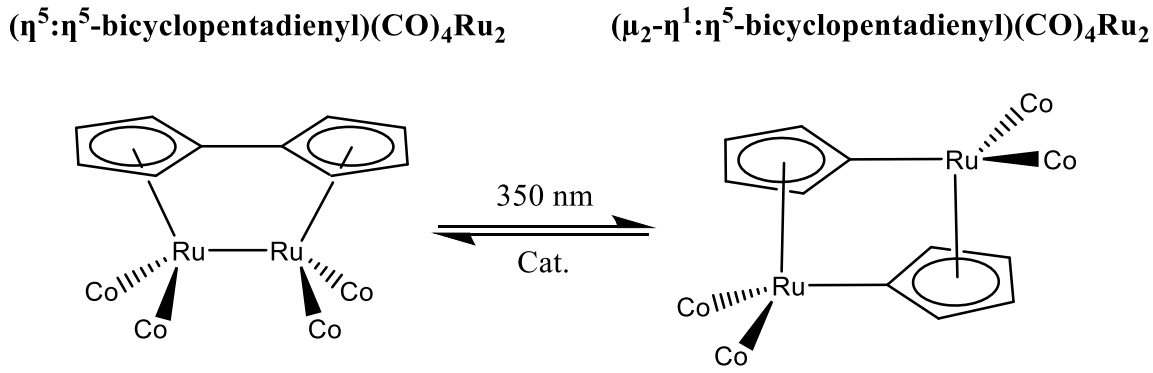

Figure 7: The photochromic reaction of (η^5:η^5-bicyclopentadienyl)$(CO)_4Ru_2$ to (μ_2-η^1:η^5-bicyclopentadienyl)$(CO)_4Ru_2$. [33]

Figure 7 shows the (η^5:η^5-bicyclopentadienyl)$(CO)_4Ru_2$ photoisomer being converted to an energetically higher, metastable (μ_2-η^1:η^5-bicyclopentadienyl)$(CO)_4Ru_2$ photoisomer. The fulvalene dimetal system also shows an inferior quantum yield to the norbornadiene to quadricyclane system with an average quantum yield at 350 nm of 0.15.[34]

In contrast to the norbornadiene to quadricyclane system, the fulvalene dimetal system shows a good total solar irradiance spectrum match with the low energy isomer showing absorption at 350 nm.[33] As well as this, the fulvalene dimetal system has a strong thermal stability due to the strength of its internal bonds and high steric hindrance, with an activation energy of ~282 J g^{-1}.9,[35] However, due to the use of ruthenium, the cost of the fulvalene dimetal system is high, as well as having a very high molecular weight of 442 g mol^{-1} with alternative metals showing decreased energy densities.[33] Finally, the fulvalene dimetal system also suffers from being unable to isomerise without the use of solvents therefore, the actual energy density of this system is lower than those reported.

1.5.3. Stilbene

The stilbene system offers a low molecular weight of ~180 g mol^{-1} compared to the norbornadiene to quadricyclane and fulvalene dimetal systems, making it one of the lightest STF systems. They are well-studied and have a relatively simple synthesis. The stilbene photoreaction is shown in Figure 8 below.

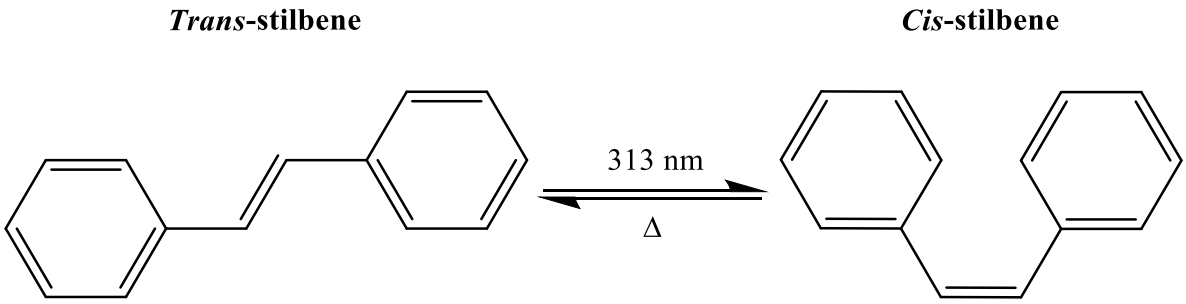

Figure 8: The photochromic reaction of trans-stilbene to cis-stilbene. Thermal energy (Δ).[36]

Figure 8 shows the reversible photoisomerisation of *trans* to *cis* stilbene.[36] Despite its low molecular weight, the stilbene reverse-isomerisation is not able to store as much energy in its metastable state as its competitors and therefore, has a low energy density of 27.7 J g^{-1} which is much lower than the norbornadiene to quadricyclane, fulvalene dimetal and azobenzene systems, therefore, has not been considered as a viable STF material.[36]

The *trans* to *cis* quantum yield of stilbene is reported as 0.50 at a temperature of 25 °C, a relatively high value compared to the norbornadiene to quadricyclane and fulvalene dimetal systems.[37] Despite the low energy density, the stilbene system does offer a good total solar irradiance spectrum match, with the lower energy *trans* photoisomer absorbing at 313 nm.[37] The stilbene system is also unable to photoisomerise without the use of a solvent and therefore, the energy density offered by the system is even lower than reported.

1.6. Molecular Azobenzene Photoswitches

Azobenzene is considered a well-known molecular photoswitch that exists in two isomeric states.[16] The photoisomerisation of *trans* to *cis* azobenzene is shown below in Figure 9.

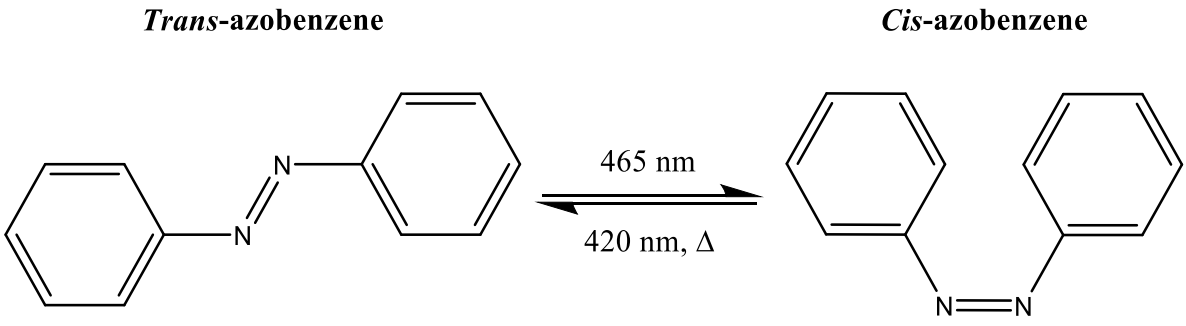

Figure 9: The photochromic reaction of trans-azobenzene to cis-azobenzene. Photon energy (hv), thermal energy (Δ).[26]

The half-life of the excited *cis*-azobenzene in solution and at room temperature is quoted as being 2 days.[15] This would be suitable for any application intended for daily repeat uses. The excitation wavelengths mentioned in section 1.3.1, facile synthesis, moderate half-life, highly

repeatable photoisomerisation cyclability and promising energy densities suggest this is the reason why azobenzene derivatives have been posed as one of the most promising STF materials. The range of excitation wavelengths are perhaps the largest benefit of the azobenzene STF with a good total solar irradiance spectrum overlap (between 350-625 nm), these wavelengths can be tuned to suit the needs of an application by introducing electron donating or withdrawing groups to the system.[3]

1.7. Azobenzene Based Solar Thermal Fuels

There has been a wealth of research into the reasonably large enthalpy of isomerisation for azobenzene. Kolpak *et al.* calculated a theoretical value of 260.0 J g^{-1} using DFT calculation.[8] An accurately determined experimental value of 259.6 J g^{-1} was measured by Cammenga *et al.* using differential scanning calorimetry,[57] which is sufficiently accurate and will be used for this thesis going forward. This energy density has later been followed with some liquid-state azobenzene derivatives with a branched 2-ethylhexyl group added via an ester linkage to the 4-position of the azobenzene chromophore. Isomerisation enthalpies of 192.1 J g^{-1} with a cis percentage of 68 % at an excitation wavelength of 365 nm were obtained, meaning 285.4 J g^{-1} when converted to 100 % cis percentage by Masatuni *et al*.[28] This value also has the added benefit of not requiring a solvent for isomerisation therefore, the energy density obtained is exactly that of the system rather than being decreased by the presence of a solvent.

Due to the promising properties of azobenzene mentioned earlier, there has been recent interest in the development of azobenzene-based STFs. STFs can exist in two different states, the liquid state and the solid state.

Unfortunately, the basic azobenzene system has a major flaw which is that it cannot isomerise in the solid state. The photoisomerisation of azobenzene requires a relatively large geometrical structure change that is prohibited in a crystal lattice.[38] Liquid state STFs perform well, due to providing the additional space required for structural changes that need to take place in the material upon excitation and relaxation. A strategy to combat this is to use systems which immobilise azobenzene units but allow enough steric freedom for isomerisation to occur.

1.7.1. Solid-State Templated Azobenzene STFs

Due to the practicality of azobenzene as a solid-state STF and its promising energy densities, a number of people have attempted to overcome the problem of azobenzene not switching in the solid-state by tethering it to a rigid architecture. Feng *et al.* produced closely packed, azobenzene-functionalised, multi walled carbon nanotubes (CNT).[39] They also showed that reversible photoinduced switching of the azobenzene isomers could take place

whilst adsorbed onto the multi walled carbon nanotube surface.[39] Simmons *et al.* observed that covalently attached azobenzene molecules aligned parallel to the long axis of a single walled carbon nanotube,[40] as well as showing that photoinduced switching of azobenzene isomers could take place whilst adsorbed onto the single walled carbon nanotube surface.[40] Neither Feng *et al*. or Simmons *et al*. mentioned the energy densities of these architectures. However, these papers did show that adsorbing azobenzenes onto carbon nanotubes (CNTs) was a method of immobilizing azobenzenes whilst also allowing them to photoisomerise.

Kolpak *et al.* used this knowledge to carry out their own research into azobenzene functionalised CNTs. They noted the potential for an increased volume of photoactive azobenzene groups due to the close packed and highly ordered CNT substrate; as well as the close proximity of the well-ordered photoactive azobenzene molecules compared to that of molecules free in solution, allowing for manipulation of inter and intramolecular interactions.[8] The same work also emphasised the importance of hydrogen bonds by calculating the energy densities of substituted azobenzene-functionalised single walled carbon nanotubes, with the calculations showing that, the energy density increased as a result of close packing, hydrogen bonding and orientation.[8] The azobenzene-single walled carbon nanotubes can be crystalline-like in solution allowing for greater packing interactions, allowing Kolpak *et al.* to predict a volumetric-energy density of up to 690 W h L^{-1} by using density functional theory.[8]

Inspired by this, Kucharski *et al.* carried out calculations on azobenzene-functionalised, single walled carbon nanotubes offering a theoretical azobenzene functionalisation density of 1/8 (1 azobenzene per 8 single-walled carbon nanotube carbon atoms).[41] An example of the azobenzene-single walled carbon nanotubes used in the Kucharski *et al.* report is shown in Figure 10 below.

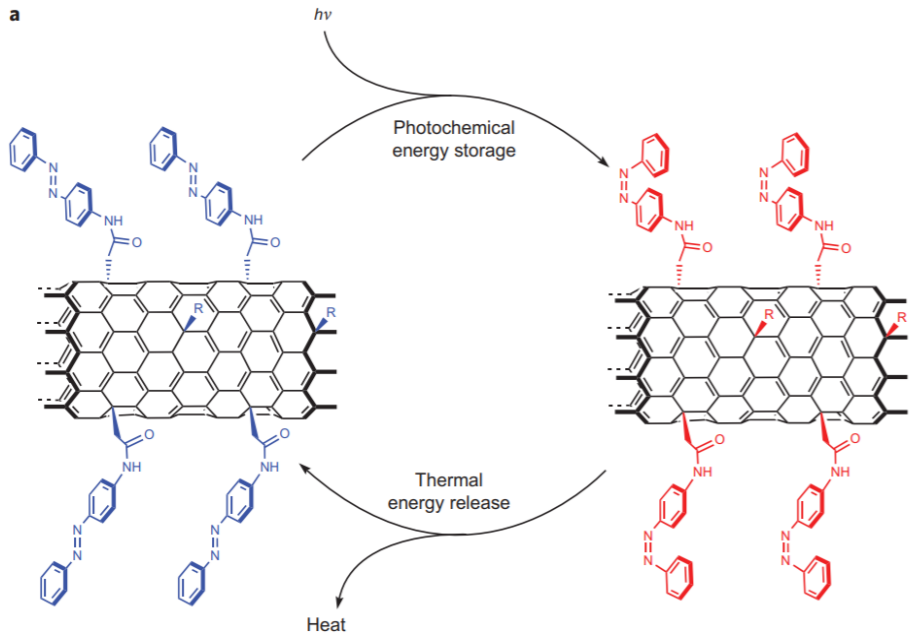

Figure *10: Reactions scheme showing the charging and discharging of azobenzene-single walled carbon nanotubes, reproduced from T. J. Kucharski, N. Ferralis, A. M. Kolpak, J. O. Zheng, D. G. Nocera and J. C. Grossman, Nature Chemistry, 2014, 6, 441–447.*[41]

Kucharski *et al.* was able to synthesise azobenzene-functionalised, single-walled carbon nanotubes with a maximum functionalisation density of ~1/18 (1 azobenzene per 18 single-walled carbon nanotube carbon atoms).[41] Dispersed in acetonitrile, this azobenzene functionalised single walled carbon nanotube had an absorbance band at ~350 nm, showing a good total solar irradiance spectrum match as well as showing an energy density of 90 ± 3 kJ mol^{-1}.[41] Intermolecular interactions between azobenzene-single walled carbon nanotubes can be increased by removal of the solvent, thus bundling the systems and inhibiting isomerisation. The energy density of the solid-state azobenzene-single walled carbon nanotube was measured as 120 kJ mol^{-1}.[41] This study showed that intermolecular interactions can have a positive effect on the energy densities of solar thermal fuel systems and the azobenzene-single walled carbon nanotube prototypes were a good proof of concept based on earlier calculations shown in the theoretical report from Kolpak *et al.* It also showed that immobilising azobenzene units onto a CNT substrate, allowed the reverse isomerisation of *cis* to *trans* azobenzene pendant units to take place.

Despite the promising energy densities shown by single walled carbon nanotubes and adjacent studies into reduced graphene oxide templating, controlling the precise locations and functionalisation densities of these systems is synthetically challenging. Therefore, other options should still be considered.[28] Kimizuka *et al.* recognised that, despite the high energy densities produced by the solid-state azobenzene-functionalised single walled carbon nanotubes in the Kucharski *et al.* report, the photoactive moieties (azobenzene pendant

groups) still required the use of dilute solvents to photoisomerise into the (charged) *cis* state, then the system was dried followed by discharging into the *trans* state.[41,28]

More recently a bridge between solid-state and liquid-state azobenzene-based STFs has been investigated in ionic liquids. Ishiba *et al.* investigated ionic crystals (ICs) formed from azobenzene derivatives that were able to photoliquify into ionic liquids (ILs).[42] They demonstrated that the phase transition between the IL and the IC state resulted in a large energy release of 97.1 kJ mol^{-1}. A phase transition between solid and liquid states, however, could prove practically difficult in certain applications.

1.7.2. Utilising Phase Change Materials for Higher Energy Densities

Systems utilising phase changes could be used to increase the overall energy density of an STF material. In Figure 1 an energy level diagram for azobenzene during isomerisation was shown. The mechanism of reaching the higher energy metastable state remains the same however, upon discharging, the material crystallises, creating a larger energy gap between the metastable state of the material and its ground state. The recrystallisation of the polymer would create an additional exotherm to the one generated by isomerisation. This is illustrated in Figure 11 below.[43]

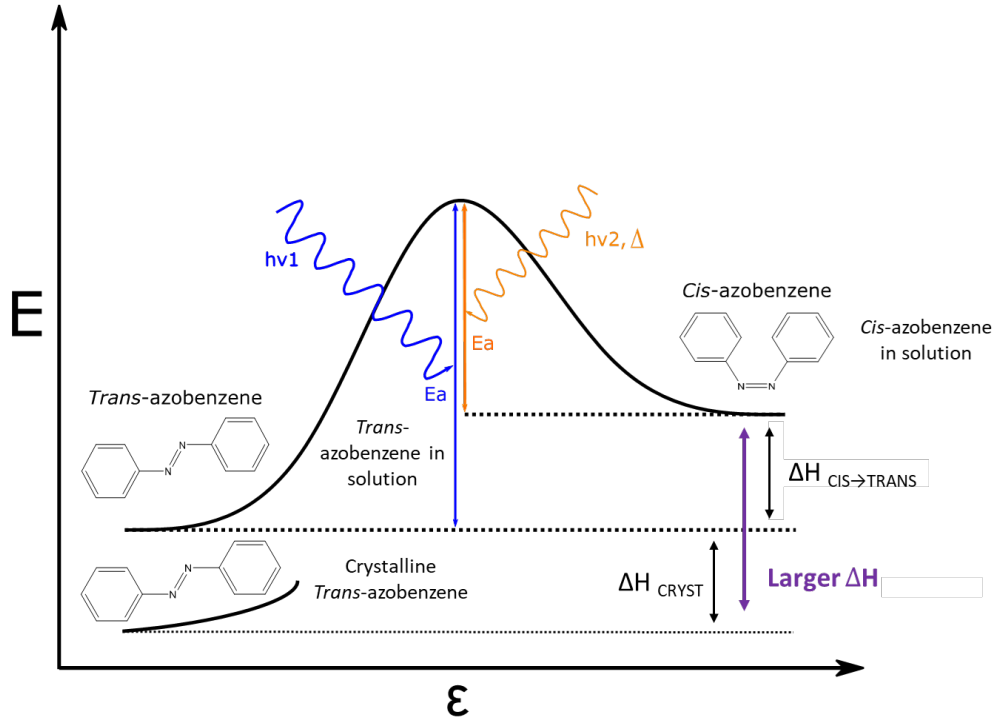

Figure 11: An energy level diagram of trans-azobenzene photoisomerising into the metastable cis-azobenzene conformation via a transition state, showing the lower energy state of trans-azobenzene in a crystalline state.[16,17] $\Delta H_{CIS \rightarrow TRANS}$ = Enthalpy of isomerisation of cis to trans, ΔH_{CRYST} = Enthalpy of crystallisation, E_a = Activation energy of; the trans to cis isomerisation (blue), the cis to trans isomerisation (orange), $\mathcal{E}$ = Reaction progress.

The main problem with utilising this additional energy is overcoming the lattice energy density via irradiation – a balance must be struck between the level of crystallisation in the lower energy ground state and the ability of the solar thermal fuel material to be charged following a photo-induced phase change.[43] This balance can be avoided by dissolving the material in solvents however, using solvents massively decreases the actual energy density of solar thermal fuel systems.[28] Therefore, using azobenzene-based materials that can tailor their levels of crystallinity, as well as keeping their effective photoswitch properties, is the next step in attempting to increase the energy densities in solar thermal fuels.

Polymers can crystallise depending on the structure of their backbone and any functional groups added as pendant units. They are a highly tuneable material that can display any level of crystallinity aside from 100%, a major factor in tuning polymer crystallinity involves the tacticity of the polymer, this will be mentioned later.

1.7.3. Azobenzene Based Solid-State Polymer STFs

Following the earlier azobenzene-functionalised single walled carbon nanotubes work by Kucharski *et al.* and conditions for future solid-state STFs, Zhitormirsky *et al.* noted that a rich monomer and polymer backbone chemistry would allow for tailoring of the solid-state properties and scaling of a polymer. Their initial polymer system was simple however, would allow for many different derivatives, to tune the solid-state polymer properties. The polymer system Zhitormirsky *et al.* chose is shown below in Figure 12.[9]

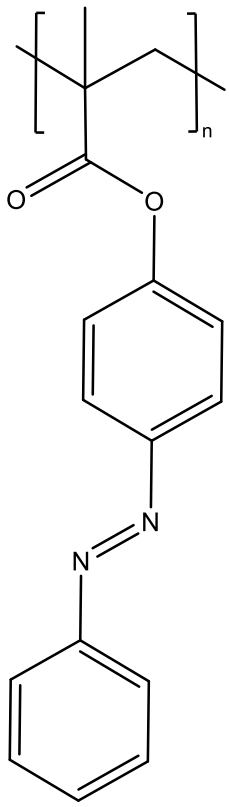

Figure *12: Azobenzene based homopolymer used by Zhitormirsky et al.*[9]

Figure 12 shows the polymer that Zhitormirsky *et al.* used to create their potential solid-state STF. They generated an azobenzene-based polymer consisting of azobenzene pendant units as the polymer side chains, a 2-step procedure which was reported as possibly allowing easy scalability and cheap production.[9]

Just as with previous azobenzene systems, the *trans*-azobenzene will be excited into the higher-energy metastable *cis*-azobenzene state, storing energy in chemical bonds, which can be released upon application of a thermal or photochemical trigger.

The conversion of monomer to polymer showed very little to no change in absorption wavelength and only a minor decrease in the intensity of the azobenzene absorption peak at ~320 nm, shown in Figure 13 below.

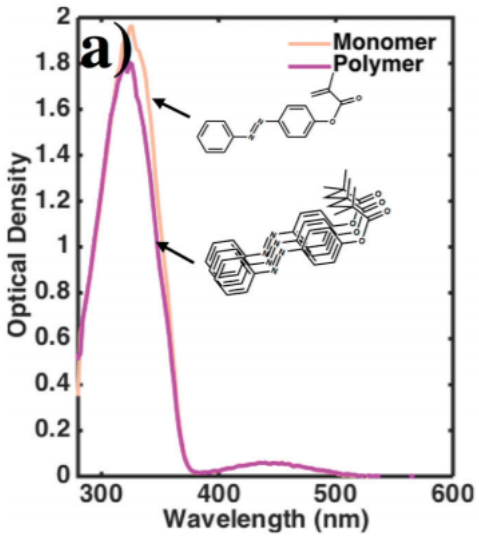

Figure 13: Solution absorption spectra comparing the azobenzene monomer and solid-state STF polymer.[9] *Picture taken from D. Zhitomirsky, E. Cho and J. C. Grossman, Advanced Energy Materials, 2016, 6, 1–8.*

The Zhitormirsky *et al.* solid-state polymer system displayed a moderate room temperature half-life of 55 ± 1 hours.[9] This timescale would be device specific and the half-life properties of an azobenzene system could be altered through derivatives, by adding different functional groups to the monomer.

A thin-film of the Zhitormirsky *et al.* solid-state STF was generated via spin-coating, they produced a solar thermal energy capacitor to allow charging and discharging. It was concluded that it is possible to produce highly uniform, smooth and crack-free thin films of the solid-state STF. The Zhitormirsky *et al.* polymer system had a reported energy density of 104.4 ± 7.2 J g^{-1} when charged in a solution of toluene and 93.6 ± 3.6 J g^{-1} when charged in the solid state, redissolved into solution and then dried within a DSC pan. The decrease in energy density in the solid state can be due to a number of effects; a variation in the quantum yield, highest absorption wavelength or changes to thermal reversion barriers.[9]

The large amount of synthetic diversity of the azobenzene system as well as the promise of solid-state STF led Zhitormirsky *et al.* to conclude that solid-state STF systems present a tremendously attractive avenue for, renewable energy storage and heat release.[9] This study, however, did not discuss the structure, local ordering, the morphology of the polymer or even the glass transition temperature of the polymer.

Towards this end, Jeong *et al.* investigated the morphological properties of azobenzene-based polymers via differing the processing solvent and investigating polymer-solvent interactions in the solid-state.[44] To test this, Jeong *et al.* used a syndiotactic-rich polymethylmethacrylate (PMMA) based azobenzene-polymer, using this polymer allowed them to achieve similar distances between azobenzene units to those in azobenzene-

functionalised single wall carbon nanotubes.[44] The group however, did not focus much on the glass transition temperature of the polymer.[44,45]

1.7.4. Solvent Effects on Energy Densities of Azobenzene-Based Polymer STFs

Jeong *et al.* also found that when solid-state azobenzene-based polymers were obtained by dissolving the polymer in THF and DCM and then removing these solvents via evaporation, tetrahydrofuran (THF) from the sample, the energy densities achieved were significantly and consistently higher than when dichloromethane (DCM) was used, with the average energy densities achieved for samples dried from DCM being 110 ± 25 J g^{-1} and those dried from THF being reportedly 510 ± 115 J g^{-1}. They produced differential scanning calorimetry spectra to display exotherms for both solvents, shown in Figure 14a below.[44]

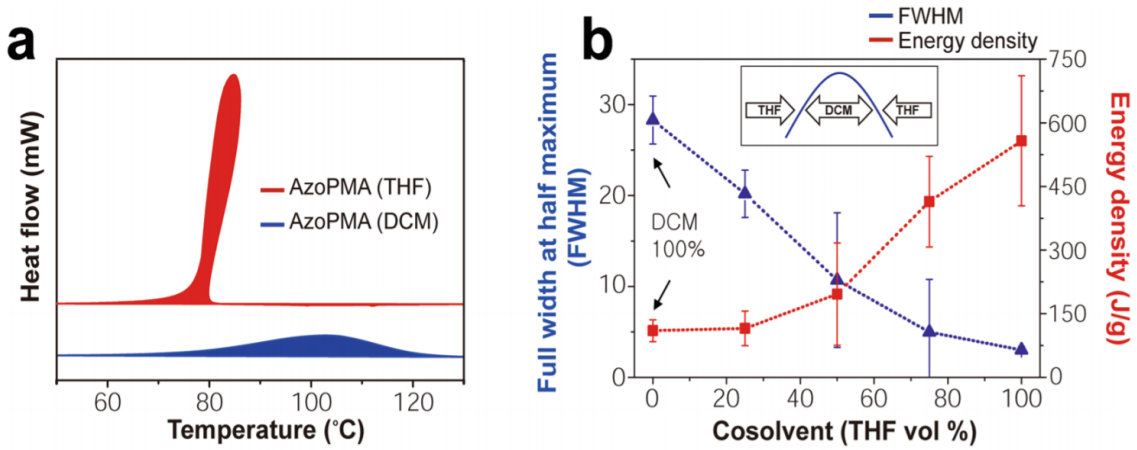

Figure 14: a) First heating cycle DSC exotherms of cis-azobenzene-based polymer when dried from THF (red) and DCM (blue). B) Full width at half maximum of energy density cosolvent tests starting from 100% DCM:0% THF to 0% DCM:100% THF. Pictures taken from S. P. Jeong, L. A. Renna, C. J. Boyle, H. S. Kwak, E. Harder, W. Damm and D. Venkataraman, Scientific Reports, 2017, 7, 1–12.[44]

Figure 14a shows the first heating cycle of a irradiated-azobenzene-based polymer sample when dried from THF and DCM. Figure 14b shows how the energy densities of the azobenzene-based polymer increases as the percentage of THF increases in tests using differing amounts of DCM and THF together.[44] This data allowed Jeong *et al.* to conclude that the processing solvent used for the syndiotactic azobenzene-based polymers is important for achieving high energy densities.[44]

The Jeong group used wide angle x-ray scattering (WAXS) to determine the crystallinity of the polymer and also the distance between azobenzene moieties. These distances are represented in Figure 15.

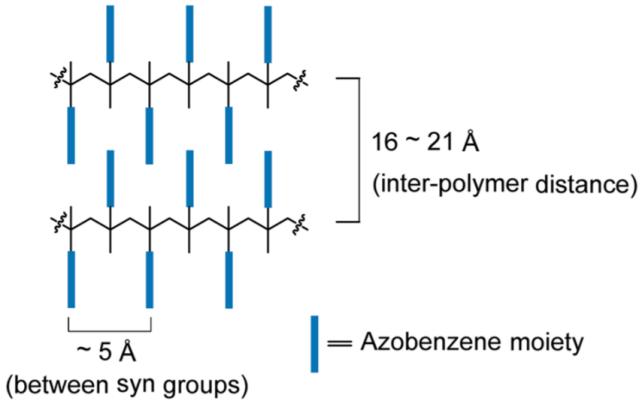

Figure 15: Graphical representation of the azobenzene polymer morphology, displaying the inter-polymer distance and distance between azobenzene moieties.[44]

The group concluded that using DCM caused the inter-polymer distance to decrease when in the *cis*-state therefore, indicating an increased polymer packing of polymer chains.[44] Following this, the effect of the dipole moments of the *cis* and *trans* polymer states was explored, using Kelvin force probe microscopy. This would allow Jeong *et al.* to see any orientational differences in films dried from DCM or THF. The group found that the potential energy surfaces of the films differed, this is shown in Figure 16.

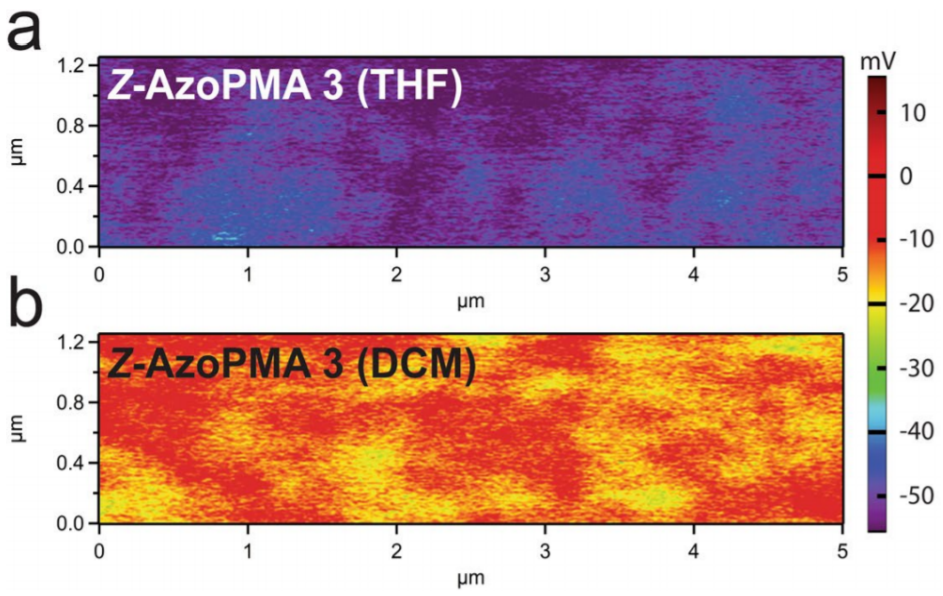

Figure 16: Surface potential spectra of the azobenzene-based polymer when dried from a) THF b) DCM.[44]

Figure 16 shows the more-negative surface potentials of the azobenzene-based polymers dried from THF. Due to the *cis-trans* isomer ratio being similar in both films, the group concluded that the physical structure of the films is different. The group postulated that the difference in potential energies was down to opposing dipole moments being cancelled out in the more disorderly and closely packed azobenzene-based polymer dried from DCM. The

polymer dried from THF reported more orientations perpendicular to the surface. This led Jeong *et al.* to speculate that the lower energy densities achieved in films dried from DCM are due to the more compact nature of the solid-state polymer, leading to decreased room for the physical geometric changes during isomerisation.[44] This could suggest the presence of more ordered polymer strands.

The polymer-solvent interaction parameter (χ) for PMMA-DCM is -0.15 to 0.09, and 0.44 to 0.46 for PMMA-THF, the lower the value of χ, the more interaction there is with the polymer backbone. The increased packing of films dried from DCM is likely caused by the increased PMMA-backbone interaction with DCM. This increased affinity for the PMMA backbone leads to less solvation of the *cis*-azobenzene dipole, which causes aggregation in solution thus, a more disordered arrangement of azobenzene moieties and less free volume available for efficient π- π stacking.[44]

Jeong *et al.* concluded that the processing solvent used in azobenzene-based polymers should solvate the dipole moment formed in the *cis* state of the azobenzene pendant group, in order to reduce the aggregation of the polymer in solution and allow for efficient π- π stacking.[44] This study however, does not investigate the exact polymer structure after using the different solvents as wide angle x-ray scattering only gives vague information regarding packing in the solid state.

The results obtained from the Jeong *et al.* paper, could be the result of additional contributions through crystallisation of that polymer systems, as a result of different polymer environments in different solvents. Using further DSC investigations and other techniques such as solid-state NMR (SSNMR) and optical microscopy (OM) may give more information towards gaining a greater understanding of the polymer morphology in similar polymer systems to those researched in the paper by Jeong *et al*.

Ultimately, the polymers mentioned in the Jeong paper are still unable to be charged in the solid state due to the polymers being too crystalline.

1.8. Project Aims

Due to the inability of currently designed azobenzene based polymers to photoisomerise in the solid state, this project aims to make an azobenzene based PMMA polymer that can be charged in the solid state. Tuning the level of crystallinity contributions to the overall energy density of the polymer solar thermal fuel system, via close packing or π-π stackings as a result of polymer tacticity will also be discussed.

The project will aim to cover a small molecular weight system known to isomerise in solution but also that is known to crystallise in the solid state. The energy storage properties and any

crystallisation contributions to the overall energy density in the smaller molecular weight system, will be explored. The project will also aim to synthesise an azobenzene-based PMMA polymer by free radical polymerisation for its structure, solid state morphology and energy storage properties in solution and in the solid state.

Following this, the project will then explore any additional energy density contributions in the azobenzene-based polymer system due to solvent differences or differences in the level of crystallinity in the system.

2. Synthesis and Experimental Section

2.1. General Information

2.1.1. Chemicals Information

All reagents and solvents used in monomer synthesis were available commercially and used as supplied, without further purification. Accurate masses were obtained using a Mettler Toledo XPE205 DeltaRange balance.

2.1.2. Chromatography Methods

The monitoring of reactions was carried out by thin-layer chromatography (TLC) using Merck silica gel 60 F254 plates (0.25 mm). TLC plates were visualized using UV light (254 nm). Purification of the synthesised monomer was carried out by using Flash column chromatography using silica gel (VWR) 40-63 μm in collaboration with a 17.5:1 (heptane : ethyl acetate) solvent system specified in the procedure, utilising a dry loading method.

2.1.3. Standard Solvent Removal Methods

The products of monomer and polymer synthesis were dried using high vacuum lines. Reactions using anhydrous conditions or solvents were conducted in oven-dried glassware under an inert atmosphere of argon. The removal of solvents during experiments was carried out by using a combination of N_2 blowing and the use of high vacuum lines, with only timing alterations. Specific conditions for individual experiments will be discussed below.

2.2. Nuclear Magnetic Resonance (NMR)

Solution state NMR spectra were recorded using a Bruker Fourier 400 (400 MHz) NMR spectrometer at 298 K with TMS as the reference. The NMR spectra were viewed using TopSpin NMR software and plotted using Origin.

Solid state NMR (SSNMR) spectra were recorded using a Bruker Fourier 400 (400 MHz) NMR spectrometer at 298 K with TMS as the reference. The SSNMR spectra were viewed using TopSpin NMR software and plotted using Origin.

2.3. Molecular Weight Determination

Molecular weights and molecular weight distributions of the synthesised polymer were determined by gel permeation chromatography (GPC). Analysis was performed using a GPC system comprising of a Shimadzu DGU-20A5R degassing unit, an LC-20AD pump, a SIL-20AHT autosampler, a CTO-20AC column oven, and an RID-20A refractive index detector. Analysis was performed at 40 °C using THF (Chromatography GPC Grade, Fisher Scientific) at a flow rate of 1.0 mL/min with a Phenomenex Phenogel Linear (2) column (5.0 um, 7.8 × 300 mm) fitted with a Phenomenex Security Guard Cartridge (GPC, 4 × 3 mm).

Samples were dissolved in mobile phase at an approximate concentration of 1 mg/mL and allowed to dissolve over night before filtration through syringe filter (0.2 µm). An injection volume of 100 µL was used for both samples and standards. Data was calculated by column calibration using polystyrene standards (Agilent Technologies) dissolved in THF to generate calibration curves.

GPC revealed values for the number average molecular weight (M_n): 5526 and the weight average molecular weight (M_w): 25477 for polymer P1. Using the equation below, it was calculated that P1 had an average of 22 repeat units per polymer:

$$\text{Number of repeat units} = \frac{\text{M}_\text{n}}{\text{M}_\text{r} \text{ of 1 polymer repeat unit}}$$

$$\text{Number of repeat units} = \frac{5526}{252.3} = 21.9$$

2.4. UV-Vis Spectroscopy

UV-vis measurements were carried out using a Cary 60, in a 1 cm path length quartz cuvette. The UV-vis spectra were collected between 200 nm – 800 nm at 200 nm min^{-1} using Cary WinUV software. Samples were prepared in DCM, to a concentration of 4.69×10^{-3} g L^{-1} for monomer M1 and 5.08×10^{-3} g L^{-1} for polymer P1. Precise concentrations were obtained by weighing the 206 sample on a Mettler Toledo XPE205 DeltaRange balance and diluting using volumetric flasks with an error of $\pm 0.015 \times 10^{-4}$ g L^{-1}.

UV-vis spectra of an irradiated sample were obtained from samples irradiated at 365 nm in DCM solution for a period 1 hour at a distance of 10 cm from the light source. The light source was set to 50 % intensity. Cuvettes were sealed with PTFE stoppers to prevent solvent evaporation during irradiation, with cuvettes and samples shielded from external light sources during exposure, transit, and measurement by use of aluminium foil.

Table 2: The absorption maxima and extinction coefficients of π→π and n→π* transitions, recorded for monomer M1 and polymer P1 in DCM. Values for irradiated samples acquired after exposure to 365 nm light for a duration of 1 hour.*

Sample	π→π* λ_{max} (nm)	π→π* Ε (L cm^{-1} mol^{-1})	n→π* λ_{max} (nm)	n→π* Ε (L cm^{-1} mol^{-1})
Unirradiated M1	325	4.97×10^4	442	1.43×10^3
Irradiated M1	285	1.45×10^4	428	3.34×10^3
Unirradiated P1	322	1.09×10^5	439	2.97×10^3
Irradiated P1	291	3.23×10^4	437	7.30×10^3

2.5. Polymer Irradiation

The OmniCure® LX500 Ultra-compact UV LED spot curing system was used to charge the polymer samples utilising a 365 nm UV LED spot curing head with a power of ~5000 mW/cm^2 15 mm. Polymer samples were dissolved in THF unless stated otherwise, in a sealed vial to avoid solvent evaporation and irradiated at 100 % intensity from a distance of 10 cm from a clamped 365 nm UV LED spot curing head. With samples shielded from external light sources during exposure, transit, and measurement by use of aluminium foil. The population of cis isomers was determined at this wavelength via ^{1}H NMR.

Table 3: Experimental data of photoisomerisation experiments to determine the population of cis isomer at the photostationary state upon irradiation with 365 nm light of monomer M1 and polymer P1

Experiment	Thesis Section	Irradiation Time (Minutes)	*Trans* Integral	*Cis* Integral	Percentage of *Cis* Isomer (%)
P1 Irradiated in DCM, Dried from DCM	***4.2***	60	0.4894	1	67.14
Solid State Charging of P1	***4.3***	60	4.1382	1	19.46
P1 Irradiated in THF, Drying Method 1, Dried from THF	***5.1***	60	1.6403	1	34.87
P1 Irradiated in THF, Drying Method 1, Dried from DCM	***5.1***	60	1.9275	1	31.16
P1 Irradiated in THF, Drying Method 2, Dried from THF	***5.1***	60	2.0750	1	32.52
P1 Irradiated in THF, Drying Method 2, Dried from DCM	***5.1***	60	1.5992	1	38.47
P1 Irradiated in THF, Drying Method 3, Dried from THF	***5.1***	60	3.0041	1	24.97
P1 Irradiated in THF, Drying Method 3, Dried from DCM	***5.1***	60	3.5006	1	22.22
P1 Irradiated in THF, Dried from DCM	***5.2***	60	0.6150	1	61.92
P1 Irradiated in THF, Dried from THF	***5.2***	60	0.5859	1	63.06
P1 Irradiated in DCM, Dried from DCM	***5.4***	120	0.5134	1	66.08

2.6. Differential Scanning Calorimetry (DSC)

DSC was carried out on a Mettler Toledo DSC 1 with STARe acquisition and analysis software calibrated against an indium standard.

Experiment	Thesis Section	*Cis* Percentage (%)	Recorded Energy Density (J g^{-1})
P1 Irradiated in DCM, Dried from DCM	***4.2***	67.14	-134.00
Solid State Charging of P1	***4.3***	19.46	-27.28
P1 Irradiated in THF, Dried from DCM	***5.2***	61.92	-83.64
P1 Irradiated in THF, Dried from THF	***5.2***	63.06	-90.96

2.7. Wide Angle X-ray Spectrometry (WAXS)

WAXS patterns were measured with a Rigaku SmartLab X-ray diffractometer with a 9 kW rotating anode Cu-source equipped with a high-resolution Vertical θ/θ 4-Circle Goniometer and D/teX-ULTRA 250 High-Speed Position-Sensitive Detector System in reflectance mode. The system was configured with parallel-beam optics and a Ge(220) 2 bounce monochromator on the incident side. Samples were mounted on zero background holders made of off-cut Si(911) single crystal wafers. The measurements were performed as θ/2θ scans with a step size of 0.01 degrees, and a scanning rate of 3 degrees per minute.

2.8. Synthesis of Monomer M1 and Polymer P1

2.8.1. Synthesis of *Trans*-4-methacroloyloxyazobenzene monomer (M1)

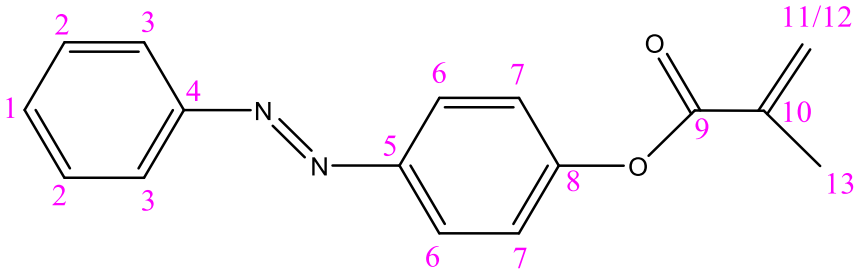

To synthesise the monomer, tetrahydrofuran (75 mL) was added to 4-phenylazophenol (6.6 g, 33 mmol), with the resulting solution added to triethylamine (4.62 mL, 33.3 mmol) and 2-6-di-tert-butyl-p-cresol (3.0 mg). The solution was then purged in argon gas and stirred for 30 minutes at 21 °C. Methacroloyl chloride (9.6 mL, 99 mmol) was added dropwise under inert conditions with the solution temperature held to ≤5 °C in an ice bath. The reaction flask was left to stir for 48 hours at room temperature (21 °C). The resulting precipitate was filtered off with the solution diluted 4 times with a 3:1 mix of dichloromethane and water. Any remaining

Methacroloyl chloride was hydrolysed by washing and extracting the organic phase with saturated sodium bicarbonate (100 mL), sodium hydroxide (1 M), sodium hydroxide (0.5 M), hydrochloric acid (1 M) and saturated brine solution. The organic phase was dried with sodium sulphate and the residual solvent removed under vacuum. The resultant material was purified in silica via dry loading of the crude monomer using 17.5:1 heptane and ethyl acetate and dried in vacuo.

Yield: orange powder, 1.2 g, 13.5 %, repeat resulted in 1.59 g, 17.9 %. Difficulties in product separation led to a large loss of product over multiple recovery attempts.

1H NMR (400 MHz, $CDCl_3$) δH (ppm): 8.02 (dt, 2H, J = 8.9 Hz, H6), 7.97 - 7.93 (m, 2H, H3), 7.58 - 7.48 (m, 3H, H1 and H2), 7.33 (dt, 2H, J = 9.1 Hz, H7), 6.42 (t, 1H, J = 1.1 Hz, H11 *cis*), 5.83 (q, 1H, J = 1.5 Hz, H12 *trans*), 2.12 (dd, 3H, J = 1.1, 1.5 Hz, H13).

13C NMR (100 MHz, $CDCl_3$) δC (ppm): 165.5 (C9); 153.0 (C8); 152.6 (C4); 150.2 (C5); 135.7 (C10); 131.1 (C1); 129.1 (C2); 127.7 (C11/12); 124.1 (C7); 122.9 (C3); 122.3 (C6); 18.4 (C13).

2.8.2. Synthesis of poly(trans-4-methacroloylazobenzene) (P1)

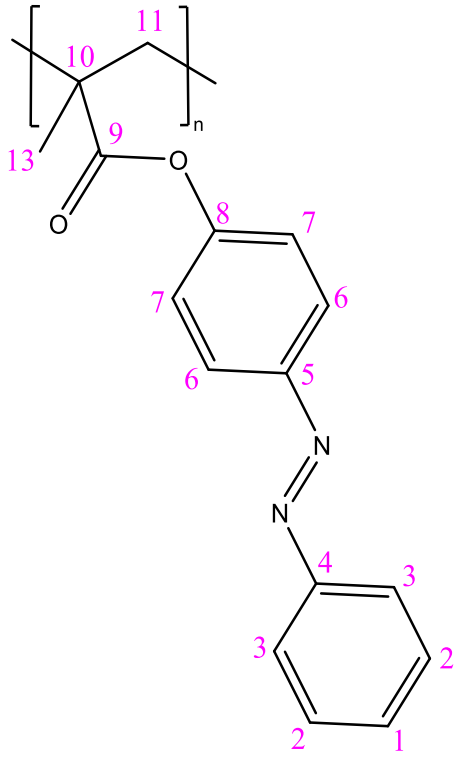

To synthesise the polymer, azobisisobutyronitrile (AIBN) (9 mg) was added to a solution of *trans*-4-methyacroloylazobenzene (M1) (0.3 g, 1.1 mmol) in unstabilised THF (3.0 mL). The solution was then subjected to 3 freeze/pump/thaw cycles. This was then followed by leaving the solution to stir under inert conditions for 3 days at 65 °C. The resulting polymer was then

precipitated with methanol (200 mL) whilst stirring and collected and dried by filtration under vacuum.

Yield: Orange powder, 0.79 g, 83.5 %, with one repeat using only 0.71 g of monomer M1 producing 0.54 g, 76.0 % and another using 0.56 g of monomer M1 producing 0.49 g, 86.6 %.

1H NMR (400 MHz, $CDCl_3$) δH (ppm): 8.05 - 7.70 (b, 4H, H3 and H6), 7.58 - 7.36 (b, 3H, H1 and H2), 7.36 - 7.15 (b, 2H, H7), 2.76 – 2.15 (b, m, 2H, H11), (1.89 - 1.20 (b, m, 3H, H13)

13C NMR (100 MHz, $CDCl_3$) δC (ppm): 175.2 (C9); 152.4 (C8); 152.3 (C4); 150.4 (C5); 131.1 (C1); 129.0 (C2); 124.2 (C3); 123.0 (C6); 121.9 (C7); 46.0 (C13); 25.6 (C11); 23.4 (C10).

GPC:

Mn (THF): 5526 g mol^{-1}

Polydispersity (M_w/M_n) = 4.61.

DSC:

T_g = 129 °C (10 °C min^{-1}).

2.9. Solvent Effects Investigation

P1 (40 mg) was dissolved in THF (2 mL). The solution was then placed in the polymer charging system (Omnicure lamp) for 60 minutes, 10 cm away from the light source at 365 nm, with a lamp intensity of 100 %. The irradiated solution was then split into two equal 1 mL solutions, each with its own flask labelled T (THF) and D (DCM). N_2 was blown across the surface of both solutions at the same time to remove most of the remaining solvent. Both flasks were then placed in a desiccator connected to a Schlenk line for 1 hour. Following this, the flask labelled D (DCM) was removed from the desiccator and 1 mL of DCM was added to the flask, dissolving the dry sample within. Once the solid was dissolved, N_2 was then blown across the surface of the P1 in DCM solution in flask D to leave a dry orange solid residue, followed by placing flask T and D in the desiccator connected to the Schlenk line for a further 2 hours under high vacuum. DSC samples for each solid sample were collected, alongside submission of NMR samples.

3. Exploring the Thermal Properties of Azobenzene

To test the theory behind crystallinity contributing to the energy density of a material mentioned in Section 1.7.2 and the effects of solvent on this energy density highlighted in Section 1.7.4, it was important to explore a simple, low molecular weight system with photoswitchable properties, that was known to crystallise readily. This system could both be irradiated and discharged whilst also crystallising and melting to explore the effects of both phenomena on the energy density of the material.

3.1. Using Crystallinity to Increase Energy Densities

The enthalpy of isomerisation is generally well known for a lot of low molecular weight, photoswitchable, compounds. As described previously, a good example of this is azobenzene, a photoswitchable compound that produces an exotherm upon conversion from a *cis* isomer to its lower-energy *trans* isomer. There are many ways to characterise the isomerisation of a compound like azobenzene, one of these ways is to look at the thermal properties of azobenzene using differential scanning calorimetry (DSC).

3.1.1. Differential Scanning Calorimetry

DSC is a characterisation method which measures the amount of heat flow applied from a furnace to a sample, relative to the heat flow from the same furnace to a reference sample. The reference crucible can be empty, or it can contain different standards. A DSC trace plots the measured heat flow against the temperature of the furnace and allows the measurement of exothermic energy release or endothermic energy intake, caused by phase transitions in the material and also glass transition temperatures (T_g).

As an example, if crystallisation occurs resulting in an exotherm, heat would be released from the sample to the surrounding furnace. This heat release would result in less heat flow being required to increase the temperature of the sample in that moment, compared to the reference sample therefore, the applied heat flow from the DSC decreases. A decrease in applied heat flow in a DSC trace is recognisable as a ‘dip’ or ‘trough’, whereas an increase in applied heat flow is seen as a ‘peak’, with glass transitions being recognised as a ‘step’ in a DSC trace.

3.1.2. Differential Scanning Calorimetry of Azobenzene

To investigate the thermal properties of azobenzene and the effect of drying trans-azobenzene from DCM and THF solutions on the crystallinity of trans-azobenzene, samples of irradiated and unirradiated azobenzene were investigated by DSC. Each sample was submitted to a heat-cool-heat cycle at 10 °C min^{-1}. Details of the procedure can be found in the experimental Section 2.9.

The DSC trace of unirradiated azobenzene dried from THF and DCM solutions, is shown below in Figure 17.

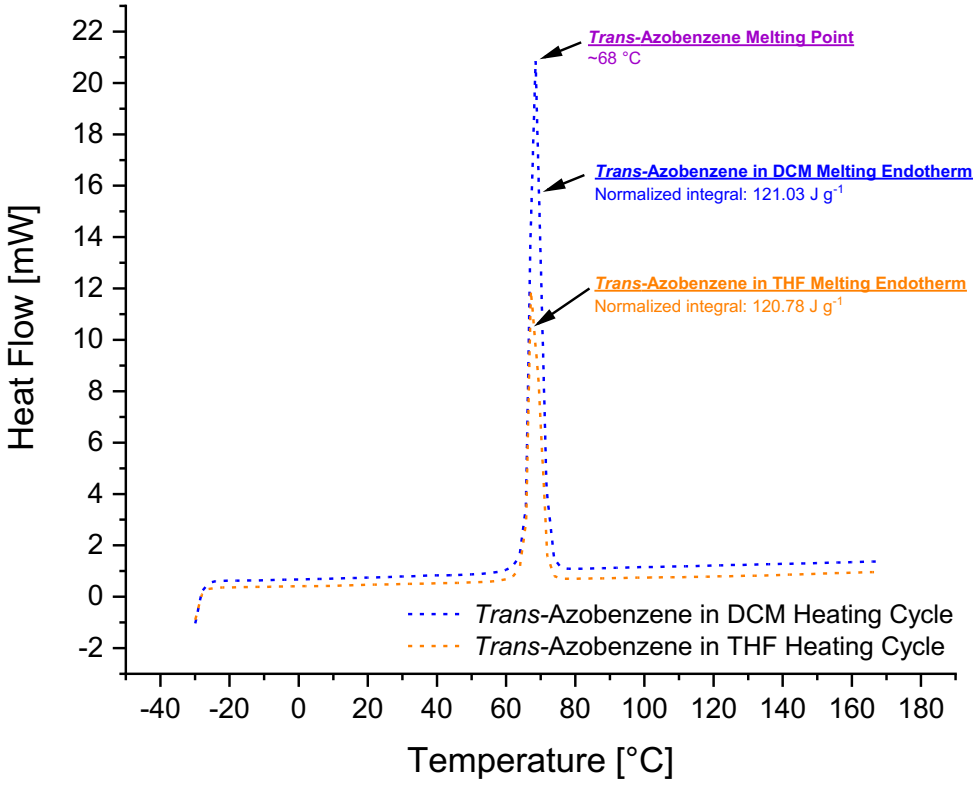

Figure 17: DSC Trace of the 1st heating cycle of unirradiated-azobenzene following evaporation of DCM (blue) and THF (orange) from the sample. Range: -20 to 170 °C, Heating Rate: 10 °C min^{-1}, 2 cycles for each solvent.

Figure 17 shows a large endotherm for *trans*-azobenzene of 121 J g^{-1} dried from DCM and 120.8 J g^{-1} dried from THF, with the melting point of *trans*-azobenzene dried from both solvents being ~68 °C. The peak for trans-azobenzene dried from DCM is approximately twice the size of that of the peak shown for trans-azobenzene dried from THF however, when normalised by the mass of the sample used, the melting endotherms are very similar. The similarity of the endotherms produced by trans-azobenzene dried from both solutions, suggests that the crystallinity of the material is not altered heavily by the use of either solvent.

As shown in Figure 4, the UV-Vis spectrum of azobenzene shows the ratio of molar absorption coefficients is much higher for the *trans* isomer than the *cis* isomer, at a wavelength of ~350 nm. Irradiation at 365 nm would still allow us to exploit this in order to gain a high *cis* percentage photostationary state. Therefore, a 20 g L^{-1} solution of azobenzene in DCM was irradiated using a high-power 365 nm LED lamp at 50 % intensity

for 1 hour. The solution was then split into two round bottom flasks containing 1 mL of irradiated azobenzene in DCM, followed by N_2 being blown over the surface of the solutions to quickly remove the solvent. The solid films left in the round bottom flasks were then placed onto a Schlenk line at full vacuum, to fully remove any remaining DCM. One of the flasks was then removed from the Schlenk line and the solid within this flask was redissolved in THF, followed by N_2 blowing and then removal of the remaining THF by being placed back onto the Schlenk line at full vacuum. The remaining solid-state irradiated azobenzene in both round bottom flasks, was then collected into separate DSC pans for analysis of their thermal properties, with ^{1}H NMR samples of each also submitted. The DSC trace of the irradiated azobenzene samples is shown below in Figure 18.

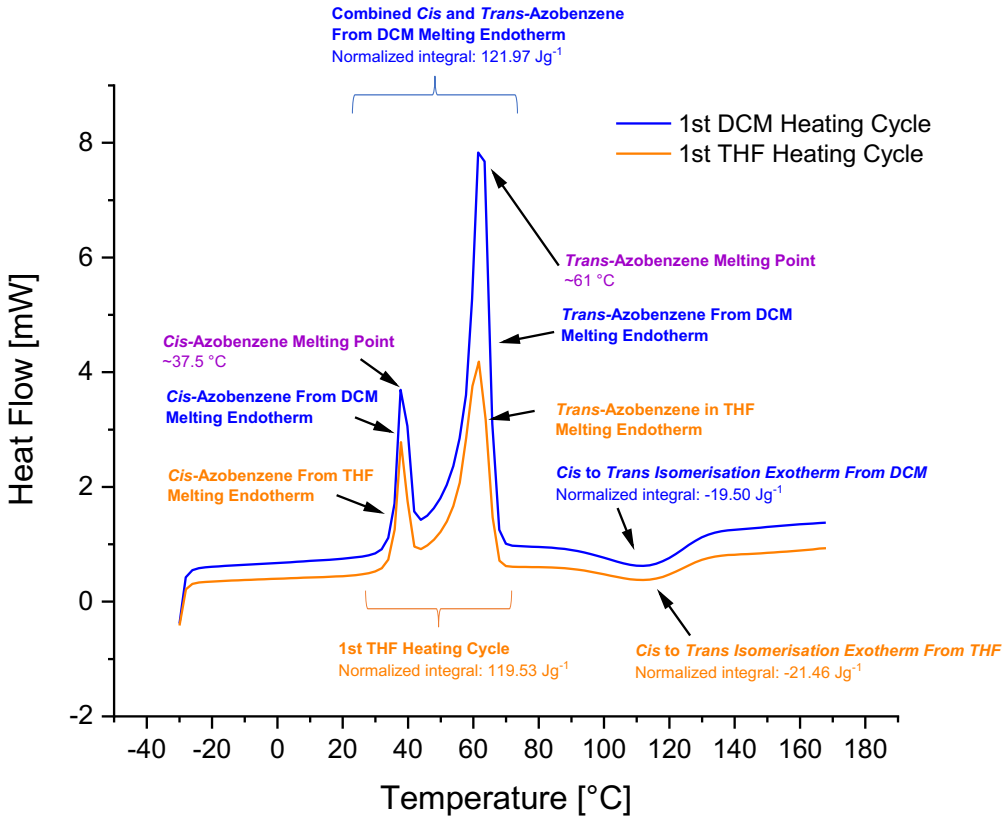

Figure 18: DSC trace of the 1st heating cycle of irradiated azobenzene following evaporation of DCM (blue) and THF (orange) from the sample. Range: -20 to 170 °C, Heating Rate: 10 °C min^{-1}, 2 cycles for each solvent.

Figure 18 shows the first heating cycles for irradiated azobenzene from evaporated DCM and THF. The first heating cycle for irradiated azobenzene appears to show melting of both *cis* and *trans* azobenzene based on the assumption of successful irradiation. For the sample dried from DCM, a *cis*-azobenzene melting endotherm of ~25 J g^{-1} is present, followed by the *trans*-azobenzene melting endotherm of ~95 J g^{-1}. Both endotherms combine to make an

overall melting endotherm of ~122 J g^{-1}, the same value of the *trans*-azobenzene melting endotherm in Figure 17, suggesting that melting could be the only process occurring here. The melting points of *cis* and *trans*-azobenzene is shown to be 37.5 °C and 61 °C respectively, with the latter being shifted lower than the melting point shown in Figure 17 (68 °C). Further details about the experiment can be found in the experimental section. The lower melting point of the *cis* isomer is significant, as this could offer a potential avenue to providing an easier to isomerise, solution-like state, for the *cis* isomer to revert back to the *trans* isomer, avoiding any steric hinderances to the reverse-isomerisation process. The similarity in the normalised endotherms and exotherms for irradiated azobenzene, suggests that the system is not heavily affected by drying from DCM and THF solutions.

The first heating curve can further be characterised by the presence of the broad exotherm at between 95 – 130 °C, this exotherm is caused by the reverse isomerisation of azobenzene from its *cis* to *trans* isomer. An interesting observation from the first heating cycle of irradiated azobenzene, is that the *cis* to *trans* reverse isomerisation occurs in a molten state.

The size of the exotherm produced by the crystallisation of *trans*-azobenzene is relatively large, combining this with the exotherm produced by the *cis* to *trans* reverse-isomerisation would produce a larger overall energy output over one heating and cooling cycle. Figure 19 below, shows the first heating and cooling cycles in the DSC trace of irradiated azobenzene dried from DCM:

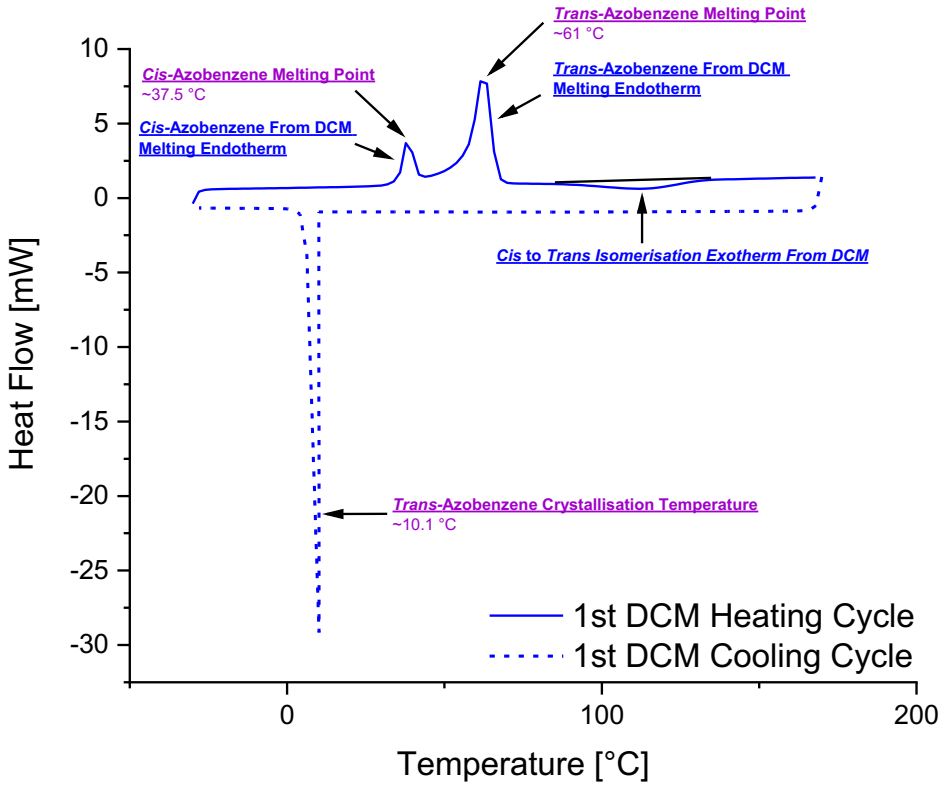

Figure 19: DSC trace of the first and second heating curves of irradiated-azobenzene dried from DCM. Range: -20 to 170 °C, Heating Rate: 10 C min^{-1}, 1 cycle.

The value for the reverse isomerisation exotherm is -22.18 J g^{-1}, which is low compared to other reported literature values mentioned earlier. This is likely due to the use of the 50 % intensity setting of the UV LED lamp rather than 100 % resulting in a much lower *cis* percentage but also, with the time between irradiation of the sample and submission of the samples to DSC being ~3 hours, some *cis*-azobenzene molecules could have returned to their *trans* state. The crystallisation exotherm is -103.18 J g^{-1} and combining the two creates an overall exotherm of -125.36 J g^{-1}. However, the energy input for the melting of both the *cis* and *trans* isomers, would determine the net energy output over one heating and cooling cycle. The ability of sunlight to overcome this particular energy barrier naturally, is currently unknown.

The DSC traces shown in Figures 18 and 19 clearly show that the azobenzene samples are majority *trans* isomers therefore, the combined enthalpy of the system is not representative of what a system comprised mostly of *cis* molecules would be. A system with a higher *cis* percentage would show a higher isomerisation exotherm, with the crystallisation exotherm likely to remain the same, a higher energy output should be seen as mentioned in Section 1.7.2. With a lower melting point for *cis* azobenzene isomers, this could allow for a higher net energy output by using the ambient heat of a system to overcome the *cis* isomer melting endotherm.

This is an extreme example of using the additional exotherm of crystallisation in a system, to gain a higher energy output that is hindered by two factors: a very high melting endotherm and also that solid, molecular azobenzene does not isomerise easily due to steric issues mentioned previously. Utilising the crystallisation enthalpy of a material, alongside the isomerisation enthalpy is currently being explored by the use of photochemical phase transition materials. An example of this is given by Zhang *et al*. who developed pyrazolylazophenyl ethers that are able to isomerise from *trans* to *cis* while in the solid state upon irradiation with 365 nm light, storing energy in the bonds of the higher energy metastable isomer.[43] Due to the melting point of the *cis* isomer being at or lower than room temperature, the *cis* isomer melts due to ambient heat, with this process of harvesting both photon energy and thermal energy happening progressively with longer irradiation times.[43]

Upon reversal of this process, the *cis* to *trans* isomerisation occurs in the liquid state. This is followed by crystallisation of the reformed *trans* isomers, releasing both the stored energy from isomerisation and crystallisation. Energy densities of 300 to 400 J g^{-1} were reported, which are much higher than energy densities between of 100 and 200 J g^{-1} gained from typical azobenzene systems utilising *cis* to *trans* isomerisation alone.[43]

In mobile or disordered systems such as an azobenzene based polymer, there could be some degree of crystallisation of azobenzene units through intermolecular interactions, that could produce a similar effect to the phase transitions reported in the work by Zhang *et al.* and give an additional crystallisation exotherm and higher energy output. This would, however, need to be carefully balanced against the propensity for the material to isomerise, in a repeat charging step as the cycling of a solar thermal fuel is a very important characteristic.

This trade-off between the higher energy densities achieved and the cyclability of the material, would be better explored in polymer systems where local ordering and therefore, crystallinity is more difficult to achieve, due to the increased degrees of freedom compared to lower molecular weight compounds. The level of crystallinity achieved in a polymer can be tailored by changing the polymer backbone and altering any functional groups it may have thus, altering intermolecular interactions in the system. As mentioned in Section 1.7.4, azobenzene-based polymers have been shown to achieve very high energy densities with the use of certain solvents.[45] As explained in Section 1.7.4, the use of solvents in this case may induce different levels of crystallinity in the material utilising the same concept used by Zhang *et al*. mentioned above. This will be explored further once the characterisation of our own azobenzene-based polymer P1 is discussed.

4. Exploring the Thermal Properties of an Azobenzene-Based Polymer

In section 3, the thermal properties of unirradiated and irradiated samples of azobenzene were explored and it was discussed that, the level of crystallinity in an STF system could lead to harvesting both solar and thermal energy to produce high energy densities. It was postulated that an irradiated, azobenzene-based polymer displaying a certain level of crystallinity could have a higher overall energy output of the STF system, than a polymer not displaying any level of crystallinity. This would utilise the varied tunability of polymers, to alter the level of crystallinity in the system, with this trait needing to be balanced against the propensity of the polymer to isomerise. To explore this prospect further, a suitable monomer for an azobenzene-based polymer was synthesised, followed by free radical polymerisation with the polymers thermal properties explored via DSC.

4.1. Synthesis and Characterisation of *Trans*-4-methacroloyloxyazobenzene (M1)

To investigate the thermal properties of an azobenzene-based polymer, we first systematically characterised the structural properties of both the monomer and the polymer. Hence, the monomer trans-4-methacroloyloxyazobenzene (M1) was synthesised using a single step reaction from 4-phenylazophenol, using a method by Zhitomirsky *et al*.[9] The Zhitomirsky method was a slight adaptation from the original method used by Moniruzzaman *et al*.[46] The procedure required an additional step, to ensure the hydrolysis of any excess methacroloyl chloride to methacrylic acid. The yield from the reaction was 17.9 %, which was very low compared to yields of between 70-80 % for Zhitomirsky *et al.* and 70 % for Moniruzzaman *et al*. This low yield stems from difficulties in product separation leading to a large loss of product over multiple recovery attempts.

The synthetic route for generating monomer M1 is shown in Figure 20 below.

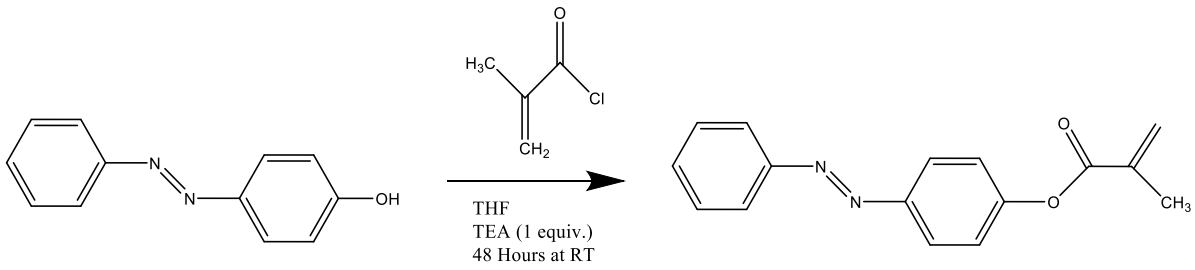

Figure 20: Scheme for the generation of trans-4-methacroloylazobenzene (M1)

4.1.1. Structural Characterisation of Monomer M1

The confirmation of the structure of M1 was carried out using ^{1}H NMR. This is shown in Figure 21 below.

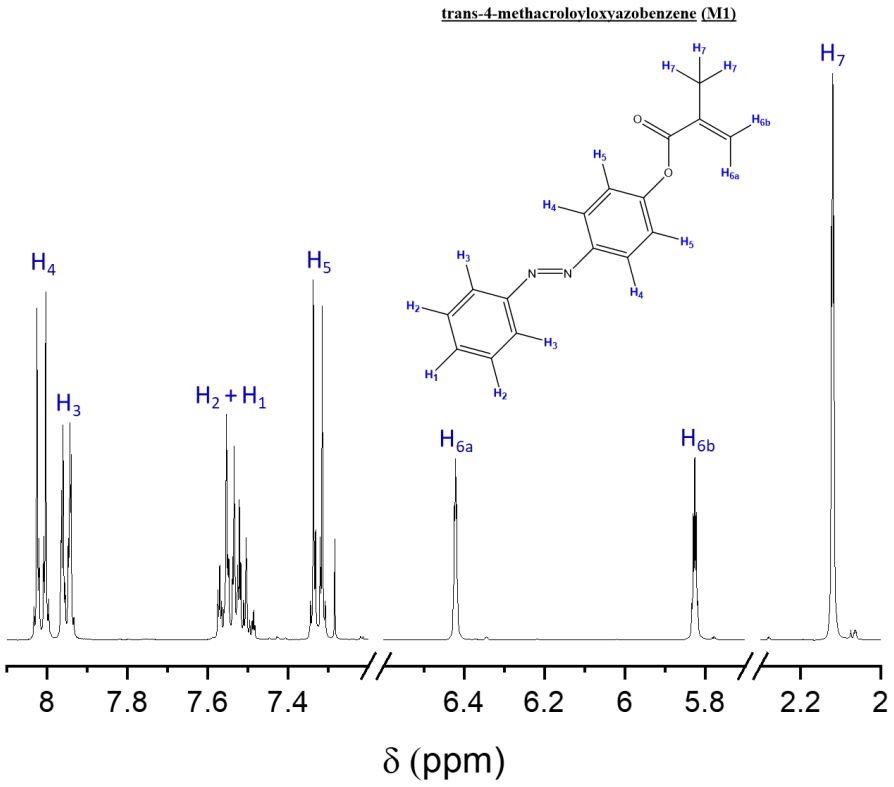

Figure 21: ^{1}H NMR spectrum of trans-4-methacroloylazobenzene monomer (M1)

Figure 21 shows a peak at 2.15 ppm as a doublet of doublets caused by H_7 coupling with H_{6a} and H_{6b}. Quintets at chemical shifts of ~6.45 ppm and ~5.85 ppm are formed from geminal coupling between hydrogens H_{6a} and H_{6b} respectively, alongside coupling with the 3 hydrogens at H_7.

The aromatic region of the spectrum contains protons H_5 at ~7.3 ppm (multiplet), H_2 and H_1 at ~7.55 ppm (multiplet) and the least de-shielded protons H_4 and H_3 at ~7.95 ppm (multiplet) and ~8.05 ppm (multiplet) respectively. This result confirms the presence of aromatic protons in the product. These chemical shifts are consistent with the structure of M1 and also with previously reported ^{1}H NMR spectra by Moniruzzaman *et al*. [46]

4.2. Synthesis and Characterisation of Poly(trans-4-methacroloyloxyazobenzene) (P1)

Despite the low yield in the synthesis of M1, there was still enough of the monomer to continue to the polymerisation stage. The monomer M1 was used to synthesise polymer P1 using a free radical polymerisation, with AIBN used as a radical initiator. The polymerisation time for the reaction was 3 days, in line with the method used by Zhitomirsky *et al*.[9] An additional step to remove oxygen by use of 3 freeze/pump/thaw cycles was added under N_2, which contributed to a yield of 83.5 %.

The synthetic route for the polymerisation of monomer M1 to polymer P1 is shown below in Figure 22.

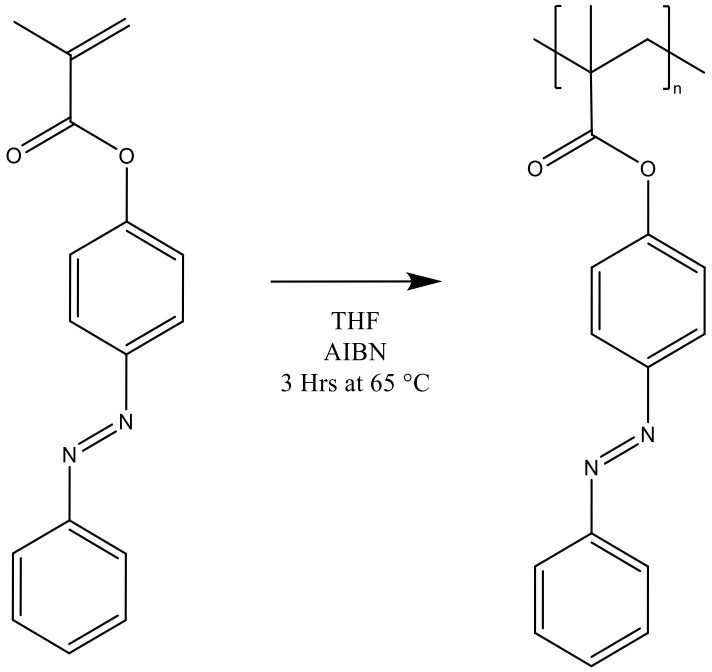

Figure 22: Scheme for the generation of poly(trans-4-methacroloylazobenzene) (P1).

The synthesised polymer P1 was characterised using gel permeation chromatography (GPC). The number average molecular weight (M_n) of P1 was measured at 5.53×10^3 g mol^{-1}, with a polydispersity value of 4.61. Previously reported synthesis of P1 has shown an M_n value of 1.20×10^4 g mol^{-1},[9] suggesting that the synthesised polymer P1 has shorter polymer strands than previously reported, with a larger range of polymer strand lengths.

4.2.1. Structural Characterisation of P1

Following the polymerisation, the polymer was then investigated by solution ^{1}H NMR to check the polymer purity, shown in Figure 23 below:

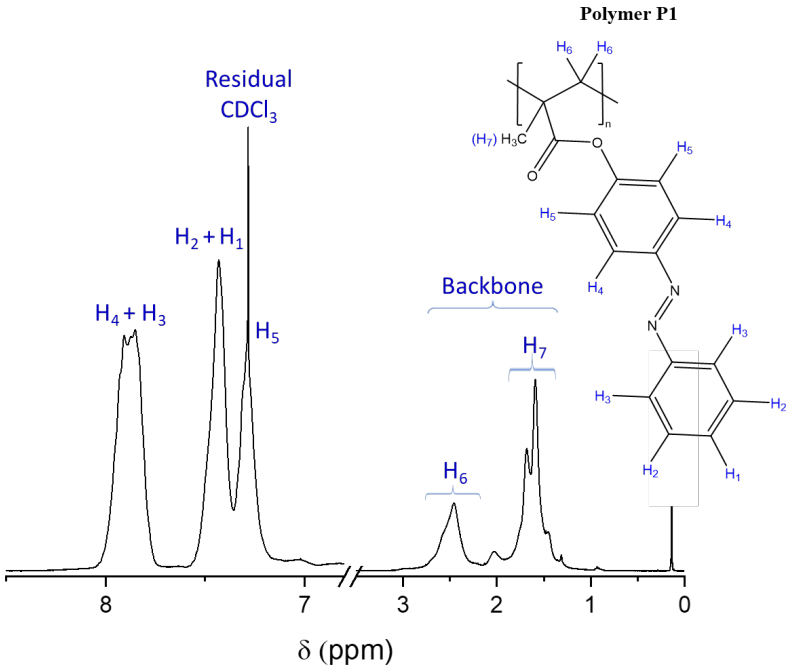

Figure 23: ^{1}H nmr spectrum of poly(trans-4-methacroloylazobenzene) P1

The P1 spectrum contains broader peaks and the shifts for aromatic protons ($H_{1\text{-}5}$) are moved slightly downfield compared to those in the M1 spectrum. Confirmation of successful free radical polymerisation and purification is the lack of peaks at 6.45 ppm and 5.85 ppm characterised by the double bond protons present in M1.

The chemical shift of H_7 has also shifted downfield caused by a more shielded environment due to the double bond anisotropy being removed. The hydrogens at H_6 are no longer geminally coupled to each other, due to removal of the double bond allowing free rotation around the backbone single bond.

The H_7 protons allow us to look deeper into the structural properties of the synthesised polymer. These protons can help us visualise tacticity differences in the polymer, due to each proton having a slightly different environment depending on the placement of the proton on the carbon backbone. Tacticity is an important factor to consider due to the potential of differing orientations of pendant groups (azobenzene units) on the polymer backbone causing a difference in the intermolecular interactions of the polymer and therefore, altering the local ordering of the system.

Although free radical polymerisation cannot lead to fully tactic polymers, some tacticity has been reported when using free radical polymerisation, leading to slight syndiotacticity in some PMMA based polymers.[47,48]

4.2.2. Absorption Properties of Unirradiated Monomer M1 and Polymer P1

Following the synthesis of polymer P1, the UV-Vis absorption properties of unirradiated monomer M1 and polymer P1 were measured in DCM, to see if there were any changes in the absorption properties compared to azobenzene. Both M1 and P1 solutions were of known concentrations of 4.69×10^{-3} g L^{-1} for M1 and 5.08×10^{-3} g L^{-1} for P1.

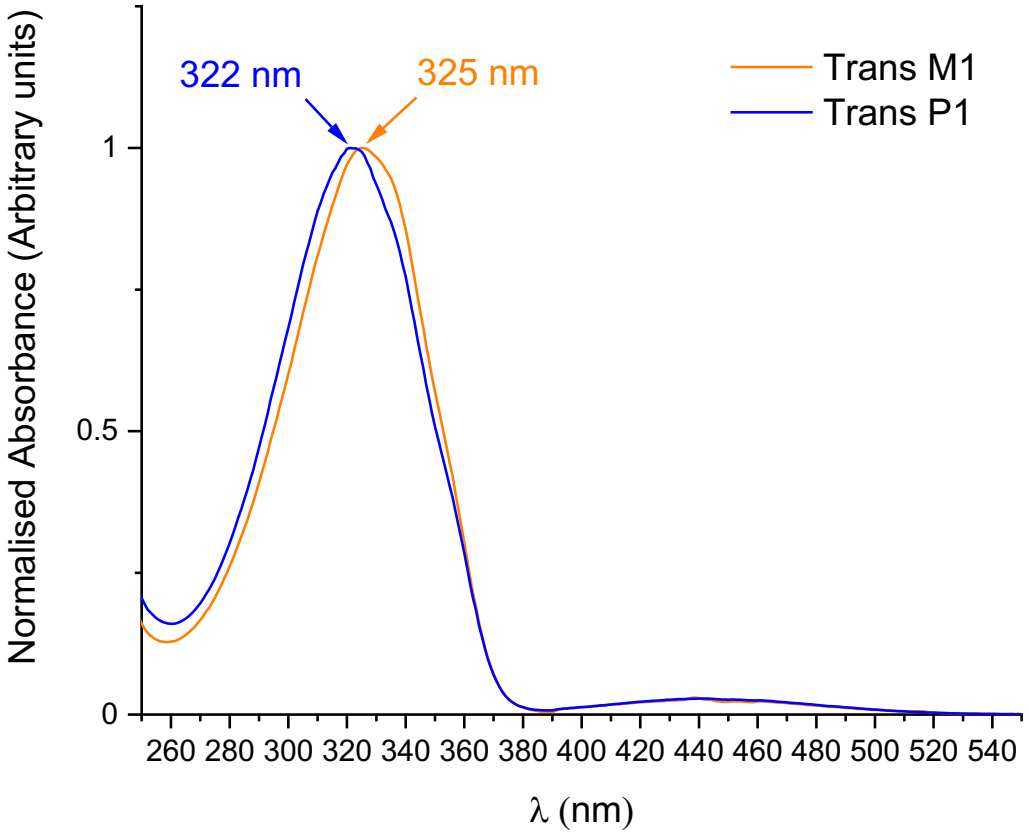

Figure 24: UV-Vis absorption spectra of unirradiated M1 and P1. With absorption values normalised to equal 1 for comparison of absorption maxima.

It has been shown previously that monomer M1 and polymer P1 maintain their STF properties that stem from their azobenzene pendant groups, following successful synthesis and polymerisation.[49]

Figure 24 shows, that *trans* monomer M1 exhibits absorption wavelengths of 325 nm and 442 nm, attributed to π→ π* and forbidden n→ π* electronic transitions respectively. Polymer P1 shows very similar π→ π* absorption wavelengths at 322 nm with the forbidden P1 n→ π* electronic transition showing an absorption at 439 nm. Comparing both monomer M1 and polymer P1 to azobenzene, we see a minimal shift from the π→ π* absorption

wavelength at 320 nm as well as a small shift in the absorption of the forbidden n→ π* absorption at 442 nm.

4.2.3. P1 Tacticity Investigation

Tacticity is a consequence of the arrangement of polymer pendant groups on the polymer backbone, arising from polymerisation conditions used when combining monomer units. Polymer P1 could have 3 possible tacticities for its azobenzene side groups to form into, these include:

- Atacticity, where there is no consistent 'pattern' in the position of pendant groups on the polymer backbone.
- Syndiotacticity, where pendant groups alternate in their positions.
- Isotacticity, where pendant groups remain on the same side as each other on the polymer backbone.

These tacticities can be analysed by NMR, as the orientation of repeat units can change the environment of hydrogens on other adjacent repeat units. They can be illustrated using triads (three repeat units) and pentads (five repeat units) from combinations of diad (two repeat units) configurations. A mesomeric (**m**) diad contains pendant groups on the same side of the polymer backbone. A racemic (**r**) diad contains pendant groups on opposite sides of the polymer backbone. As shown in Figure 25; the amount of a certain tacticity present depends on the type of polymerisation used to form the polymer.[47] In this investigation, we aimed to show the type and level of tacticity present in the synthesised polymer P1. Both ^{1}H NMR and ^{13}C NMR can elucidate the differences between triads and pentads within PMMA based polymers.[47,48,50,51]

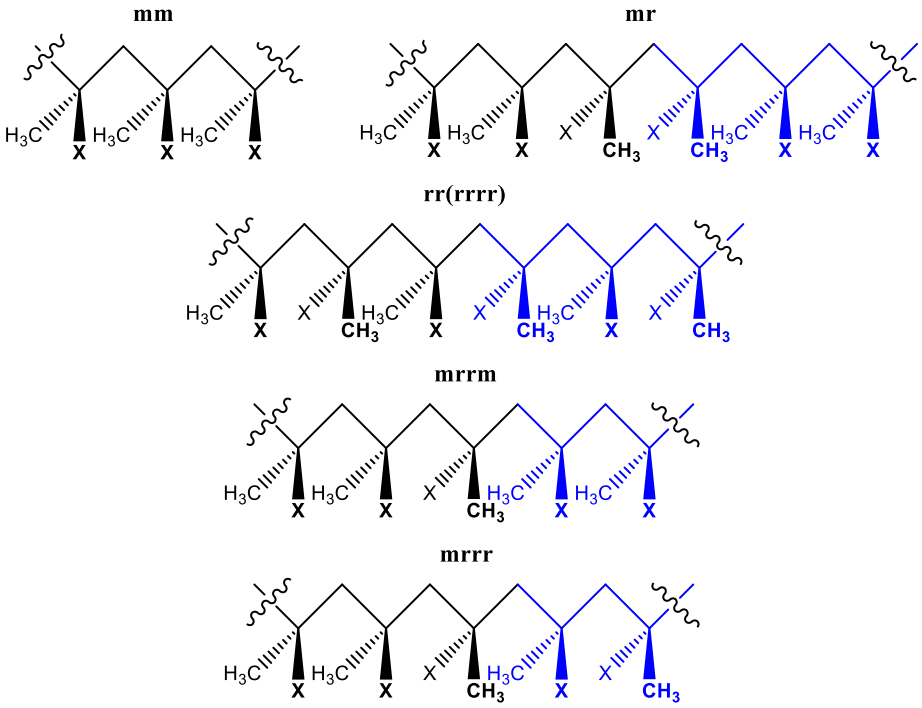

Figure 25: Possible triad and pentad tacticity variations of P1. Where: X is an azobenzene unit, as displayed in Figure 22, m is a mesomeric diad and r is a racemic diad.

The tacticities of polymethylmethacrylate (PMMA) polymers under different conditions is well known, this was used as a reference, as PMMA is the backbone of polymer P1 and contains very similar hydrogen environments, with chemical shifts varying only slightly. Figure 26 shows relative peak shapes and heights in the α-methyl region of the PMMA polymer, for the three main tacticities possible in PMMA in $CDCl_3$ via ^1H NMR.[52]

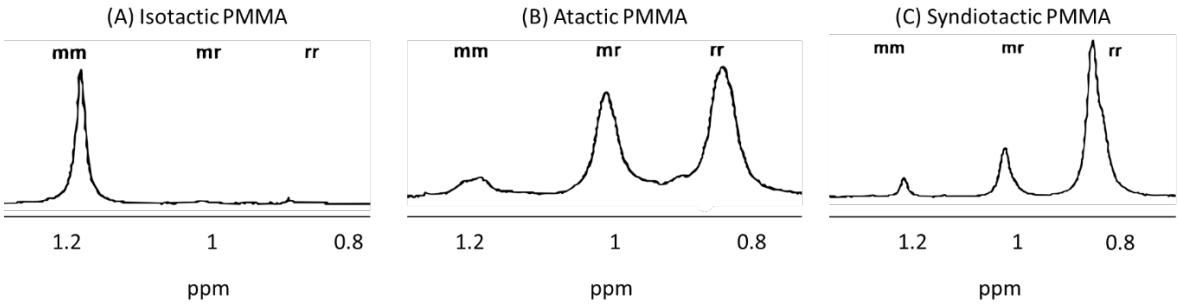

Figure 26: α-Methyl peaks of ^1H NMR spectra of (A) Isotactic PMMA in $CDCl_3$; (B) Atactic PMMA in $CDCl_3$; (C) Syndiotactic PMMA in $CDCl_3$. Spectra taken and adapted from P. Carriere, Y. Grohens, J. Spevacek and J. Schultz, Langmuir, 2000, 16, 5051–5053.

Due to the PMMA backbone in polymer P1, the ^1H NMR peak shapes and distribution should remain very similar despite changes in chemical shift, for each tacticity. Therefore, these methyl peak shapes can be used to aid the process of defining the tacticities in polymer P1, but these are not quantitative. To test the tacticity of our synthesised polymer P1

quantitatively, ^{1}H and ^{13}C NMR spectra were obtained from a polymer P1 sample of a concentration of 100 mg mL^{-1} at a resolution of 400 MHz.

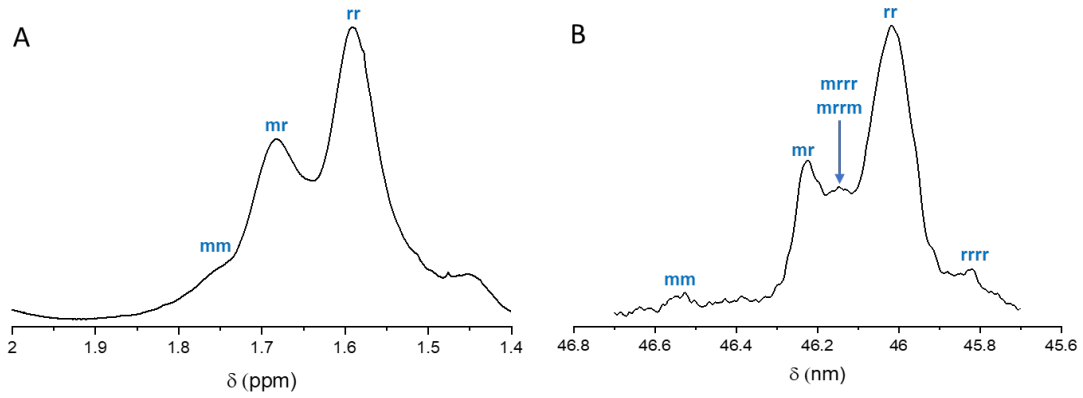

Figure 27: ^{1}H NMR and ^{13}C NMR of the α-methyl regions of polymer P1, highlighting peaks caused by different triad/pentad configurations.

Figure 27 shows the methyl regions of ^{1}H (A) and ^{13}C (B) NMR spectra for polymer P1 and labels for NMR peaks caused by differences in triad and pentad proportions in the P1 system. Mesomeric diads lead to methyl groups being adjacent to each other, leading to slight de-shielding of the methyl group, causing the **mm** triad to be at higher chemical shifts than the more shielded opposite **rr** triads. The cause of this shielding has been explored previously however, the relationship between a triad and its shielding seems to be complex, requiring computational calculations to separate the different contributions that lead to the shielding and de-shielding effects.[53,54,55]

The integral of each triad or pentad can be translated into relative percentage values to show the proportion of **rr** and **mm** triads and all 'mixed-diad' triad or pentad proportions in between. Peak deconvolution was used to separate triad peaks in close proximity to each other, which could contribute to higher integral values. An example of peak deconvolution used in the ^{1}H NMR of polymer P1 is shown below in Figure 28.

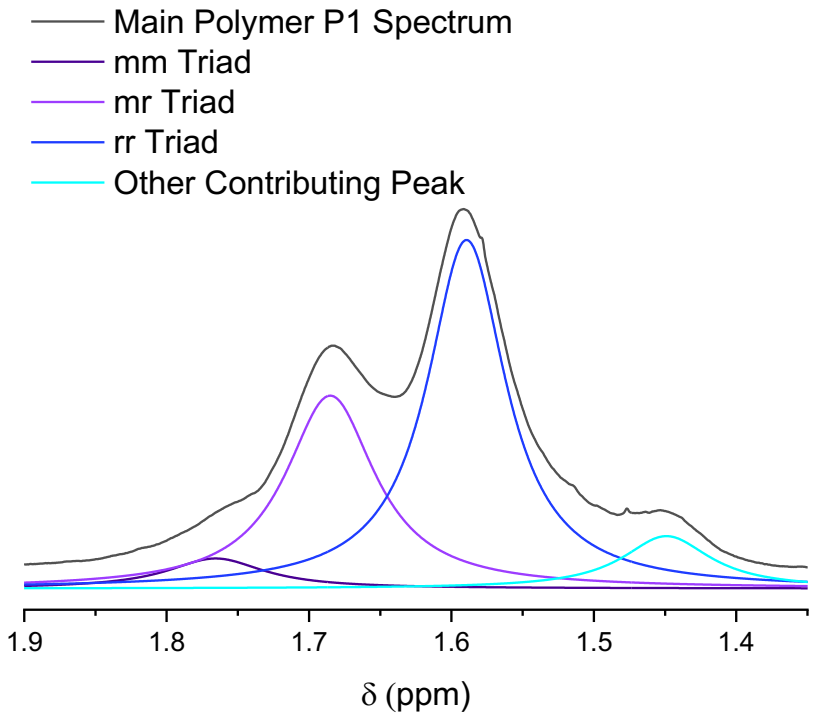

Figure 28: Methyl Region of ^{1}H NMR of polymer P1, with peak deconvolution traces of the mm triad (dark purple), mr triad (light purple), rr triad (dark blue) and another peak which contributes to the overall size of the peak attributed to the rr triad (light blue).

The deconvoluted, relative integrals of triads and pentads present in the methyl region of the ^{13}C and ^{1}H NMR spectra of P1 are shown below in Tables 2 and 3:

Table 4: Table showing the relative integral percentages of peaks within the methyl region of ^{1}H P1 spectrum. The relative integral percentages do not fully add to 1 due to 1 unassigned peak on the far left with a value of 4.55%.

^{1}H NMR Methyl Region Deconvoluted Peak Assignments		
Chemical Shift	Peak Assignment	Relative Integral
1.76	(CH_3) mm	0.0577
1.68	(CH_3) mr	0.3417
1.61	(CH_3) rr	0.6007

Table 5: Table showing the relative integral percentages of peaks within the methyl region of ^{13}C P1 spectrum.

^{13}C NMR Methyl Region Deconvoluted Peak Assignments		
Chemical Shift	Peak Assignment	Relative Integral
46.53	(CH_3) mm	0.0122
46.22	(CH_3) mr	0.1542
46.15	(CH_3) mrrr, (CH_3) mrrm	0.1090
46.02	(CH_3) rr	0.7134

45.82	(CH_3) rrrr	0.0113

The relative proportion of **rr** and **mm** triads and associated pentads can be converted into a probability, describing the likelihood of **r** or **m** diad formation,[48]

$$Pm = mm + 0.5(mr) \quad (2)$$

$$Pr = 1 - (mm + 0.5(mr)) \quad (3)$$

Where relative triad percentages are given as decimal values.

Using the following equations, we can calculate the P_r value and therefore, the tacticity of P1. This can be done for both ^{1}H and ^{13}C NMR as shown below:

P_r value from P1 ^{1}H NMR spectrum:

$$\mathrm{Pr\ (1H\ NMR\ P1)} = 1 - (0.0577 + 0.5(0.3417))$$

$$\mathrm{Pr\ (1H\ NMR\ P1)} = 0.77$$

Despite some pentads being considered within the ^{13}C methyl region, they are not well resolved and therefore, for this calculation, only the peaks defined by **mm**, **mr** and **rr** triads are being considered. This means that the relative integrations of these three triads must be scaled up to equal 1.

$$0.0122\ (\mathrm{mm}) + 0.1542\ (\mathrm{mr}) + 0.7134\ (\mathrm{rr}) = 0.8798$$

therefore,

$$\frac{0.0122\ (\mathrm{mm})}{0.8798} + \frac{0.1542\ (\mathrm{mr})}{0.8798} + \frac{0.7134\ (\mathrm{mm})}{0.8798} = 1$$

$$0.0139\ (\mathrm{mm}) + 0.1753(\mathrm{mr}) + 0.8109\ (\mathrm{rr}) = 1$$

$$\mathrm{Pr\ (13C\ NMR\ P1)} = 1 - (0.0139 + 0.5(0.1753))$$

$$\mathrm{Pr\ (13C\ NMR\ P1)} = 0.90$$

P_r values with their corresponding tacticities are shown below in table 6:

Table 6: List of potential polymer tacticities and corresponding P_r values

P_r Value	Tacticity
1	Purely syndiotactic
0.5	Atactic polymer
0 (P_m value of 1)	Purely isotactic
0.51 to 0.99	Slightly syndiotactic to highly syndiotactic
0.01 to 0.49	Highly isotactic to slightly isotactic

Both P_r values indicated by ^{1}H and ^{13}C NMR suggest that polymer P1 is syndiotactic. However, the P_r value of 0.90 obtained by the use of ^{13}C NMR suggests that polymer P1 is highly syndiotactic. This value appears to overestimate the level of tacticity in the polymer, as the use of free radical polymerisation to synthesise P1 is unlikely to result in such a high level of syndiotacticity, when compared to controlled polymerisation methods. The P_r value of 0.77 obtained by the use of ^{1}H NMR, appears to be a much more realistic value, suggesting a mild syndiotacticity in polymer P1.

Previously synthesised polymer P1 using free radical polymerisation, has been shown to have a P_r value of 0.89 using ^{13}C NMR, claiming a high level of tacticity in this polymer.[44,45] To our knowledge there has been no known previous ^{1}H NMR analysis of polymer P1 reported however, a free radical polymerisation of monomer M1 into polymer P1 is more likely to produce a polymer of mild syndiotacticity or atacticity and therefore, the P_r value of 0.77 and corresponding level of mild syndiotacticity, will be used in this thesis going forward.

Producing a mildly syndiotactic polymer, highlighted an important part of the polymer P1 morphology, allowing the exploration of whether the level of syndiotacticity in polymer P1 would display any form of crystallinity and its potential effect on the energy storage properties of P1.

4.3. Thermal Properties of Unirradiated P1

To further characterise P1, DSC was used to show the thermal properties of the unirradiated polymer. Any crystallinity present in the polymer could be shown as an endotherm, along with the glass transition temperature of the polymer. To this end, samples of unirradiated P1 collected directly after synthesis and placed in a vacuum oven for 5 days at 70 °C, were investigated by DSC. Each sample was submitted to a heat-cool-heat cycle at 10 °C min^{-1}. Further details of the procedure can be found in the experimental section. The DSC trace of unirradiated P1 following synthesis, is shown in Figure 29 below:

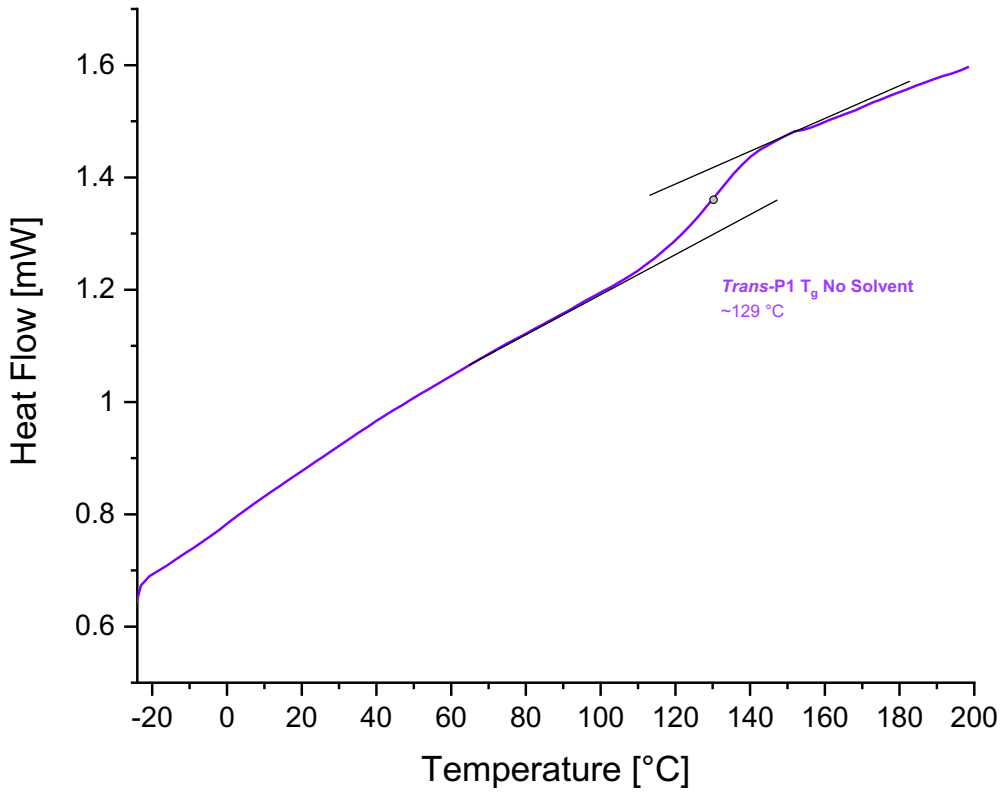

Figure 29: Second DSC heating curve of unirradiated P1 following synthesis with glass transition temperature (T_g) shown. Cycle from -30 °C to 200 °C and 200 °C to -30 °C at a heating rate of 10 °C per minute.

In Figure 29 a glass transition (T_g) is evident at ~129 °C, shown as a step. This value is similar to the T_g shown (~126 °C) in unpublished research by Wallace *et al*.[24] Figure 29 shows no sign of a melting endotherm, indicating that the slightly syndiotactic polymer shows no levels of crystallinity following precipitation by adding methanol in the final step of the polymer synthesis.

4.3.1. Solvent Effect on Unirradiated P1

Once the thermal properties of unirradiated P1 were explored, the effect of solvents on unirradiated P1 was explored. To do this, unirradiated P1 was dissolved in DCM and THF with a concentration of 15 g L^{-1}, the solution was then pipetted onto a microscope slide and left to dry within a desiccator under vacuum. The sample was then collected and submitted to DSC with a heat-cool-heat cycle at 10 °C min^{-1}. Further details of the procedure can be found in the experimental section, Section 2. The DSC of unirradiated P1 dried from DCM and THF, compared to P1 without solvents, is shown below in Figure 30.

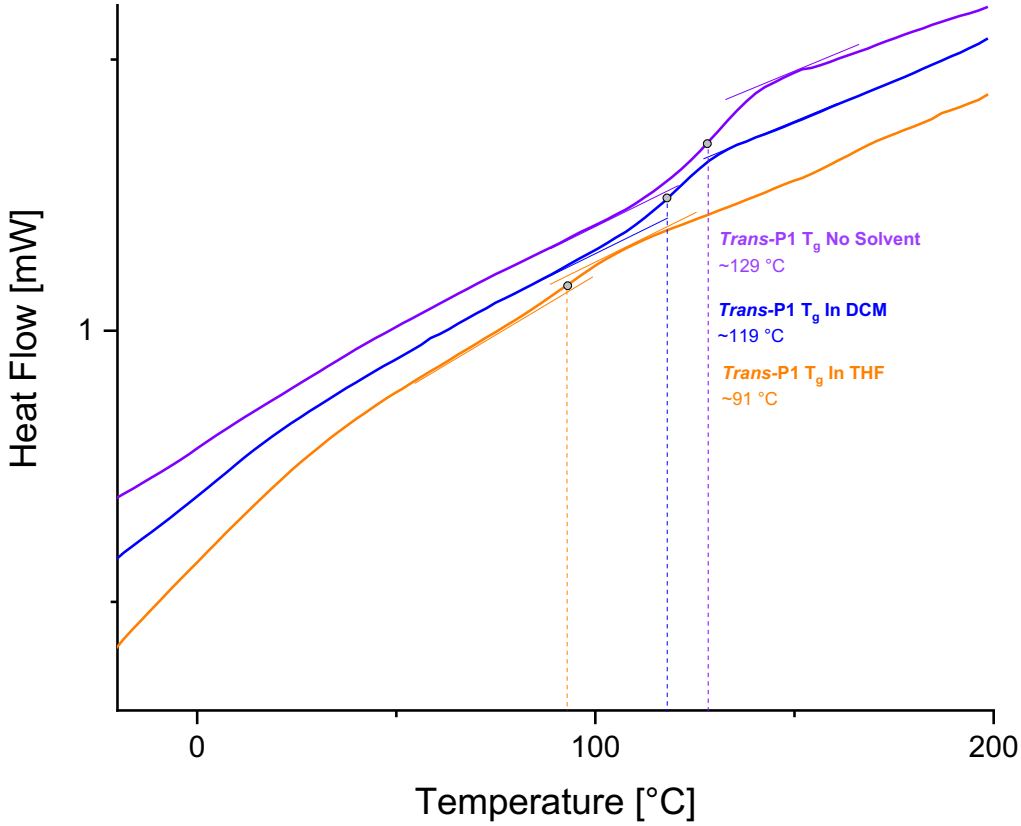

Figure 30: Second DSC heating curves of unirradiated P1 dried from THF (orange), DCM (blue) and no solvent (purple) following synthesis with glass transition temperature (Tg) shown. Cycle from -30 °C to 200 °C and 200 °C to -30 °C at a heating rate of 10 °C per minute.

Figure 30 shows the glass transition temperatures of unirradiated P1 dried from DCM, THF and directly after synthesis. There is a clear difference between the T_g values, with unirradiated P1 samples dried from THF showing the largest difference in T_g values at ~91 °C compared to the T_g of ~129 °C of P1 with no solvent interaction. Samples dried from DCM also show a lower T_g but to a smaller degree, with a T_g value of ~119 °C. The differences in T_g values suggests that solvents have a strong influence on the morphology of polymer P1.

Unfortunately, THF samples appeared not to dry effectively compared to that of DCM samples, meaning that the DSC spectra of unirradiated P1 dried from THF are inconclusive, with too many solvent features. These solvent features are highlighted more clearly when investigated by optical microscopy.

4.3.2. Optical Microscopy of Unirradiated P1

To aid the characterisation of the thermal properties of unirradiated P1, we used polarised light optical microscopy alongside DSC, to see any changes to the polymer that were visible to the naked eye. To do this, unirradiated P1 was dissolved in DCM and THF with a concentration of 15 g L^{-1}, the solution was then pipetted onto a microscope slide and left to

dry within a desiccator under vacuum. Once the samples were dried, the microscope slides were placed into a hot stage mounted below a bright field light microscope. Images were taken at 10 °C steps in a 30 to 200 °C heating cycle, followed by images being taken at 5 °C steps upon a 200 to 30 °C cooling cycle, to imitate conditions in a DSC trace. Further details of the procedure can be found in the experimental section.

Figure 31 shows an unirradiated P1 sample prepared from DCM, with specific temperatures selected to highlight important landmarks within the DSC trace itself:

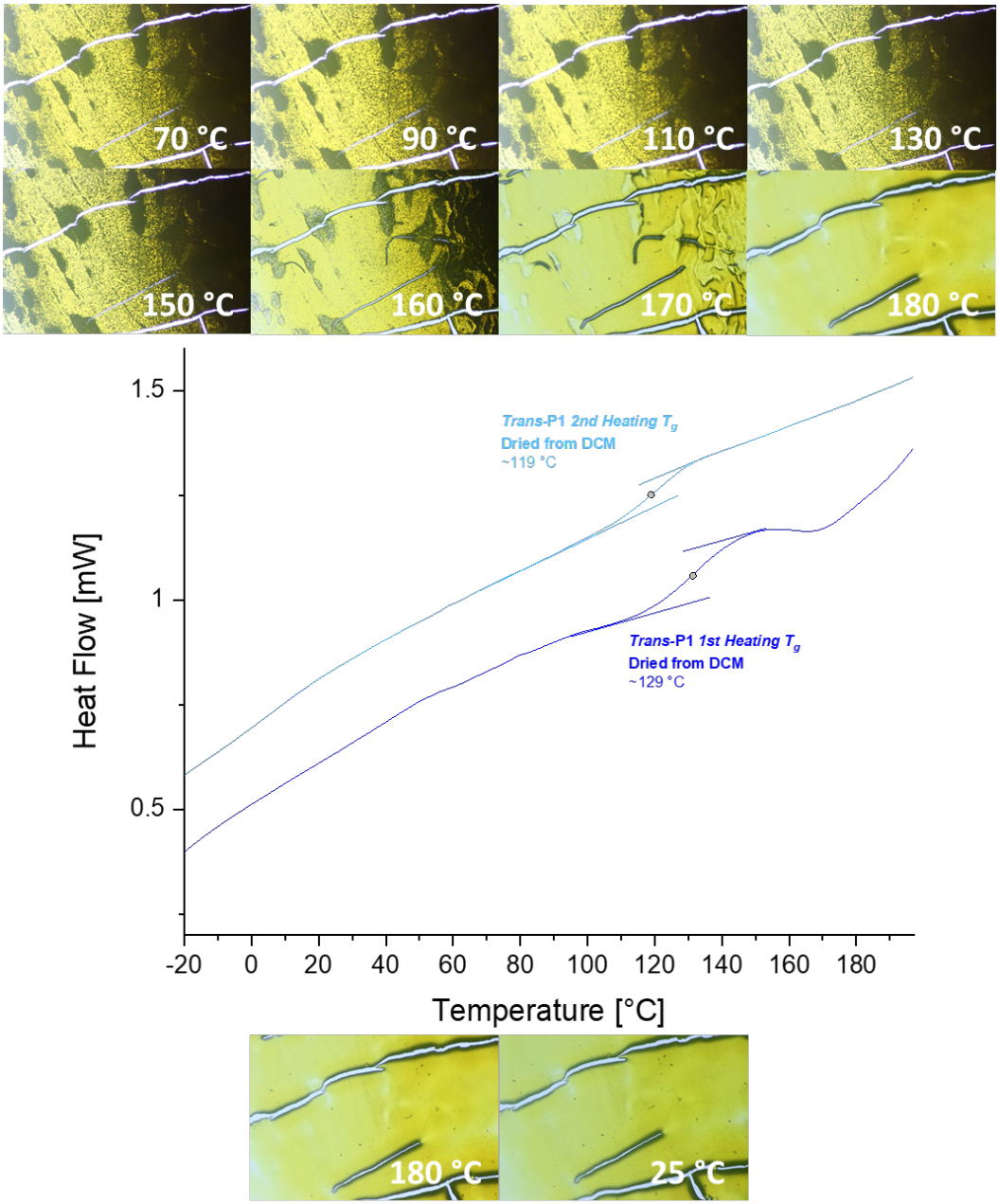

Figure 31: DSC trace of the first and second heating curves of unirradiated P1 dried from DCM, accompanied by optical microscopy images of unirradiated P1 films dried from DCM while heating (above DSC Trace, 70 °C to 180 °C) and while cooling (below DSC trace, 180 °C to 25 °C), with temperatures of interest highlighted.

The images shown in Figure 31 show very little change in the appearance of the unirradiated polymer P1 for temperatures up to 150 °C. For temperatures between 160-200 °C the texture of polymer P1 changes, with darker regions of the polymer film being progressively less visible. This change in polymer texture could be a delayed effect of the polymer becoming softer, following the glass transition. The darker regions visible in the range of 30-150 °C are likely due thicker layers of polymer P1, that were free to move and thin out following the glass transition temperatures being surpassed, allowing light to pass through these areas.

There is little to no indication of crystallinity in the unirradiated polymer P1 dried from DCM from the optical microscopy images. Another observation to be made, is that there appears to be no changes in the texture of polymer P1 upon cooling. The optical microscopy data obtained from the unirradiated P1 dried from THF system, can be seen in Figure 32 below.

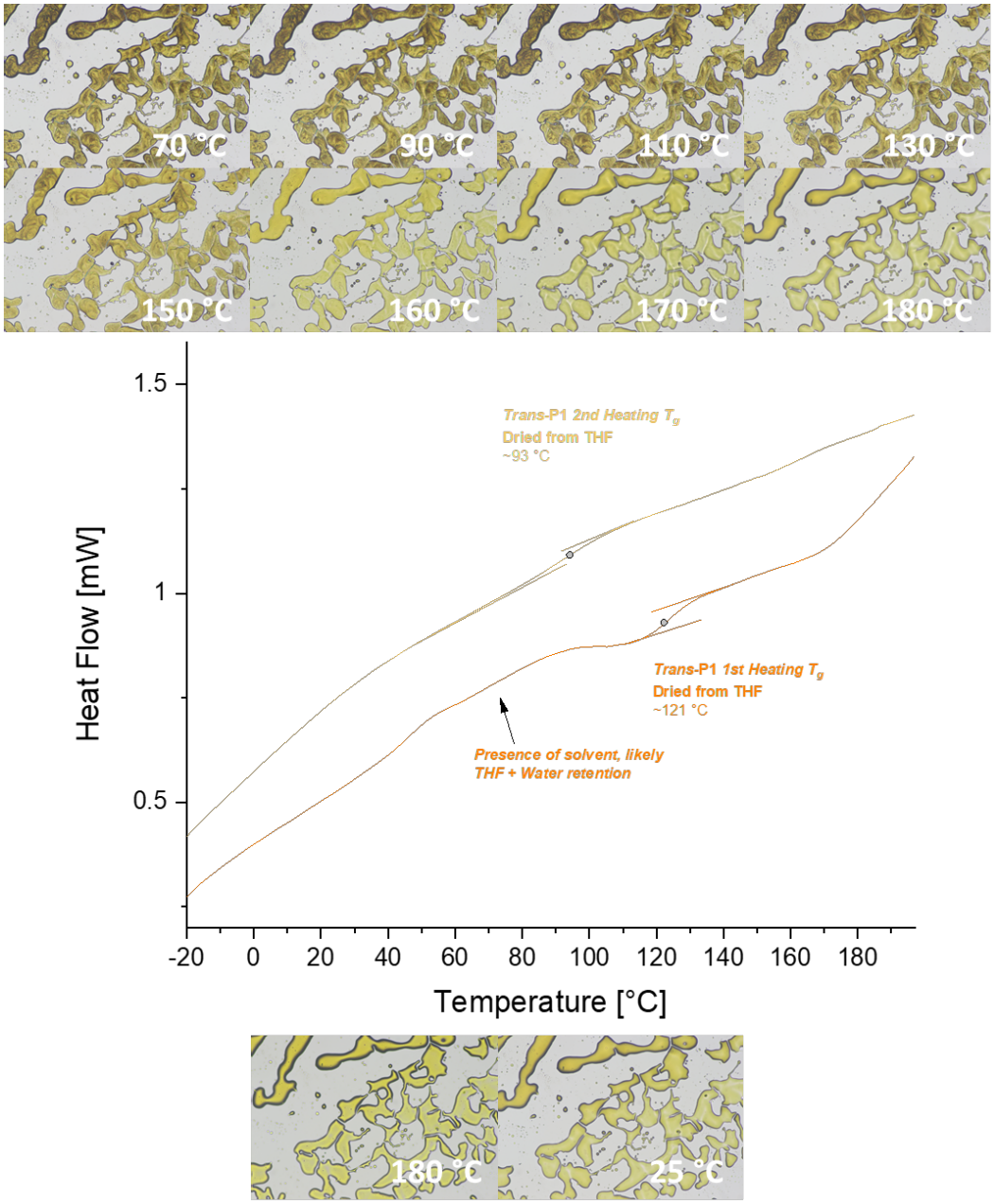

Figure 32: DSC trace of the first and second heating curves of unirradiated P1 dried from THF, accompanied by optical microscopy images of unirradiated P1 films dried from THF while heating (above DSC Trace, 70 °C to 180 °C) and while cooling (below DSC trace, 180 °C to 25 °C), with temperatures of interest highlighted.

The unirradiated polymer P1 sample, dried from THF optical microscopy data shows similar features to the system dried from DCM. The main difference between the two are the type of films formed following the drying stage, the THF system appears to retain moisture and form globule-like films, rather than the even films formed by the DCM system. The DSC trace of the THF system seems to explain why, with what appears to be a broad solvent peak between 50-100 °C. The broadness of this peak suggests that THF is not the only solvent present, and that water could have been absorbed by the THF during the drying process, making the drying process less efficient. The THF system also shows darker regions of

thicker layer of unirradiated polymer P1 for temperatures up to 150 °C, which disappear in the region of 160-200 °C.

The lack of a melting endotherm in both the THF and DCM systems suggests that the mild syndiotacticity present in polymer P1, does not appear to form any crystallinity following analysis by DSC and optical microscopy. Other methods of analysing the crystallinity present in a polymer include wide angle x-ray scanning (WAXS) and solid-state NMR (SSNMR).

4.4. Wide Angle X-ray Scanning of Unirradiated P1

Wide angle X-ray scattering (WAXS) is a method that can be used to analyse sub nanometre microstructures of a material or polymer, by measuring the intensity of scattered X-rays at different angles. The scattering of X-rays is due to the interaction of the incoming X-ray beam and the material. Bragg's law is used to describe the scattering of X-rays in this way,[56]

$$\sin\theta = \frac{\lambda}{2\mathrm{d}} \tag{4}$$

Where 2θ is the scattering angle, λ is the X-ray wavelength and d is the distance between crystal planes. Due to the scattering angle of X-rays being dependent on the wavelength of the X-ray beam, q is often used to describe the process, as described below. [56]

$$\mathrm{q} = \frac{4\pi}{\lambda}\sin\theta \tag{5}$$

Where q is related to the distance as described below,

$$\mathrm{q} = \frac{2\pi}{\mathrm{d}} \tag{6}$$

Our polymer P1 WAXS data is plotted in terms of q. If polymer P1 showed any signs of crystallinity due to its mild syndiotactic nature, a peak would be expected to appear in the WAXS spectra.

Figure 33, shows the WAXS spectra of unirradiated P1 dried from both THF and DCM:

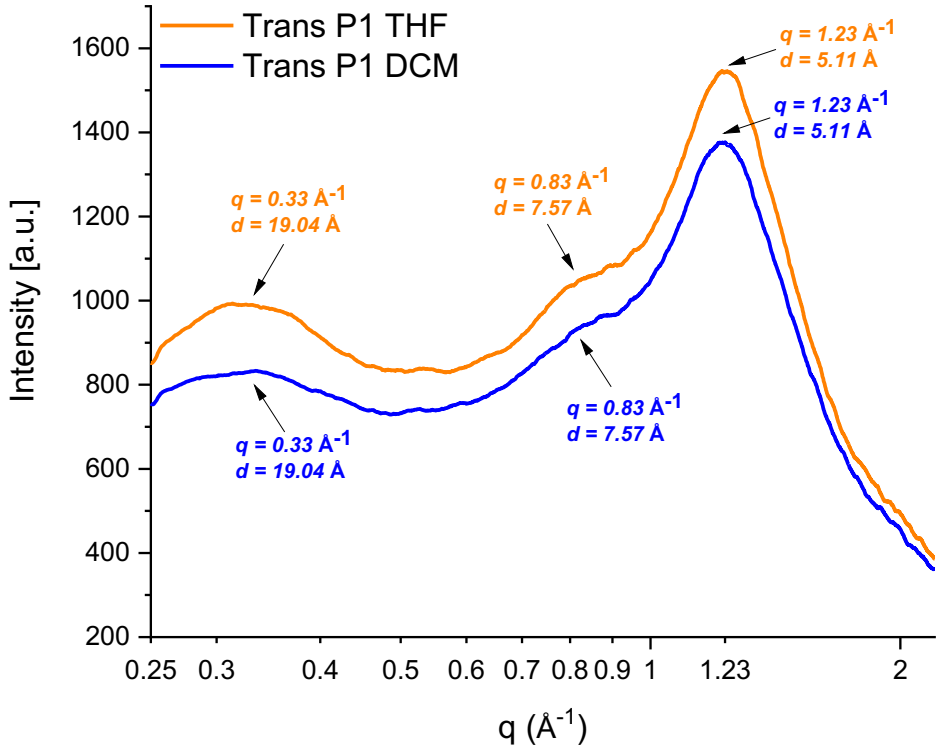

Figure 33: WAXS spectrum of unirradiated polymer P1 dried from THF and DCM.

Figure 33 shows a large peak at around a q value of 1.23 $Å^{-1}$, corresponding to a d-spacing of 5.11 Å after conversion of q to d, using equation 3 above, for unirradiated P1 dried from both DCM and THF. This q value is attributed to the distance between syn azobenzene polymer pendant units, these units are a consistent repeated structure in the polymer, which does not appear to vary between drying from DCM or THF for the unirradiated polymer. The spectrum also contains peaks at a q value of 0.33 $Å^{-1}$, corresponding to a d-spacing of 19.04 Å, attributed to the ordered spacing between polymer layers.

These results appear to contradict the DSC traces shown in Section 4.3.2, which suggested that there was no crystallinity present in unirradiated polymer P1 samples prepared with or without THF and DCM as an initial solvent. This data means that a contribution to the energy storage properties of unirradiated polymer P1 crystallinity, could still be seen in further research involving irradiated P1 despite it not being observed here.

4.5. Solid State ^{13}C NMR of Unirradiated Polymer P1

To further explore the unirradiated polymer P1 system and its structural properties, unirradiated P1 was dissolved in both THF and DCM with concentrations of ~20 g L^{-1}. The samples then had their solvents removed, by blowing under N_2 followed by 1 hour under vacuum. 40.1 mg of unirradiated P1 dried from THF and 50.2 mg of unirradiated P1 dried from DCM, was collected and submitted for a ^{13}C cross-polarisation (CP) magic-angle

spinning (MAS) NMR experiment. The ^{13}C cross-polarisation (CP) magic-angle spinning (MAS) NMR spectra for unirradiated polymer P1 dried from DCM and THF are shown below in Figure 34:

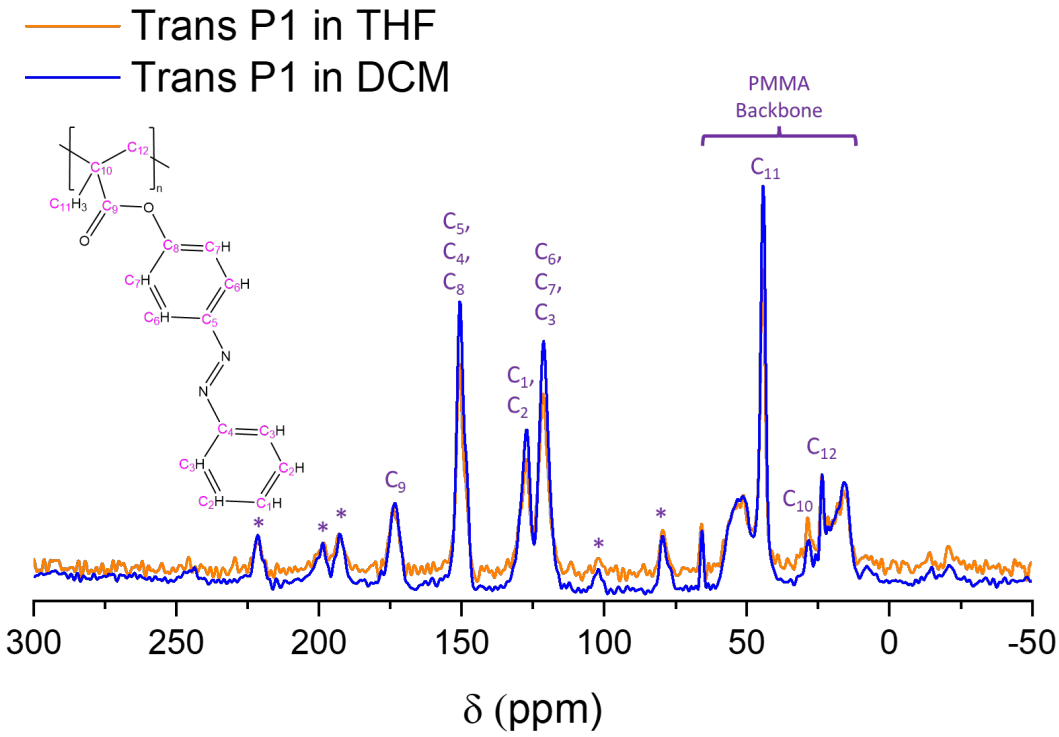

Figure 34: ^{13}C cross-polarisation (CP) magic-angle spinning (MAS) NMR spectra of unirradiated P1 dried from DCM and THF. Peaks marked with an asterisk are attributed to spinning side bands caused by the instrument.

Figure 34 shows that resonances obtained from SSNMR are comparatively broad compared to solution state NMR due to the intrinsic disorder in the solid-state polymer P1 structure. Figure 34 also shows that a single resonance is observed at ~150 ppm, corresponding to aromatic carbons in the azobenzene pendant units that are adjacent to the central N_2 double bond. There is also a pair of peaks present at 127 and 121 ppm, representing the remaining aromatic carbons in the azobenzene pendant groups. The aliphatic region shows a combination of broad and sharp peaks, which suggests that parts of the backbone are quite mobile.

Figure 34 shows no apparent difference in the structural properties of unirradiated polymer P1 when dried from THF and DCM, with no apparent difference in local ordering of polymer chains. SSNMR appears to not be sensitive to these large inter-polymer distances. Finally, it is important to note that when using magic-angle spinning, the temperature of the sample is increased by ~20 °C above room temperature, meaning the sample would reach temperatures at around 40-45 °C. This temperature is not close enough to the glass transition temperatures of the polymer, therefore, presents no issues for the spectra.

5. Exploring the Irradiated P1 System

Once the thermal properties of the unirradiated polymer were known, the irradiated polymer was obtained through solution state charging.

5.1. Solution State Charging of Polymer P1 Method

A solution state charging method allowed us to achieve successful photo switching of the *trans* polymer P1 into the *cis* photoisomer, achieving a high *cis* percentage photostationary state (PSS).

To achieve a high percentage of *cis* isomers, a solution of unirradiated P1 in THF of a concentration of 20 g L^{-1} was placed under stirring and irradiated with a 365 nm UV-lamp placed 10 cm away. The solution was irradiated for 1 hour with a 100 % lamp intensity. All charging in solution was done in THF to avoid differences in *cis* percentages at the PSS in samples prepared from different solvents. The *trans* to *cis* photoisomerisation for P1 can be visually confirmed, by the solution becoming a darker shade of orange. Once the irradiation of the P1 solution was complete, both samples were divided into two 1 mL solutions and were covered by aluminium foil. The samples were dried using N_2 blowing for 15 minutes, followed by 1 hour under vacuum. Once dry, one of the dried samples was redissolved in DCM, followed by N_2 blowing for 15 minutes and then 1 hour under vacuum.

For all solution state charging the setup outlined in Figure 35 was used.

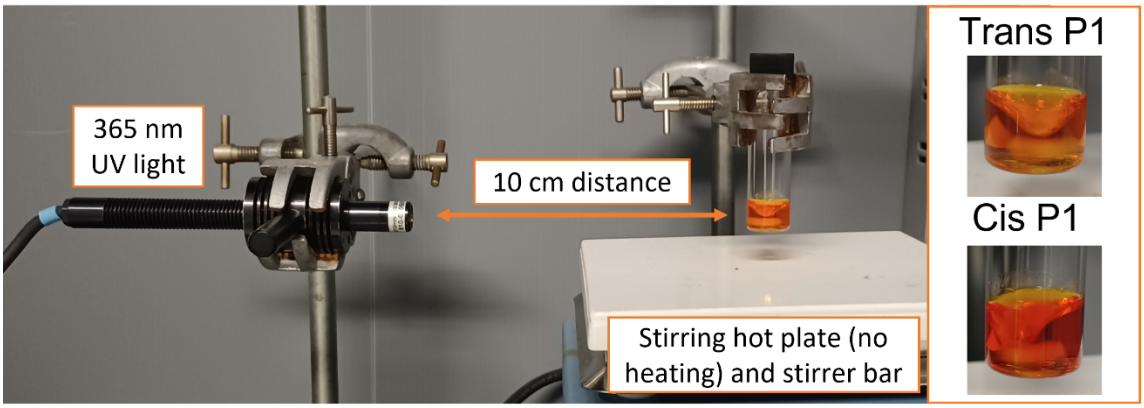

Figure 35: Image taken of P1 solution charging setup. After an hour of charging the light orange Unirradiated P1 solution becomes a dark orange Irradiated P1 solution.

Figure 35 shows a 365 nm UV-lamp placed 10 cm away from a vial containing a 2 mL solution of polymer P1 in THF with a stirrer bar in the bottom of the vial. Stirring was used to allow for increased diffusion and a more even charging of the solution, as without stirring, percentage *cis* levels were lower. This increased *cis* percentage is likely caused by increased diffusion of unirradiated P1 polymer strands, that would ordinarily be out of reach of the full intensity of the UV-lamp. Initially a lamp intensity of 50 % was used however, this

led to a low percentage of *cis* isomers (30-40 % *cis*) therefore this was changed to a 100 % intensity, leading to a consistently high percentage *cis* PSS (60-70 % *cis*). The method of calculating these percentages is shown below in Section 5.3.

5.2. UV-Vis Absorption Properties of Irradiated M1 and P1

Following irradiation of the monomer M1 and polymer P1 samples from UV-Vis Section 4.2.2, UV-Vis spectra were prepared by submitting the irradiated samples of M1 and P1 in DCM with known concentrations of 4.69×10^{-3} g L^{-1} for M1 and 5.08×10^{-3} g L^{-1} for P1.

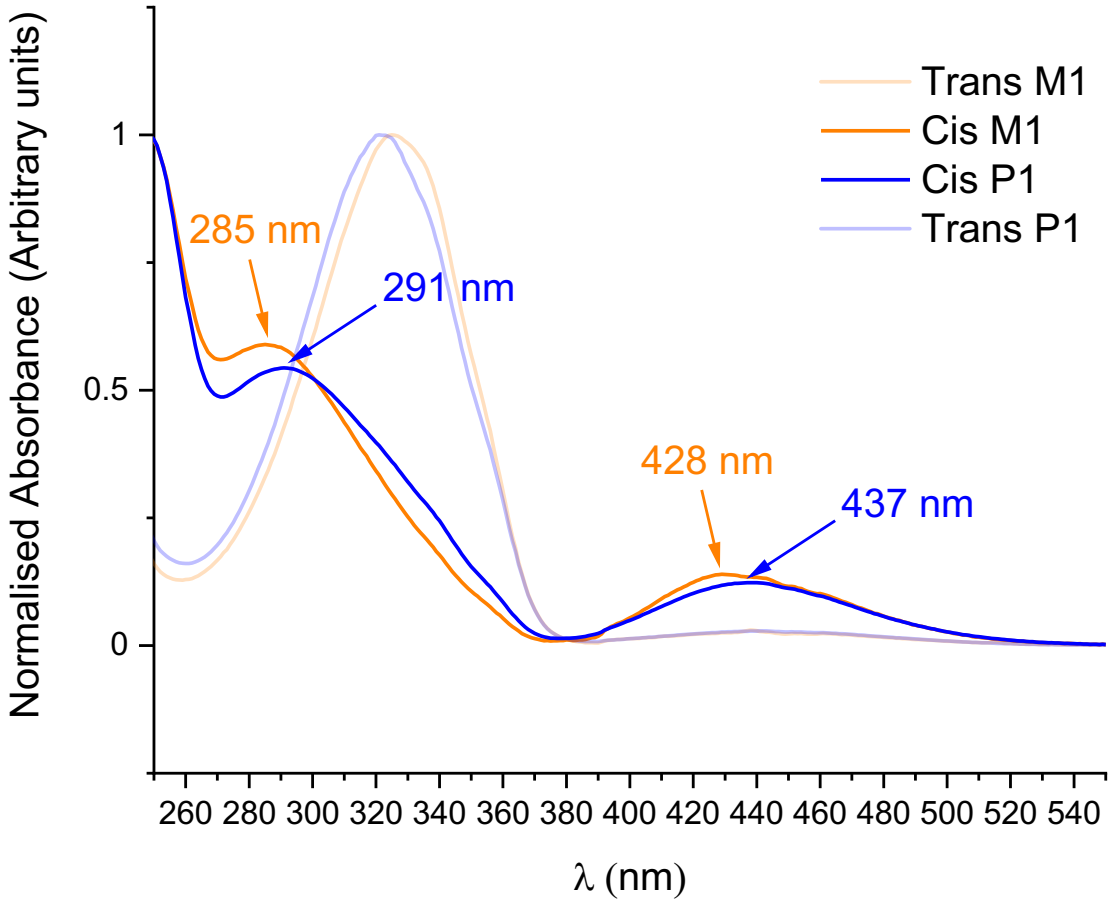

Figure 36: UV-Vis absorption spectra of irradiated M1 and P1. With the previously submitted unirradiated M1 and P1 samples made to be transparent in the spectra background for reference. The absorption values are normalised to equal 1 for comparison of absorption maxima.

Figure 36 shows the UV-Vis absorption spectra of the irradiated monomer M1 sample, with a large shift from a previous π→ π* absorption wavelength of 325 nm to 285 nm, with the forbidden n→ π* electronic transitions showing an absorption wavelength of 428 nm compared to the previous 440 nm. The irradiated polymer P1 sample shows an equally large shift from a previous π→ π* absorption wavelength of 322 nm to 291 nm, with the forbidden

n→ π* electronic transitions showing an absorption wavelength of 437 nm compared to the previous 439 nm.

5.3. Calculating the Photostationary State of Irradiated Polymer P1

To calculate the percentage of *cis* P1 present in the irradiated solution, a quantitative NMR integration method, using the ratio of *trans* to *cis* peaks in the aromatic region of the irradiated polymer P1 system, was used to calculate a percentage of *cis* molecules. A 15 g L^{-1} solution of unirradiated P1 in $CDCl_3$ was irradiated for 1 hour, under stirring, using the method and setup described in Section 4.1 Figure 32. The aromatic region of an irradiated polymer P1 with the highest recorded *cis* percentage, is shown below in Figure 37:

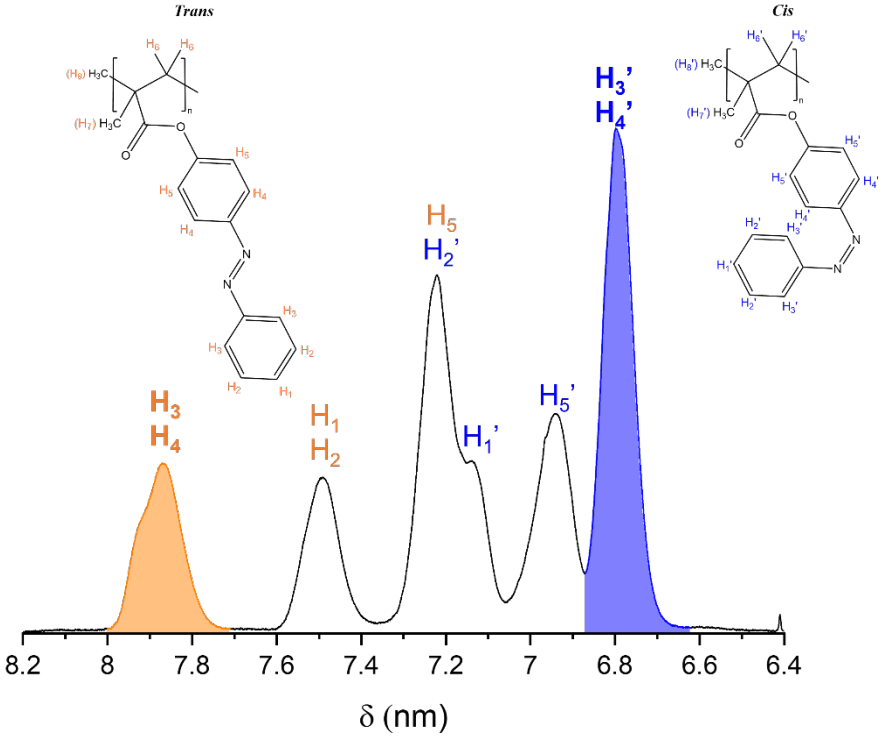

Figure 37: The aromatic region of a ^{1}H NMR spectrum of irradiated P1. Hydrogens present in trans P1 are highlighted in orange and hydrogens present in cis P1 are highlighted in blue. Integrated regions considered for the cis percentage calculation are shaded beneath the curve.

Equation 7, allows us to convert the NMR integrals of *trans* and *cis* into a 'percentage of *cis*' value, as shown below:

$$Cis\ \% = \frac{\left(\frac{\text{Cis peak area}}{\text{Cis peak protons}}\right)}{\left(\frac{\text{Cis peak area}}{\text{Cis peak protons}} + \frac{\text{Trans peak area}}{\text{Trans peak protons}}\right)} \times 100 \qquad (7)$$

Using the integrals generated in figure 37, we were able to calculate a *cis* percentage for this particular irradiated P1 system. The integrals of the H3' and H4' peak for *cis* P1 in this

system were calibrated to equal 1 therefore, the relative integrals for *trans* were also scaled as a result:

$$Cis\ \% = \frac{\left(\frac{1}{4}\right)}{\left(\frac{1}{4} + \frac{0.4623}{4}\right)} \times 100 = 68.39\%$$

5.4. Theoretical Maximum Energy Density for irradiated P1

Prior to recording a DSC of irradiated polymer P1 samples, we calculated the maximum energy density possible for an azobenzene system, to gauge the largest amount of energy produced from the *cis* to *trans* isomerisation alone, without any outside influences such as the presence of crystallinity.

Using a known value for the enthalpy of the *cis* to *trans* isomerisation of azobenzene, 49.1 kJ mol^{-1} and the molar mass of a P1 repeat unit, 252.293 g mol^{-1}, we were able to calculate the theoretical maximum energy density (ΔH_{max}) from P1 isomerisation assuming a *cis* % of 100%. As shown below.

$$\Delta H_{max} = \frac{49.1\ \text{kJ mol}^{-1}}{252.293\ \text{g mol}^{-1}} = 0.195\ \text{kJ g}^{-1} = 195\ \text{J g}^{-1}$$

Following this, using the known value for the enthalpy of fusion (ΔH_{fusion}) of azobenzene 22.53 kJ mol^{-1},[57] and the molar mass of azobenzene, 182.22 g mol^{-1}, we calculated the energy density of azobenzene crystallisation.

$$\Delta H_{fusion} = \frac{22.53\ \text{kJ mol}^{-1}}{182.22\ \text{g mol}^{-1}} = 0.12\ \text{kJ g}^{-1} = 120\ \text{J g}^{-1}$$

Adding these two energy densities would give us the maximum theoretical energy density for P1 isomerisation alongside any azobenzene crystallisation effects. This is shown below.

$$\text{Max Theoretical Energy Density} = 195\ \text{J g}^{-1} + 120\ \text{J g}^{-1} = 315\ \text{J g}^{-1}$$

Once this maximum theoretical energy density was known, any energy density values that surpassed this value, could initially be considered as being affected by something other than isomerisation alone.

5.5. Irradiated P1 Thermal Properties

To explore the thermal properties of irradiated P1, 20 g L^{-1} samples of unirradiated P1 in DCM were irradiated at 365 nm for 1 hour with a lamp intensity of 100 %, from 10 cm away. The solvent was removed by blowing the irradiated sample with N_2, followed by 1 hour under vacuum. The first and second heating curve of irradiated P1 dried from DCM were recorded

using DSC, to assess the energy density that could be reached in the charged polymer and compare it to previously reported values.

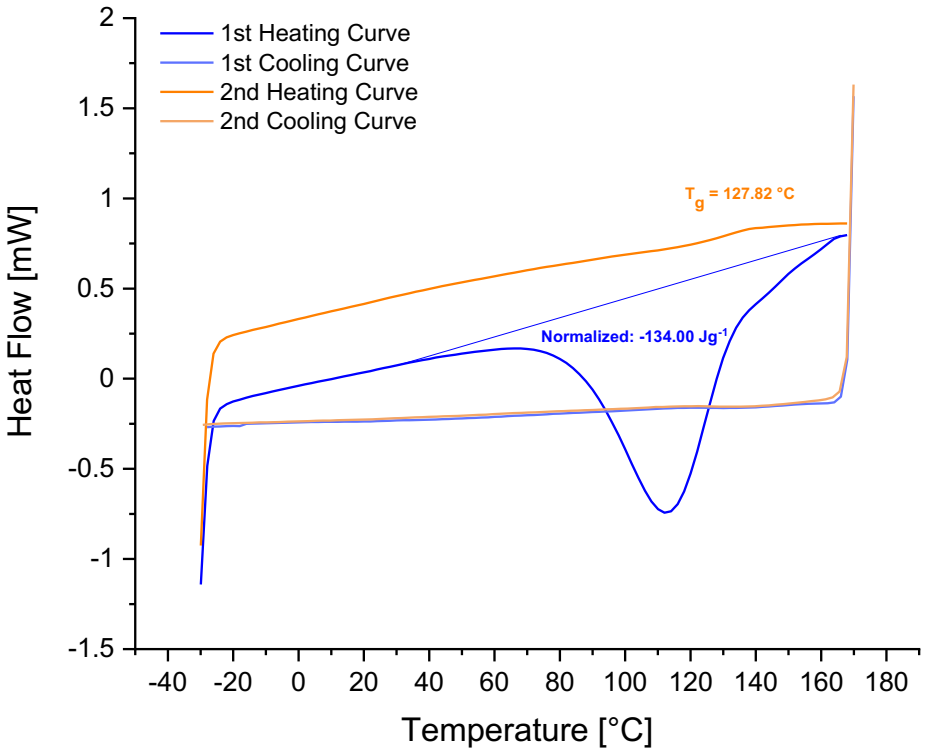

Figure 38: DSC Trace of the first heating curves of Irradiated P1 from DCM (Dark Blue) and the second heating curves (Dark Orange). Heating rate: 10 C min^{-1}, Range: -30 °C to 200 °C.

Figure 38 shows two irradiated P1 heating curves, the first heating curve (dark blue line) displays a large exotherm of 134.00 J g^{-1}, caused by the conversion of the *cis* polymer P1 back to the lower energy *trans* polymer with a *cis* percentage PSS value of 67.1 %, determined by ^{1}H NMR. The second heating curve (dark orange line) shows only the T_g at a temperature of 127.82 °C, confirming that all of the *cis* polymer molecules have returned to the *trans* state. If we were to assume a *cis* percentage of 100 % for the *irradiated* P1 system, the energy released would scale to ~200.3 J g^{-1} however, a *cis* percentage this high is unlikely to be achieved. The energy density value for P1 of 134.0 J g^{-1} at the *cis* percentage PSS of 66.8 %, is higher than previously reported exotherm values for the irradiated P1 system. These are reported to be -104.4 ± 7.2 J g^{-1} by Zhitomirsky *et al.* with no mention of the *cis* percentage PSS of the system and -95.45 J g^{-1} by Wallace *et al*. that provided a *cis* percentage PSS value of 64.2 %.[9,24] There appears to be no recrystallisation exotherm upon cooling of the now *trans* P1 system, consistent with the DSC traces discussed in Section

4.3.1, suggesting that the energy density recorded for the irradiated polymer P1 is through trans to cis reverse isomerisation alone.

This result allowed the exploration of whether large energy densities could be achieved by altering the solvent used in the irradiated P1 system as mentioned in Section 1.7.4, using samples prepared from DCM and THF just as reported by Jeong *et al*. in a similar azobenzene based polymer system. Jeong suggested that the use of different solvents, when producing a solid-state polymer film, caused differences in the energy density of the *cis* to *trans* isomerisation. Energy density values of 510 ± 115 J g^{-1} were reported for azobenzene based polymer films formed from THF and much lower values of 110 ± 25 J g^{-1} for films prepared from DCM.[44,45]

5.6. Solid-State Charging of Polymer P1

The true energy density of a solar thermal fuel system, that requires the solar thermal fuel material to be dissolved in a solvent during charging, is much lower than the reported energy density, due to the effects of dilution.[28] Therefore, it is ideal for the solar thermal fuel material to have the ability to be charged, to a high percentage of *cis* isomers, while it is in the solid state. In theory this would be difficult for a system utilising the photoisomerisation of azobenzene pendant units to achieve, due to azobenzene requiring relatively large geometrical structure changes with these changes being prohibited in densely packed crystal lattices.[38] However, the mildly syndiotactic nature of polymer P1 with an inconclusive amount of crystallinity, could provide enough space for these structural changes to occur.

Thus, producing an azobenzene based polymer, that could be charged in the solid state was the aim. To achieve thin and even layering of the polymer P1, the unirradiated polymer P1 was dissolved in DCM with a concentration of 26 g L^{-1}. The solution was then pipetted onto a Petri dish, with the diameter of the ‘puddle’ formed being no larger than the diameter of what could be consistently irradiated by a UV lamp. The sample was left in a desiccator overnight to achieve a dry sample. Once dry, the sample was irradiated by 365 nm light for 4 hours at a distance of 10 cm. Images were taken of the P1 samples every hour, during irradiation, as shown in Figure 39 below.

Figure 39: Top-down view of polymer P1 samples during irradiation at 365 nm, 10 cm away at 100 % intensity, In the solid state. Pictures were taken before irradiation (0 hours), followed by one picture every hour. The black line present on the Petri dish was placed to show an approximate area of coverage by the LED lamp.

The resulting irradiated P1 sample was submitted to NMR to determine the percentage *cis*, which was estimated to be being 19.5 %. Such a low *cis* percentage could be due to a number of factors. Figure 39 shows that the drying procedure used to prepare the solid-state sample has led to very polymer-dense regions rather than even layering of the polymer. These regions of higher density will be thicker than less dense regions, meaning that light will not penetrate the sample as effectively as it would though a less dense region. A way to avoid this, and achieve thin and even polymer layers, is through the use of spin-coating. However, this was not available at the time.

Due to the inability to produce thin and even solid-state polymer films and the steric issues present in azobenzene isomerisation, solution state charging was chosen as the method of choice, for achieving high *cis* percentage photostationary state polymer samples.

6. Solvent Effect on P1 Thermal Properties

As discussed in Section 1.7.4, in the work by Jeong *et al.* an azobenzene based polymer was dissolved in THF, followed by irradiation at 365 nm to achieve an irradiated azobenzene based polymer. The irradiated polymer samples in THF, were split into two separate solutions and then dried in vacuo. One of those samples was then left to dry for longer, while the other was redissolved in DCM, followed by drying of the irradiated polymer in DCM sample in vacuo. The general experiment used by Jeong *et al.* is shown below in Figure 40.

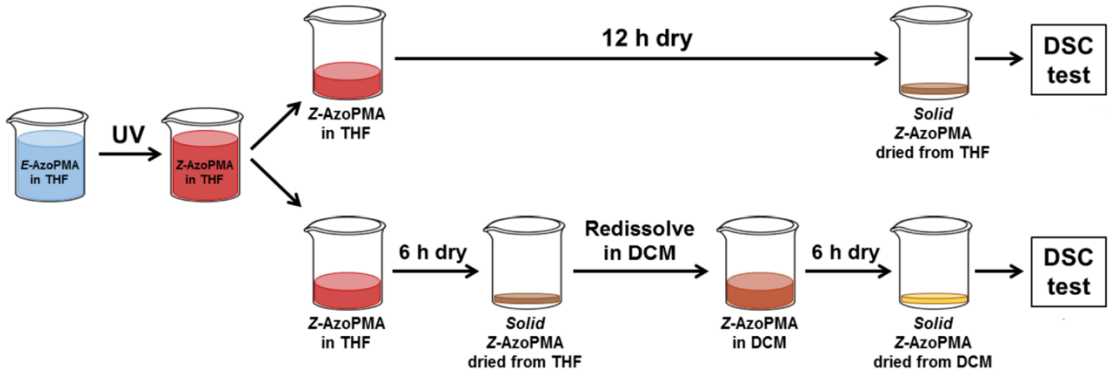

Figure 40: Scheme showing the experiment used by Jeong et al, to test their irradiated azobenzene based polymers in different solvents. Figure taken from S. P. Jeong, L. A. Renna, C. J. Boyle, H. S. Kwak, E. Harder, W. Damm and D. Venkataraman, Scientific Reports*, 2017, **7**, 1–12.*

When referencing this experiment, it was noticed that the drying times for the irradiated samples may have been too long, resulting in lower *cis* percentages and thus a similar experiment was created, that could be completed on a faster timescale, with high *cis* percentage samples. In effect, the only changes were, shorter drying times between irradiation and having a dry irradiated sample. These methods are described in Section 2**.**

6.1. Optimisation of Sample Drying Conditions

Prior to submission of irradiated polymer P1 samples to DSC, it was important that, once the P1 samples had been irradiated, the irradiated P1 films were as dry as soon possible before recording the DSC traces. Drying polymer films coated or dissolved in solvents has been modelled previously, with many industrial processes also struggling to achieve perfect drying conditions.[58,59] The removal of DCM as a solvent was much easier than removing THF from irradiated polymer P1 samples, as observed in Section 4.3.2.

Initially, 20 g L^{-1} samples of irradiated polymer P1 in THF were split into two separate round bottom flasks. The solutions were swirled to allow for air drying. Once the samples appeared dry, one of the round bottom flasks had its contents redissolved in DCM and dried using the same swirling method. Once both samples were visually dry, the irradiated P1 samples were placed under weak vacuum to remove the remaining solvent. An example of an NMR

spectra of irradiated P1 using this method is shown below, in Figure 41, showing the presence of both DCM and THF solvents, with a percentage *cis* value of 31.16 % and 34.87 % respectively.

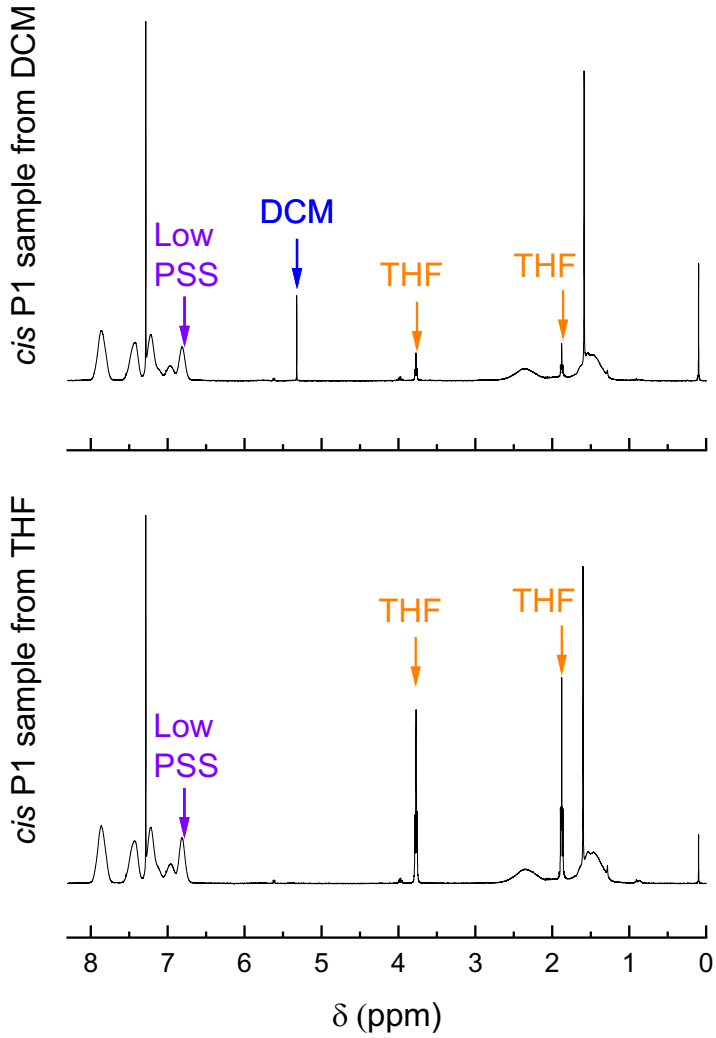

Figure 41: ^{1}H NMR of irradiated polymer P1 dried from THF and DCM, with the first drying method.

It is worth noting that, at the drying optimisation stage, the charging intensity of the 365 nm lamp was 50 % rather than the later adopted 100 % due to the charging method of the polymer not yet being optimised. Therefore, the lower *cis* percentage in all three drying methods is mostly due to this fact.

Following this, the procedure was amended to increase the surface area of the irradiated P1 drying surface, by using Petri dishes instead of round bottom flasks, while also utilising N_2 blowing to aid the drying process. The use of Petri dishes did not appear to decrease the time taken for the irradiated P1 samples to appear dry and also made sample collection unexpectedly more difficult. Following solvent evaporation through air drying, the irradiated

P1 samples were subject to overnight vacuum in a desiccator. An example of an NMR spectra of irradiated P1 using this method is shown below, in Figure 42.

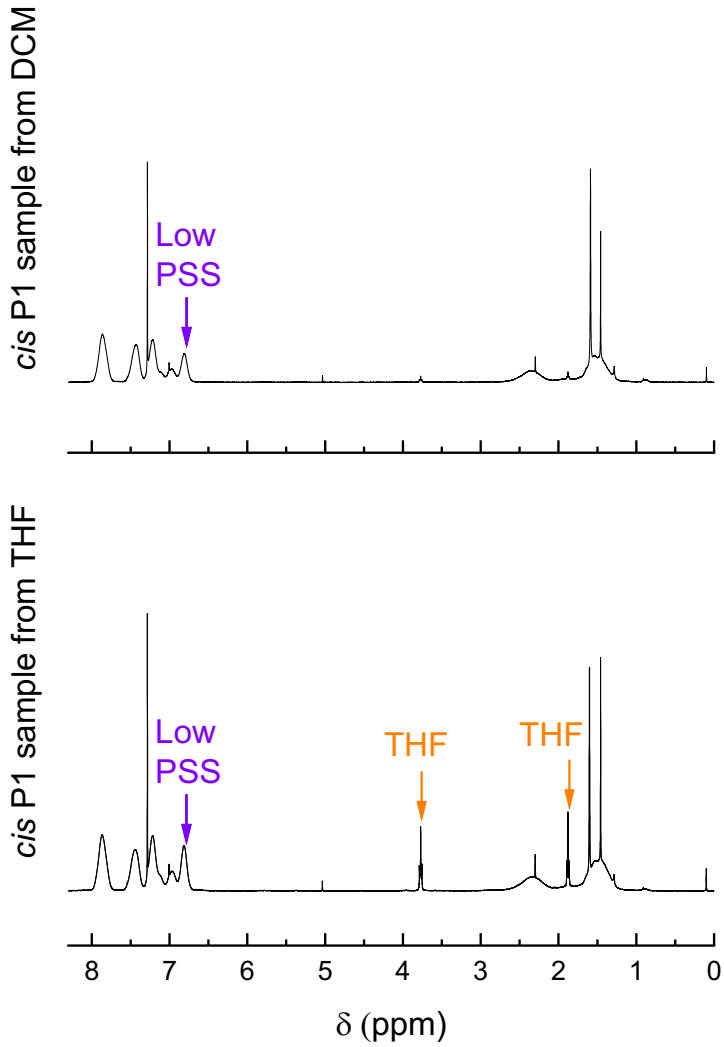

Figure 42: ^{1}H NMR of irradiated polymer P1 dried from THF and DCM, with the second drying method.

Figure 42 shows the presence of no DCM and very little THF solvents in the sample dried from DCM but samples dried from THF still show a large THF presence. The percentage *cis* values for samples dried from DCM and THF are 38.47 % and 32.52 % respectively.

Therefore, irradiated P1 samples were dried using larger round bottom flasks along with N_2 blowing, that could be attached to a Schlenk line. It is also noted that the vacuum used in the previously mentioned drying methods was weak, which was not by design but by human error therefore, once fixed, this allowed for the next drying method to utilise a full vacuum. An example of an NMR spectra of irradiated P1 using this method is shown below, in Figure 43.

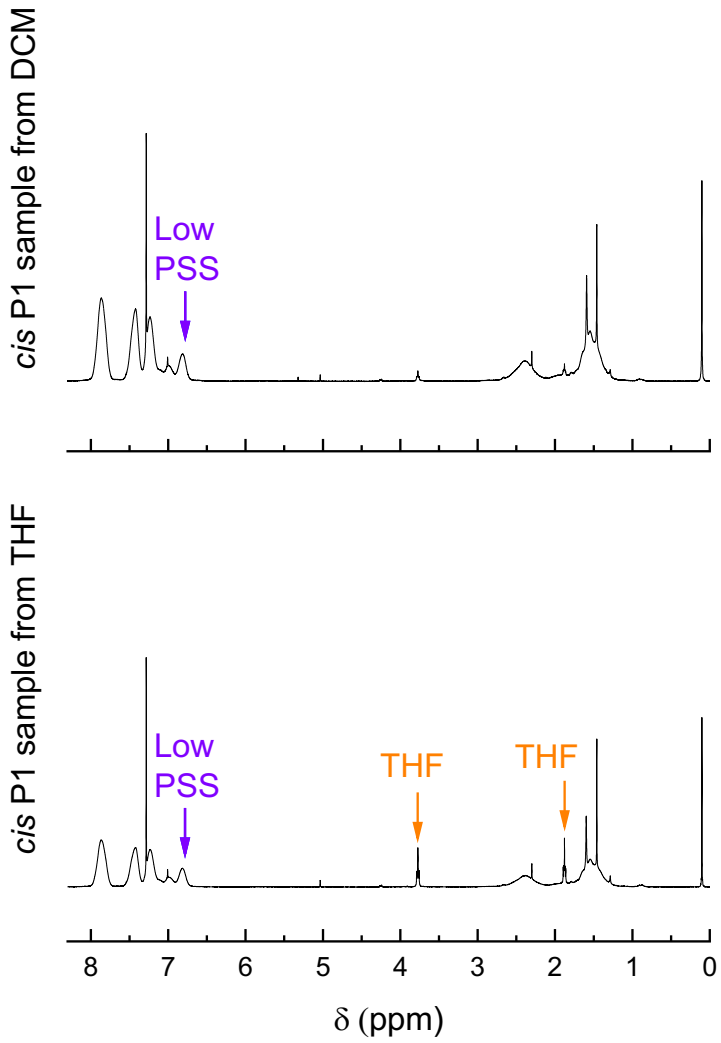

Figure 43: ^{1}H NMR of irradiated polymer P1 dried from THF and DCM, with the third drying method.

Figure 43 shows little to no presence of THF or DCM remaining in the sample dried from DCM, while the sample dried from THF still contains residual THF however, this was much less than in the first or second drying methods. The percentage *cis* values for samples dried from DCM and THF were recorded as 22.22 % and 24.97 % respectively.

Ultimately, removing the solvent THF continued to prove quite challenging, with a completely dry sample from THF appearing not to be possible. Due to time constraints, the decision was taken to choose this method as it resulted in the driest samples. The low photostationary states in all 3 methods were later improved by using 100 % intensity light during irradiation, rather than the 50 % used for these samples.

6.2. DSC of Irradiated Polymer P1

To record DSC traces of irradiated polymer P1 dried from DCM and THF, a 20 g L^{-1} solution of unirradiated polymer P1 in THF was irradiated at 365 nm for 1 hour at a distance of 10 cm away, with an irradiation intensity of 100 %. The irradiated P1 solution was then split into two

separate round bottom flasks and dried using N_2 blowing and then drying in vacuo. One of the samples was then redissolved in DCM and dried using N_2 blowing and then drying in vacuo. Once the samples were dried, they were both submitted to ^{1}H NMR to obtain the percentage *cis* of the sample and DSC curves were obtained.

The DSC traces of irradiated P1 dried from DCM and THF are shown below in Figure 44.

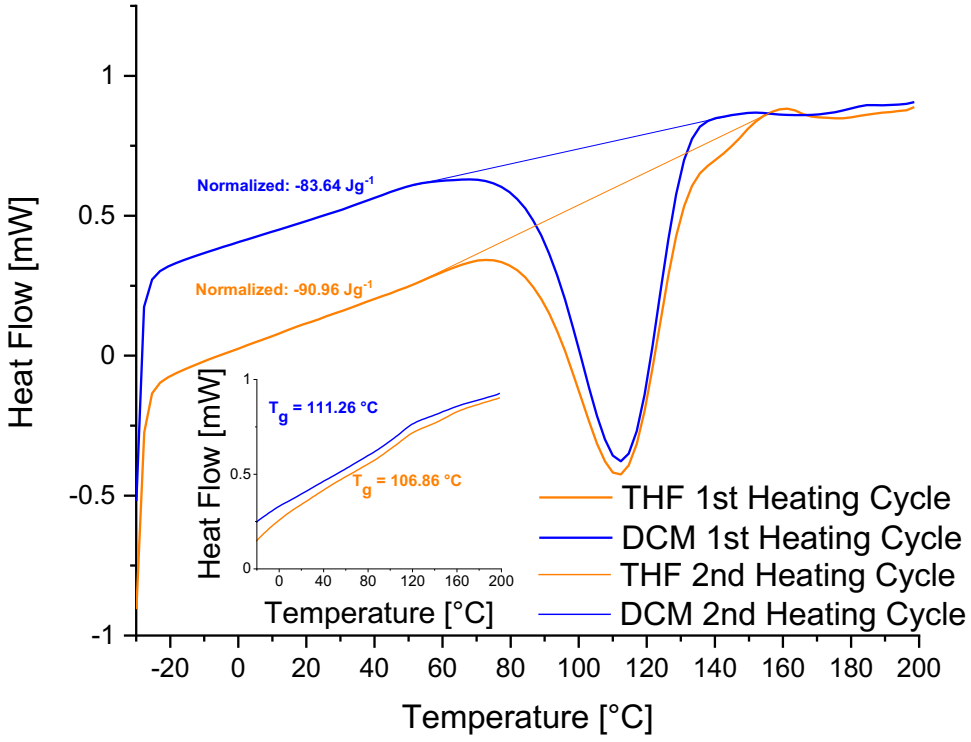

Figure 44: DSC Trace of the 1st heating curves of irradiated P1 dried from DCM (Blue curves) and THF (Orange Curves), with an inset graph of the 2nd heating curves for both. Heating rate: 10 Cmin^{-1}, Range: -30 °C to 200 °C.

The exotherms produced by *cis* to *trans* isomerisation in both of the first heating curves of P1 from DCM and THF appear to be very similar, with the recorded energy densities being -83.64 J g^{-1} (*cis* percentage: 61.8 %) and -90.96 J g^{-1} (*cis* percentage: 63.1 %) for DCM and THF respectively. Figure 44 appears to show that there is little to no difference in the energy densities between irradiated polymer P1 when dried from DCM or THF.

It is however, important to note that despite the polymer P1 samples appearing to be dry, obtaining completely dry samples of the irradiated polymer was not achieved, with both samples containing traces of THF remaining from the initial irradiated solution. Therefore, it is inconclusive on whether the energy densities of the irradiated polymer P1, would change if the samples were completely dry.

6.2.1. Optical Microscopy of Irradiated Polymer P1

Similarly, to section 4.3.2, images of irradiated P1 samples dried from DCM and THF were produced at specific temperatures, to gain an insight into how the polymer isomers change to the naked eye. Figure 45 and 46 below, show the separated DSC traces used in Figure 44, accompanied by relevant images at specific temperatures for irradiated P1 dried from DCM and THF. Samples were irradiated using the same procedure as mentioned at the beginning of Section 6.1.1, with one of the two irradiated samples being redissolved in DCM to obtain a sample dried from DCM. The irradiated solutions were then pipetted onto a microscope slide and left to dry within a desiccator under vacuum. Once the samples were dried, the microscope slides were placed into a hot stage, mounted below a bright field light microscope. Images were taken at 10 °C steps in a 30 to 200 °C heating cycle, followed by images being taken at 5 °C steps upon a 200 to 30 °C cooling cycle, to imitate conditions in a DSC trace. Further details of the procedure can be found in the experimental section. Figure 45 below shows the DSC data for irradiated polymer P1 dried from DCM, with accompanying optical microscopy images at certain temperatures.

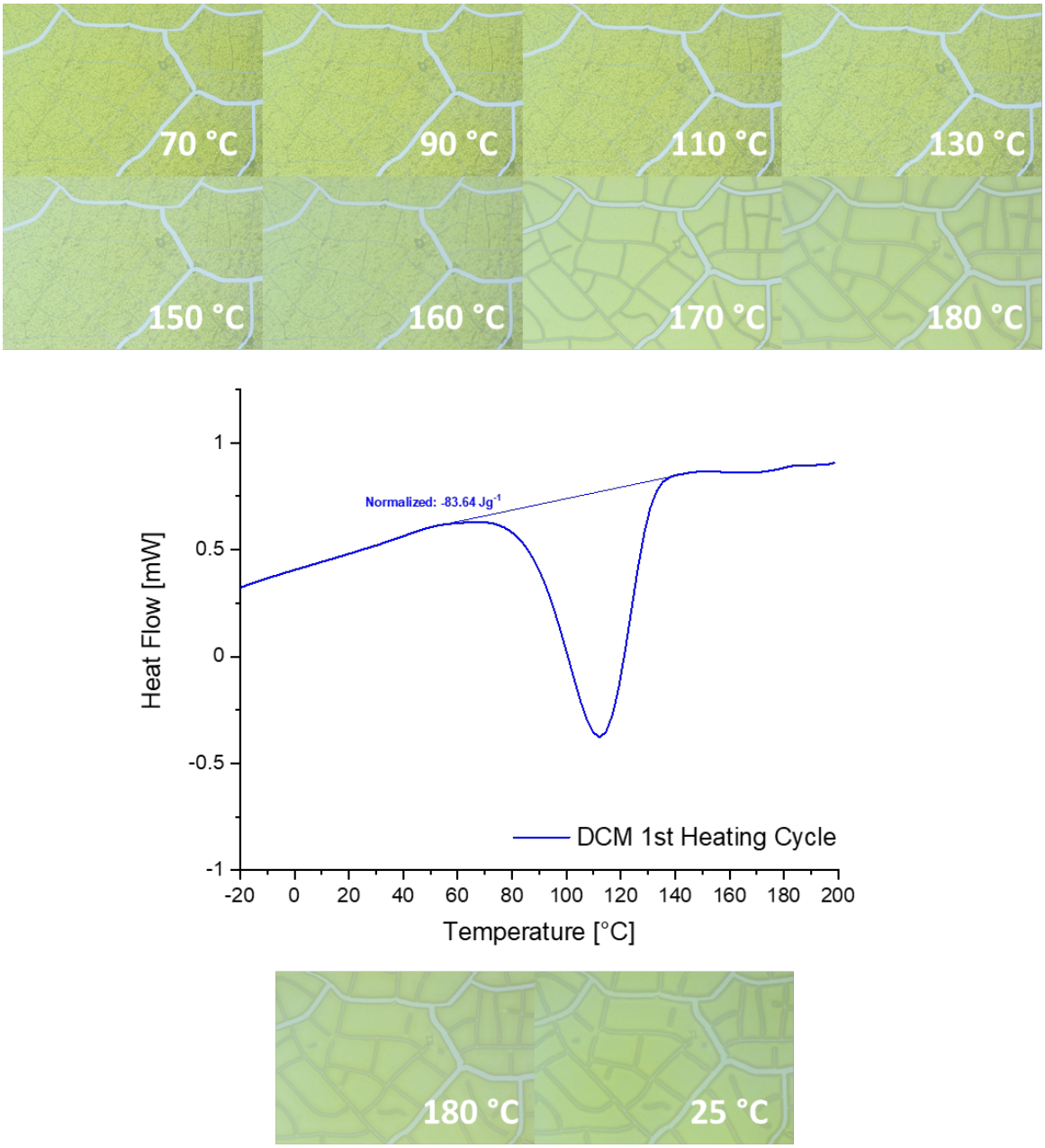

Figure 45: DSC trace of irradiated P1 dried from DCM, accompanied by optical microscopy images of irradiated P1 films formed from DCM while heating (above DSC Trace, 70 °C to 180 °C) and while cooling (below DSC trace 180 °C to 25 °C), with temperatures of interest highlighted.

In Figure 45, we can see that the irradiated P1 film formed from DCM is thin and uniform. At 70 °C, we see that the film has a slight orange hue to it suggesting a high presence of *cis* polymer P1. As the temperature increases from 70-150 °C the colour of the material changes.

There are not many other visual changes in the P1 film, other than an apparent change in texture between 160-170 °C. Just like in Section 4.3.2, with our unirradiated P1, there is little to no visual change in the polymer upon cooling at 5 °C min^{-1}. Figure 46 below, shows the

DSC data for irradiated polymer P1 dried from THF, with accompanying optical microscopy images at specific temperatures.

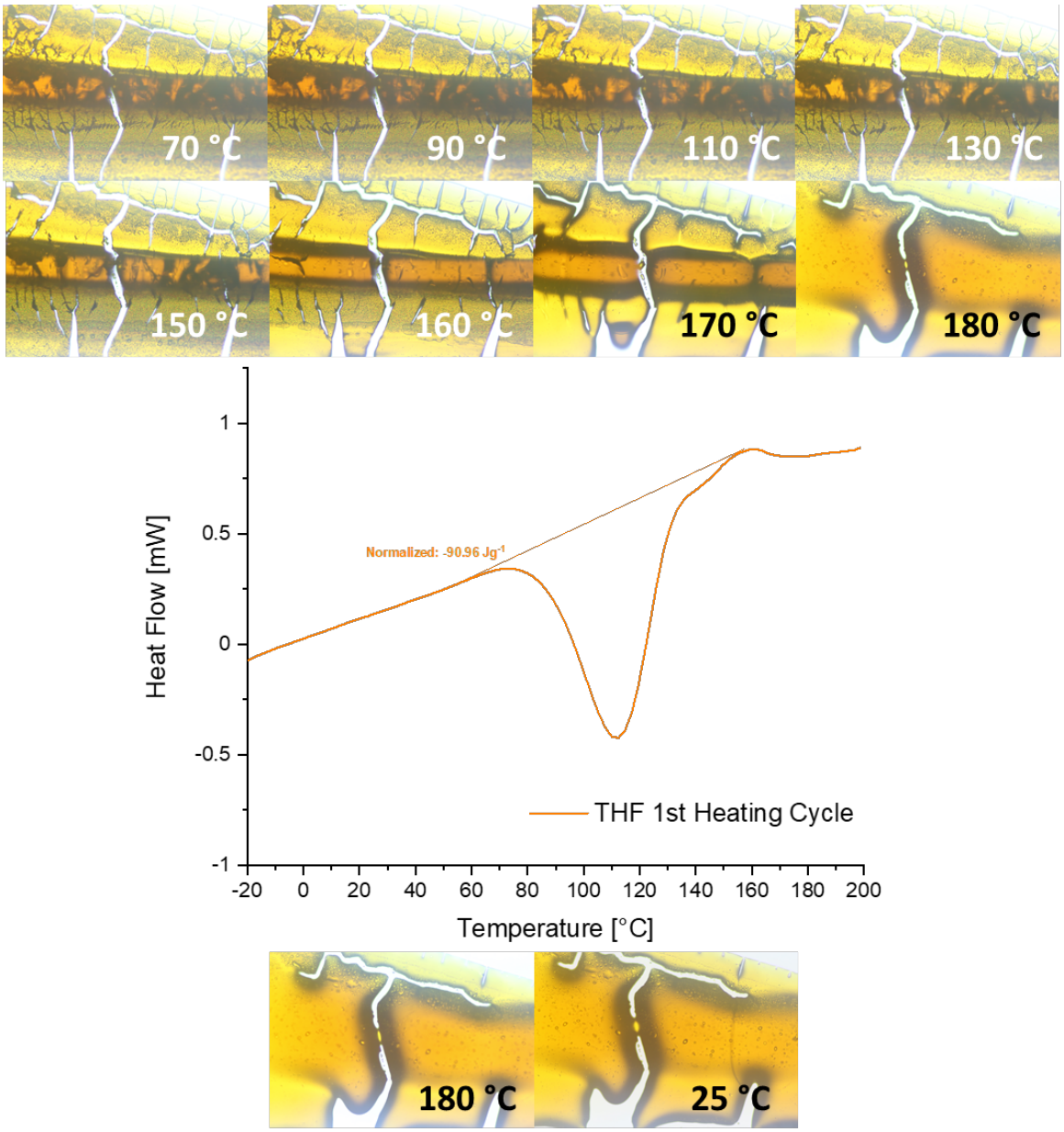

Figure 46: DSC trace of irradiated P1 dried from THF, accompanied by optical microscopy images of irradiated P1 films formed from THF while heating (above DSC Trace, 70 °C to 180 °C) and while cooling (below DSC trace 180 °C to 25 °C), with temperatures of interest highlighted

In Figure 46, the irradiated P1 film formed from THF appears to be much thicker and bolder in colour. The dark orange coloured sample appears to be too thick to show a clear colour change upon *cis* to *trans* isomerisation. In the temperature region of 160-170 °C the polymer sample appears to change texture just like its DCM counterpart. The THF sample shows little to no change upon cooling at a rate of 5 °C min^{-1}.

As expected, the polymer sample dried from THF contains bubbles, likely from retention of THF or water that could not be removed from drying. This further suggests the need for a longer drying period or a more optimised drying procedure, to see differences between these samples more clearly.

6.3. WAXS of Irradiated Polymer P1 Compared to Unirradiated P1

Earlier in Section 4.4, it was shown that the WAXS spectra for unirradiated polymer P1 samples. Irradiated polymer P1 samples were prepared using the same procedure as described in Section 6.2, with irradiated polymer P1 dried from THF and DCM samples placed in vials and submitted to the WAXS instrument.

The WAXS spectra for irradiated polymer P1 samples dried from THF and DCM is shown below.

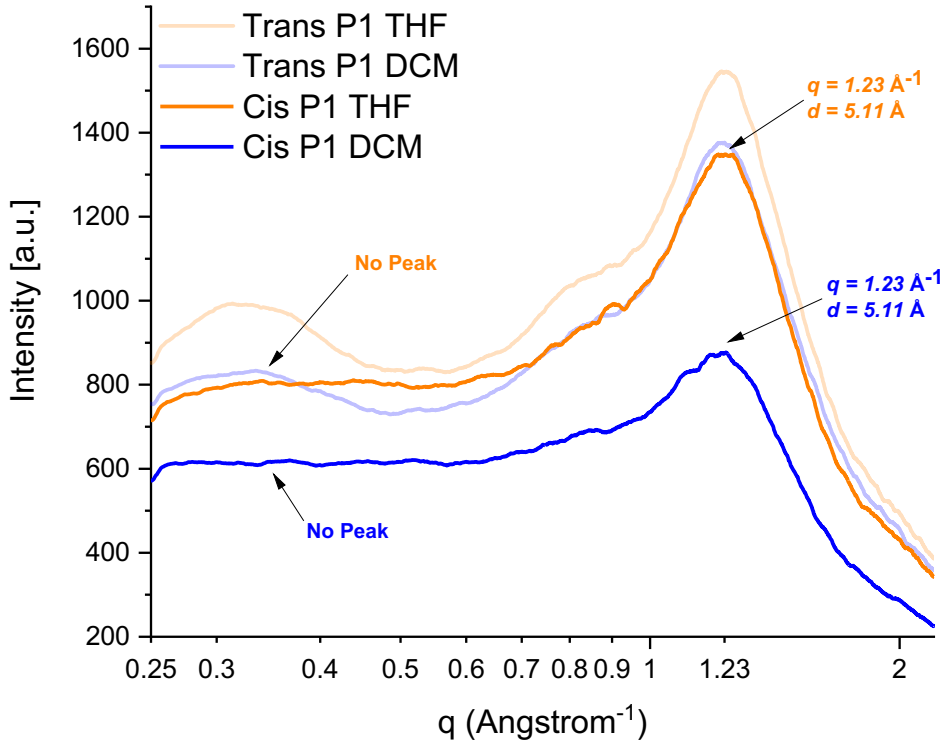

Figure 47: WAXS spectrum of irradiated polymer P1 dried from THF and DCM. The previously shown, WAXS spectrum of unirradiated polymer P1, is shown in the background for reference.

Figure 47 shows a peak at a q value of ~1.23 $Å^{-1}$, corresponding to a d-spacing of 5.11 Å, for both irradiated polymer P1 samples dried from THF and DCM. As mentioned earlier, this is the value attributed to the distance between *syn* azobenzene polymer pendant units and it is expected that this value would not change significantly, between the irradiated and unirradiated forms of the polymer.

Figure 47 also shows no sign of a peak between q values of 0.3-0.4, suggesting that there is no crystallinity in the irradiated form of polymer P1. This is in contrast to the unirradiated

polymer P1, which showed q values of 0.33 $Å^{-1}$ (19.04 Å). Both sets of WAXS data for irradiated and unirradiated polymer P1 appear to contradict the DSC data, with none of the DSC traces showing the presence of a melting endotherm or recrystallisation exotherm.

WAXS data for a similar azobenzene based polymer, with a differing end group, made by Jeong *et al*. is shown below in Figure 48.

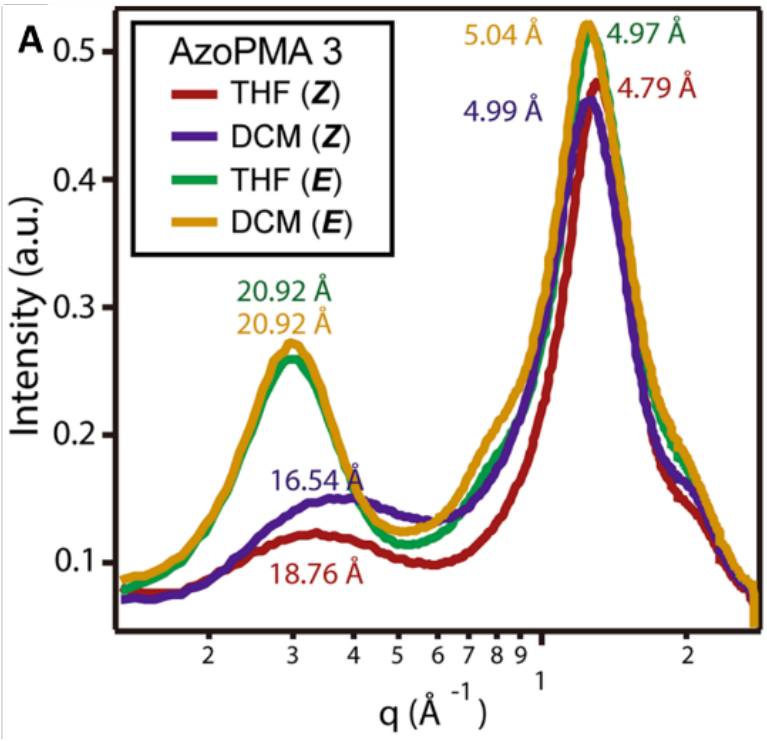

Figure 48: WAXS data for an azobenzene based polymer synthesised by Jeong et al. for the irradiated polymer in; THF (red line) and DCM (purple line) with the unirradiated polymer in THF (green line) and DCM (yellow line). Spectrum taken from S. P. Jeong, L. A. Renna, C. J. Boyle, H. S. Kwak, E. Harder, W. Damm and D. Venkataraman, Scientific Reports, *2017, **7**, 1–12.*[44]

Figure 48 appears to show crystallinity in both, the irradiated and unirradiated polymer samples. This data is certainly comparable to polymer P1 in that, the distance between *syn* azobenzene units is between 5.04-4.79 Å, with polymer P1 having d-spacings of 5.11 Å in this region. The irradiated polymer samples from the Jeong *et al.* paper also appear to show a much lower amount of crystallinity than in the unirradiated sample.[44]

The main differences between Figure 48 and polymer P1 data in Figure 47 are that the lower d-spacing values for the distance between *syn* azobenzene pendant groups does vary slightly for the azobenzene based polymer dried from THF. Also, the irradiated version of the Jeong *et al.* azobenzene based polymer does display some crystallinity in the irradiated sample, rather than none, suggesting that the irradiated polymer is much more disordered than the unirradiated polymer in both our polymer P1 and the similar polymer made by Jeong *et al*. It should be noted however, that these polymers did contain different end

groups, which could have contributed to a more ordered polymer, so direct comparisons cannot be made.

Despite this, the appearance of crystallinity could be a contributing factor to the very high energy densities of 500 ± 115 J g^{-1} achieved by Jeong *et al.* Something which we aimed to achieve with our mildly syndiotactic polymer P1.

6.4. Solid-State NMR of P1

To further analyse whether there were any structural differences between the *cis* or *trans* isomers of the polymer dried from DCM and THF, a 15 g L^{-1} solution of unirradiated P1 was placed in a vial and irradiated for 2 hours at 365 nm with a lamp intensity of 100 % from a distance of 10 cm. The irradiated polymer was then dried via N_2 blowing, followed by drying under vacuum. The dry sample was then collected, with a 39.2 mg sample submitted for a ^{13}C cross-polarisation (CP) magic-angle spinning (MAS) NMR experiment, with a 15 g L^{-1} solution state NMR also recorded to confirm the *cis* percentage of the sample, which was recorded as being 66.08 % *cis* isomers. Only irradiated polymer P1 dried from DCM SSNMR spectra were produced, due to technical difficulties in preparing irradiated polymer P1 SSNMR samples dried from THF

Figure 49 shows ^{13}C CPMAS NMR spectra of irradiated and unirradiated polymer P1 samples obtained from DCM solutions.

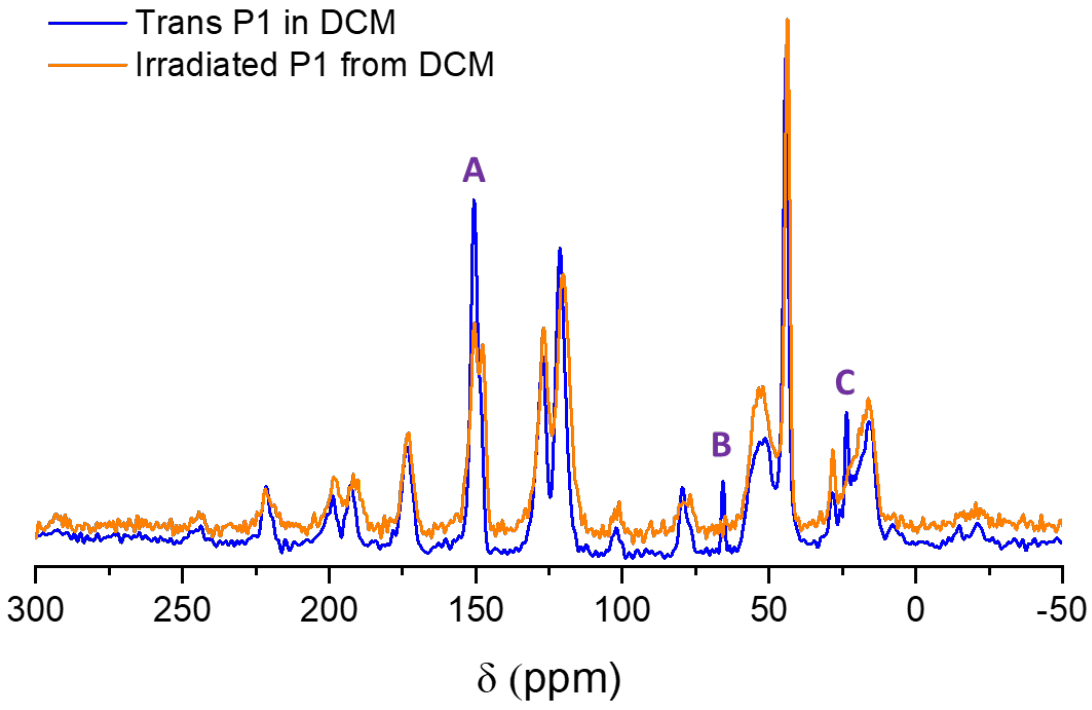

Figure 49: ^{13}C cross-polarisation (CP) magic-angle spinning (MAS) NMR spectra of irradiated and unirradiated P1 dried from DCM.

Just as in Section 4.5 Figure 34, the resonances in the SSNMR spectra are comparatively broad compared to solution state NMR. In Figure 49, point A is situated in the aromatic region, here an additional peak arises in the irradiated sample. Initially, the unirradiated sample showed a single peak at 150 ppm attributed to the aromatic carbons adjacent to the N_2 double bond of the azobenzene pendant group. Upon irradiation, the intensity of this peak at 150 ppm decreases, followed by an additional peak at 148 ppm. This is consistent with a light-induced structural change taking place in the azobenzene pendant units. Despite this difference, it is important to note that the CPMAS NMR experiment is not intrinsically quantitative therefore, any attempt to integrate this data to gain a percentage *cis* value would be impossible. However, qualitative information can be gained from relative changes in intensity.

Changes are also observed in the aliphatic regions of the spectra with points B and C, with the 2 peaks previously seen in the aliphatic region of the unirradiated sample disappearing. The disappearance of peaks B and C suggest that the structure and mobility of the PMMA backbone could be seeing subtle changes, caused by the isomerisation of *trans* polymer P1 to the *cis* isomer.

Broadening of the polymer itself while in solution combined with small natural chemical shift changes results in spectra that are similar. Overall, it appears that SSNMR is not very sensitive to changes in P1 isomers.

7. Conclusion

The overall aim of this project was to synthesise an azobenzene-based PMMA polymer that could be charged in the solid state, while also exploring the level of crystallinity contributions to the overall energy density of the polymer solar thermal fuel system, via close packing or π-π stackings as a result of the polymer tacticity. This was attempted by synthesising and investigating an azobenzene PMMA polymer, synthesised by free radical polymerisation for its structure, solid state morphology and energy storage properties in solution and in the solid state.

The polymer properties were characterised by solution state ^{1}H NMR, UV-vis, DSC, WAXS, optical microscopy and solid state ^{13}C NMR. The tacticity of the polymer was also calculated, through the use of the α-methyl region of ^{1}H NMR spectrum, giving an insight into the structure-property relationships of the polymer. It was decided that the tacticity of the polymer P1 was a mild syndiotacticity with a P_r value of 0.77, showing that a polymer synthesised by free-radical polymerisation could achieve this tacticity.

The energy release properties of the polymer were also studied, considering the theoretical limitation on the energy density of the polymer, with the limit being calculated as being 315 J g^{-1}. Irradiation of the polymer with 365 nm light, enabled the determination of the effect on the molecule's absorption properties by UV-vis. A shift from a previous π→ π* absorption wavelength of 322 nm to 291 nm and the forbidden n→ π* electronic transitions showing an absorption wavelength of 437 nm compared to the previous 439 nm confirmed a change in the polymer. The structure and purity of polymer P1 was confirmed by ^{1}H NMR and comparisons to previous literature. The percentage *cis* values for the polymer, were calculated during experiments, using the aromatic region of the ^{1}H NMR spectrum.

Irradiated polymer P1 with 365 nm light resulted in cis percentages of around 60-70 % for most experiments, with a comparatively high energy density of 134 J g^{-1} being achieved by P1 dried from DCM. Polymer P1 was dissolved in and dried from both THF and DCM following irradiation, to determine whether the energy release properties of the system would change in these solvents, there was no apparent difference in the energy densities reported with energy densities of 83.64 J g^{-1} (cis percentage: 61.8 %) and -90.96 J g^{-1} (cis percentage: 63.1 %) being recorded for DCM and THF respectively. These results are not fully conclusive due to a not fully optimal drying method for P1 films dried from THF.

The ability of the irradiated and unirradiated polymer to crystallise when dried from THF and DCM was also explored. DSC analysis showed no presence of an additional melting endotherm or recrystallisation exotherm upon cycling. WAXS data appeared to contradict

this result with an apparent small level of crystallinity in the unirradiated form of the polymer, indicated by an additional peak at the q value of 0.33 $Å^{-1}$, corresponding to a d-spacing of 19.04 Å, attributed to the ordered spacing between polymer layers. No evidence was found to support any contribution of polymer crystallinity to a higher energy density in polymer P1.

Solid-state charging of the polymer via drop casting and irradiation at 365 nm was unsuccessful with the polymer only reaching a low cis percentage of around 19.5 %. 13 C CPMAS experiments were carried out to assess the sensitivity of the experiment to differences in P1 isomers. Overall, it appeared that SSNMR was not very sensitive to changes in P1 isomers however, there were some small differences present.

7.1. Future work/ Outlook

Future works should continue to explore the P1 polymer system, with the ability to fully dry polymer films produced being a priority. Polymer P1 could be tailored by increasing the amount of π- π bonding between polymer layers, to further explore the potential of phase transitions contributing to an increased energy density of a polymer based solar thermal fuel system. On the same note, polymer P1 could potentially be altered to make the melting point of the *cis* isomer be below room temperature, to enable for ambient heat melting at or below room temperature and further explore the phase transition effect, this could be done by adding additional functional groups to the polymer backbone to enable it to move even more freely, as well as adding more branched pendant groups. The polymer P1 system could be compared to liquid crystal polymers which can show a greater degree of localised crystallinity, to explore the contribution of crystallinity to a higher energy output further. The backbone structure and T_g of a polymer could also be explored to see how they may affect the energy density.

Additionally, the drying methods for removal of THF and DCM could be improved by potentially increasing the amount of time under vacuum, while ensuring that *cis* to *trans* isomerism cannot occur readily. The choice of solvent could also be assessed, to see whether another solvent has any higher or lower affinity to the polymer P1 backbone and potentially induce more aggregation in the system. If overnight DSC samples were possible, it may have been beneficial to run longer scans to visualise heat flows in more detail and potentially spot any crystallinity in the *trans* P1 system, this could be something to explore.

Spin casting could be introduced when preparing solid-state films to allow for a more even spread of polymer sample to properly assess the materials solid-state charging ability. Also,

if there was a way to spin cast irradiated and unirradiated polymer films onto a microscopy slide, without losing too much of the *cis* percentage in the sample, this could lead to some clearer optical microscopy images.

The solid-state 13 C CPMAS experiment could be repeated to include both *cis* and *trans* forms of polymer P1 in DCM and THF, to provide an even more detailed look at the system in different solvents.

8. References

1 IPCC, Summary for policy makers, https://www.ipcc.ch/sr15/chapter/spm/. Date Accessed: 20/03/2021

2 K. Whiting, L. G. Carmona, A. Carrasco and T. Sousa, *Energies (Basel)*, 2017, **10**, 1-21.

3 T. J. Kucharski, Y. Tian, S. Akbulatov and R. Boulatov, *Energy and Environmental Science*, 2011, **4**, 4449–4472.

4 B. Looney, *Statistical Review of World Energy, 2020 | 69th Edition*, 2020, **69**, 40-68.

5 A. D. Carlo, E. Lamanna and N. Y. Nia, in *Ecohouse*, Taylor and Francis, 2014, pp. 171–202.

6 L. Dong, Y. Feng, L. Wang and W. Feng, *Chemical Society Reviews*, 2018, **47**, 7339–7368.

7 Y. Tian and C. Y. Zhao, *Applied Energy*, 2013, **104**, 538–553.

8 A. M. Kolpak and J. C. Grossman, *Nano Letters*, 2011, **11**, 3156–3162.

9 D. Zhitomirsky, E. Cho and J. C. Grossman, *Advanced Energy Materials*, 2016, **6**, 1–8.

10 D. Zhitomirsky and J. C. Grossman, *ACS Applied Materials and Interfaces*, 2016, **8**, 26319–26325.

11 E. N. Cho, D. Zhitomirsky, G. G. D. Han, Y. Liu and J. C. Grossman, *ACS Applied Materials and Interfaces*, 2017, **9**, 8679–8687.

12 D. H. Waldeck, *Chemical Reviews*, 1991, **91**, 415–436.

13 Y. Kanai, V. Srinivasan, S. K. Meier, K. P. C. Vollhardt and J. C. Grossman, *Angewandte Chemie - International Edition*, 2010, **49**, 8926–8929.

14 M. D. Kilde, M. Mansø, N. Ree, A. U. Petersen, K. Moth-Poulsen, K. v. Mikkelsen and M. B. Nielsen, *Organic and Biomolecular Chemistry*, 2019, **17**, 7735–7746.

15 H. M. D. Bandara and S. C. Burdette, *Chemical Society Reviews*, 2012, **41**, 1809–1825.

16 G. Hartley, *Nature*, 1937, **14**, 281.

17 B. L. Dale, 2020, Thesis.

18 E. Durgun and J. C. Grossman, *Journal of Physical Chemistry Letters*, 2013, **4**, 854–860.

19 J. Lemaire, *Isomerisation photochimique de l'azobenziine en solution*, 1973, **52**, 1848-1858.

20 G. Gauglitz and S. Hubig, *Journal of Photochemistry*, 1985, **30**, 121–125.

21 E. Karls, S. Hubig, 1984. Thesis.

22 Ľ. Vetráková, V. Ladányi, J. al Anshori, P. Dvořák, J. Wirz and D. Heger, *Photochemical and Photobiological Sciences*, 2017, **16**, 1749–1756.

23 J. Clark, The Beer Lambert Law, https://chem.libretexts.org/Bookshelves/Physical_and_Theoretical_Chemistry_Textbook_Maps/Supplemental_Modules_(Physical_and_Theoretical_Chemistry)/Spectroscopy/Electronic_Spectroscopy/Electronic_Spectroscopy_Basics/The_Beer-Lambert_Law. Date accessed: 10/01/2022

24 C. N. Wallace, *Solar Thermal Fuels for Automotive Applications*, 2021. Thesis.

25 B. Ernst Fischer, *Temperature Dependence of Photoisomerization Equilibria. Part I. Azobenzene and the Azonaphthalenes*, UTC, 1955, **23**, 7.

26 A. W. Adamson, A. Vogler, H. Kunkely and W. Rudolf, *J Am Chem Soc*, 1978, **100**, 1298–1300.

27 M. Park, X. Zhang, M. Chung, G. B. Less and A. M. Sastry, *Journal of Power Sources*, 2010, **195**, 7904–7929.

28 K. Masutani, M. A. Morikawa and N. Kimizuka, *Chemical Communications*, 2014, **50**, 15803–15806.

29 A. P. Kirk, in *Solar Photovoltaic Cells*, Elsevier, 2015, pp. 9–24.

30 M. Kazuhiro, T. Kazitoshi, N. Toshinori and Y. Yoshinori, *Chemical Letters*, 1980, **9**, 1259–1262.

31 D. P. Schwendiman and C. Kutal, *Inorganic Chemistry*, 1977, **16**, 719–721.

32 C. Philippopoulos, D. Economou, C. Economou and J. Maragozis, *Norbornadiene-Quadricyclane System in the Photochemical Conversion and Storage of Solar Energy*, 1983, **22**, 1-4.

33 K. Börjesson, D. Coso, V. Gray, J. C. Grossman, J. Guan, C. B. Harris, N. Hertkorn, Z. Hou, Y. Kanai, D. Lee, J. P. Lomont, A. Majumdar, S. K. Meier, K. Moth-Poulsen, R. L. Myrabo, S. C. Nguyen, R. A. Segalman, V. Srinivasan, W. B. Tolman, N. Vinokurov, K. P. C. Vollhardt and T. W. Weidman, *Chemistry - A European Journal*, 2014, **20**, 15587–15604.

34 R. Boese, J. K. Cammack, A. J. Matzger, K. Pflug, W. B. Tolman, K. P. C. Vollhardt and T. W. Weidman, *J Am Chem Soc*, 1997, **119**, 6757–6773.

35 Y. Kanai, V. Srinivasan, S. K. Meier, K. P. C. Vollhardt and J. C. Grossman, *Angewandte Chemie*, 2010, **122**, 9110–9113.

36 C. Bastianelli, V. Ciaa, G. Cum, R. Gallo, V. Mancini, *Annual Review of Biochemistry*, 1983, **24**, 3903–3904.

37 D. Gegiou, K. A Muszkat, E. Fischer, D. Gegiou, K. A. Muszkat, *Journal of the Chemical Society*, 1968, **90**, 3907-3919.

38 M. Irie, *Bull Chem Soc Jpn*, 2008, **81**, 917–926.

39 Y. Feng, W. Feng, H. Noda, A. Fujii, M. Ozaki and K. Yoshino, *Journal of Applied Physics*, 2007, **102**.

40 J. M. Simmons, I. In, V. E. Campbell, T. J. Mark, F. Léonard, P. Gopalan and M. A. Eriksson, *Physical Review Letters*, 2007, **98**, 086802.

41 T. J. Kucharski, N. Ferralis, A. M. Kolpak, J. O. Zheng, D. G. Nocera and J. C. Grossman, *Nature Chemistry*, 2014, **6**, 441–447.

42 K. Ishiba, M. A. Morikawa, C. Chikara, T. Yamada, K. Iwase, M. Kawakita and N. Kimizuka, *Angewandte Chemie - International Edition*, 2015, **54**, 1532–1536.

43 Z. Y. Zhang, Y. He, Z. Wang, J. Xu, M. Xie, P. Tao, D. Ji, K. Moth-Poulsen and T. Li, *J Am Chem Soc*, 2020, **142**, 12256–12264.

44 S. P. Jeong, L. A. Renna, C. J. Boyle, H. S. Kwak, E. Harder, W. Damm and D. Venkataraman, *Scientific Reports*, 2017, **7**, 1–12.

45 S. P. Jeong, L. A. Renna, C. J. Boyle, H. S. Kwak, E. Harder, W. Damm and D. Venkataraman, *Scientific Reports*, 2017, **7**, 1-28, Supplementary.

46 M. Moniruzzaman, C. J. Sabey and G. F. Fernando, *Macromolecules*, 2004, **37**, 2572–2577.

47 L. M. Smith and M. L. Coote, *Journal of Polymer Science, Part A: Polymer Chemistry*, 2013, **51**, 3351–3358.

48 L. M. Smith and M. L. Coote, *Supporting information for Effect of temperature and solvent on polymer tacticity in the free-radical polymerization of styrene and methyl methacrylate*.

49 C. Wallace, *Development of Solar Thermal Fuels for Automotive Applications*, 2018. Unpublished thesis work.

50 J. F. Lutz, W. Jakubowski and K. Matyjaszewski, *Macromolecular Rapid Communications*, 2004, **25**, 486–492.

51 Y. Miura, T. Satoh, A. Narumi, O. Nishizawa, Y. Okamoto and T. Kakuchi, *Macromolecules*, 2005, **38**, 1041–1043.

52 P. Carriere, Y. Grohens, J. Spevacek and J. Schultz, *Langmuir*, 2000, **16**, 5051–5053.

53 R. Born, H. W. Spiess, W. Kutzelnigg, U. Fleischer and M. Schindler, *Macromolecules* 1994, **27**, 1500–1504.

54 R. Born and H. W. Spiess, *Macromolecules* 1995, **28**, 7785–7795.

55 F. Ademma, R. Born, H. W. Spiess, C. de Rosa and P. Corradini, *Macromolecules* 1995, **28**, 6902–6910.

56 J. Engqvist, S. A. Hall, M. Wallin, M. Ristinmaa and T. S. Plivelic, *Experimental Mechanics, 2014,* **54**, 1373–1383.

57 E. Wolf and H. K. Cammenga, *Zeitschrift fur Physikalische Chemie*, 1977, **107**, 21–38.

58 B. Guerrier, C. Bouchard, C. Allah and C. Bknard, *Drying Kinetics of Polymer Films*, 1998, **44**, 791–799.

59 S. Alsoy and J. L. Duda, *Modeling of Multicomponent Drying of Polymer Films*, 1999, **45**, 896–906.